Joint compensation of I/Q impairments and PA nonlinearity in mobile broadband wireless transmitters

Bozic, M.

JOINT COMPENSATION OF I/Q IMPAIRMENTS AND PA NONLINEARITY IN MOBILE BROADBAND WIRELESS TRANSMITTERS

MILICA BOZIC

A thesis submitted in partial fulfilment of the
requirements of the University of Westminster
for the degree of Doctor of Philosophy

April 2016

ABSTRACT

The main focus of this thesis is to develop and investigate a new possible solution for compensation of in-phase/quadrature-phase (I/Q) impairments and power amplifier (PA) nonlinearity in wireless transmitters using accurate, low complexity digital predistortion (DPD) technique. After analysing the distortion created by I/Q modulators and PAs together with nonlinear crosstalk effects in multi-branch multiple input multiple output (MIMO) wireless transmitters, a novel two-box model is proposed for eliminating those effects. The model is realised by implementing two phases which provide an optimisation of the identification of any system. Another improvement is the capability of higher performance of the system without increasing the computational complexity. Compared with conventional and recently proposed models, the approach developed in this thesis shows promising results in the linearisation of wireless transmitters. Furthermore, the two-box model is extended for concurrent dual-band wireless transmitters and it takes into account cross-modulation (CM) products. Besides, it uses independent processing blocks for both frequency bands and reduces the sampling rate requirements of converters (digital-to-analogue and analogue-to-digital). By using two phases for the implementation, the model enables a scaling down of the nonlinear order and the memory depth of the applied mathematical functions. This leads to a reduced computational complexity in comparison with recently developed models. The thesis provides experimental verification of the two-box model for multi-branch MIMO and concurrent dual-band wireless transmitters. Accordingly, the results ensure both the compensation of distortion and the performance evaluation of modern broadband wireless transmitters in terms of accuracy and complexity.

TABLE OF CONTENTS

CHAPTER 1 Introduction

CHAPTER 2 Background

CHAPTER 3 Behavioural Modelling of Wireless Transmitters and Description of Digital Predistortion Techniques

CHAPTER 6 Conclusion and Future Work

LIST OF FIGURES AND TABLES

CHAPTER 1

CHAPTER 2

CHAPTER 3

CHAPTER 4

CHAPTER 5

CHAPTER 2

CHAPTER 4

CHAPTER 5

ACKNOWLEDGEMENTS

I would like to express my deepest appreciation to my Director of Studies, Dr. Djuradj Budimir, for offering me a research opportunity at the University of Westminster and helping me to stay focused and motivated throughout my doctoral programme, without your guidance this thesis would not have been possible. I would also like to thank my second supervisor, Dr. Andrzej Tarczynski, for the insightful advice and support he has given me.

The financial support provided by the Fund for Young Talents of Ministry of Youth and Sport of Serbia is greatly acknowledged.

Special thanks to my friends who have always been there to encourage me and provide me with their unconditional support.

Finally, I would like to dedicate this work to my family, for their patience and continuous support.

Milica Bozic

29/01/2016

AUTHOR'S DECLARATION

I declare that all the material contained in this thesis is my own work.

LIST OF ACRONYMS

ACPR	Adjacent Channel Power Ratio
ADC	Analogue-to-Digital Converter
ADS	Advanced Design System
AM	Amplitude Modulation
CM	Cross-Modulation
CP	Cyclic Prefix
DAC	Digital-to-Analogue Converter
DC	Discrete Current
DS	Distortion Suite
DLA	Direct Learning Architecture
DL	Downlink
DPD	Digital Predistortion
DSP	Digital Signal Processing
DUT	Device Under Test
ESG	Electronic Signal Generator
EVM	Error Vector Magnitude
ETSI	European Telecommunications Standards Institute
E-UTRA	Evolved-UMTS Terrestrial Radio Access
FFT	Fast Fourier Transform
FIR	Finite Impulse Response
1G	First Generation
FLOP	Floating Point Operation
4G	Fourth Generation

FDD	Frequency Division Duplex
GMP	Generalised Memory Polynomial
GPIB	General-purpose Interface Bus
GSM	Global System for Mobile communications
HSPA	High Speed Packet Access
ICT	Information Communication Technology
ICI	Inter-Channel Interference
IM	Intermodulation
IMD	Intermodulation Distortion
IM3	Third-Order Modulation
IP3	Third-Order Intercept Point
ILA	Indirect Learning Architecture
IFFT	Inverse Fast Fourier Transform
ISI	Inter-Symbol Interference
I/Q	In-phase Quadrature-phase
LS	Least Square
LTI	Linear Time Invariant
LO	Local Oscillator
LTE	Long Term Evolution
LUT	Look-up Table
LB	Lower band
MSE	Mean Squared Error
MP	Memory Polynomial
MIMO	Multiple Input Multiple Output
NN	Neural Network

NMSE	Normalised Mean Squared Error
OFDM	Orthogonal Frequency-Division Multiplexing
OBO	Output Back-off
PH	Parallel Hammerstein
PAPR	Peak-to-Average Power Ratio
PBO	Peak Back-off
PC	Personal Computer
PM	Phase Modulation
PA	Power Amplifier
PD	Predistorter
PSD	Power Spectrum Density
QAM	Quadrature Amplitude Modulation
QPSK	Quadrature Phase Shift Keying
QoS	Quality of Service
RatF	Rational Function
RV	Real Volterra
RVFTDNN	Real Valued Focused Time Delay Neural Network
RBS	Radio Base Station
RF	Radio Frequency
RB	Resource Block
SISO	Single Input Single Output
2G	Second Generation
3G	Third Generation
3GPP	Third Generation Partnership Project
TDD	Time Division Duplex

2D	Two-dimensional
UB	Upper band
UE	User Equipment
UL	Uplink
VSA	Vector Signal Analyser
WCDMA	Wideband Code Division Multiple Access
WL	Widely Linear

CHAPTER 1
INTRODUCTION

Almost 300 years ago, the development of wireless communications began. Without hesitation, we can say that true wireless communications were based on the works of James Clark Maxwell and Heinrich Hertz. Maxwell discovered the science of electromagnetism, which opened the door for the use of radio waves for radio, television and personal mobile communications. Moreover, he theoretically predicted and proved the existence of electromagnetic waves. All of these led to the discovery of radio waves by Heinrich Hertz, who experimentally validated that electrical energy can be transmitted using electromagnetic waves. However, the first person who proposed the use of radio waves for transmitting coded information was Nikola Tesla. Also, he proposed first radio communication systems. Nearly simultaneously, Guglielmo Marconi patented the telegraph which was the first practical system of wireless telegraphy. Using telegraph he sent (and received) Morse code across the English Channel. Therefore, Marconi became known as the "wizard of wireless". A few more years had to pass until the idea of reliable transmission of information through wireless channel could be realised. Claude Shannon is the one who is responsible for paving the way for modern communications. Nowadays, wireless communications is one of the most developed areas in the industry of telecommunications.

1.1 Introduction

During the past years, the progress of wireless communications has increased tremendously worldwide. The main goal is to provide high data capacity with low-cost services. The first generation (1G) wireless communications used analogue transmission which provided basic voice communication with limited roaming. Development of second generation (2G) of wireless communications improved capacity of the systems as well as voice quality. Also, roaming became more prevalent and low bit rate data services were supported [1-1]. Since 2G could not meet the requirements of the data rates, the progress of third generation (3G) wireless communications advanced. Moreover, introducing 3G enabled services independent of the technology platform, would be further developed by the fourth generation (4G). Furthermore, 4G enabled high data rates with good quality of service (QoS).

As it can be seen from Figure 1.1, overall mobile data traffic is expected to grow to 24.3 exabytes per month by 2019; nearly a tenfold rise over 2014. The number of wireless devices which are accessing mobile networks worldwide is increasing, which is one of the primary contributors to global mobile traffic growth [1-2].

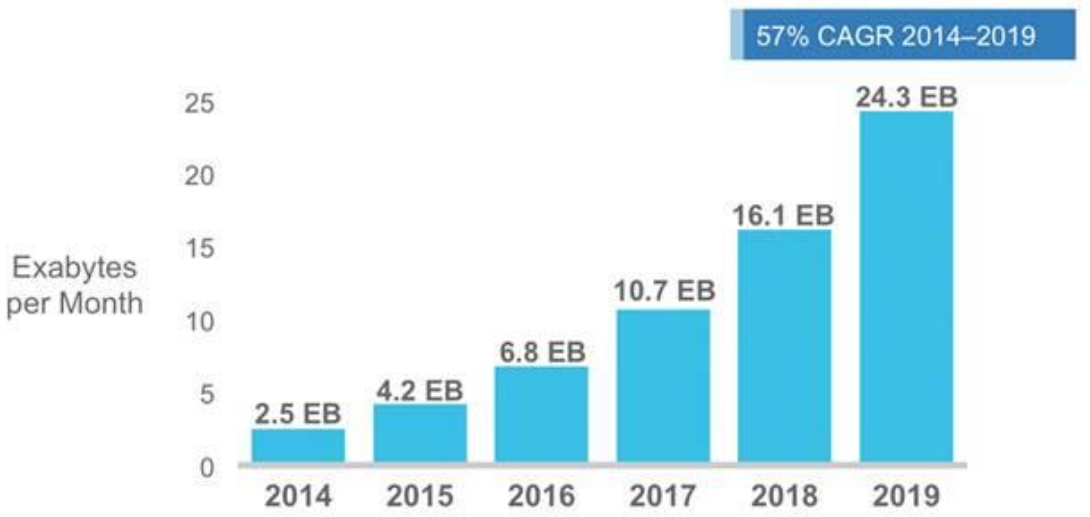

Figure 1.1: Cisco forecasts 24.3 exabytes per month of mobile data traffic by 2019 [1-2].

Therefore, wireless communications have geared to higher data rates, greater spectral efficiency, low latency, better reliability and availability. It becomes a major way of communicating and transmitting data.

Figure 1.2 illustrates basic blocks in wireless communication systems. As it can be noticed, both the transmitter and the receiver consist of two main blocks: digital and analogue. The digital block is responsible for formatting the data stream using different encoding processes, whereas the analogue block is responsible for converting signal from digital to analogue domain and from baseband to radio frequencies (RFs). Thus, these blocks format the data stream in a form suitable for transmission through wireless channels. Such wireless systems are required to work with a limited amount of energy and RF resources while the QoS is still at high level. In other words, wireless transmitters need to be highly linear and have a low power consumption.

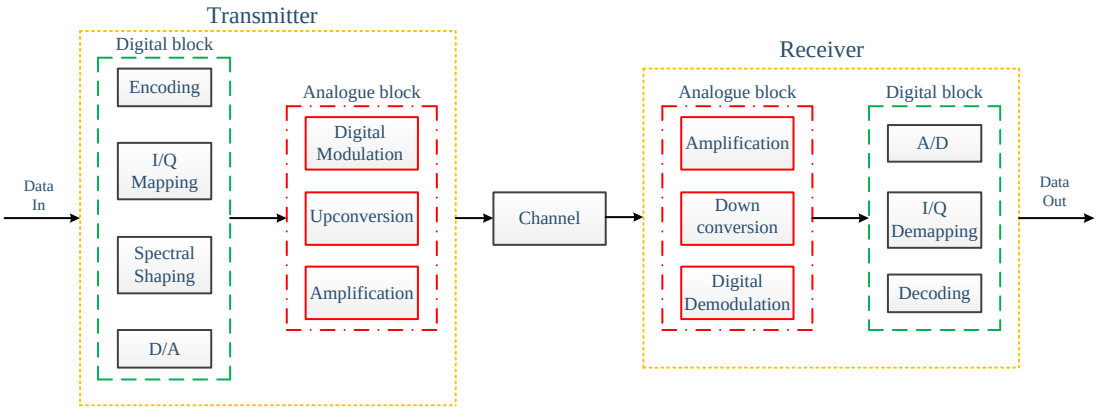

Figure 1.2: Basic blocks in wireless communications systems.

One of the main trends in the evolution of wireless transmitters is to implement more and more of the transmitter functionalities using digital signal processing (DSP). However, those modern wireless transmitters involve highly complex DSP blocks. Real wireless transmitters, like all physical systems, are not ideal, since their components introduce distortion in the transmitting signal. This distortion is mainly produced by nonlinear components in the RF front ends, such as In-phase/Quadrature-phase (I/Q) modulators and power amplifiers (PAs).

Modern wireless transmitters include complex I/Q modulators that imply generating and processing the I and Q channel inputs separately. Therefore, any differences between these two components cause imperfections, such as amplitude and phase imbalance and discrete (DC) offset. These impairments are called linear distortion [1-3]–[1-5]. The high spectral efficiency is achieved when an I/Q modulator operates near its maximum output level. Thus, the presence of nonlinear distortions caused by an I/Q modulator cannot be avoided [1-6]–[1-7]. All these impairments cause a strong degradation of the final signal quality. The nonlinear PA amplifying the wideband signals with non-constant envelope produces nonlinearities, which contribute further to signal distortion [1-8]–[1-10]. More complex multiplexing systems, such as multiple input multiple output (MIMO) are even more sensitive to I/Q impairments and PA nonlinearity than the single-carrier modulation technique [1-11]–[1-12]. Those systems appear as a promising technique which can support up to 1 Gb/s for downlink (DL) and 500 Mb/s for uplink (UL) within a bandwidth of 100 MHz. To achieve these strong service demands it is necessary to use multi-branch or multi-frequency MIMO wireless transmitters [1-13]. The main problem with multi-branch and multi-frequency MIMO wireless transmitters is that they introduce crosstalk effects and cross-modulation (CM) products as additional distortion to the signal respectively. Therefore, in recent years,

more and more attention has been shifted towards developing compensation techniques which jointly mitigate I/Q impairments and PA nonlinearity and MIMO impairments (crosstalk effects and CM products). With the increasing demands for the system performance and supported data rates on one side and the terminal flexibility and implementation costs on the other, the requirements for the suppression of nonlinear distortion in wideband multichannel wireless transmitters becomes extremely challenging to meet. Thus, the modelling and compensation of the impairments produced by imperfect hardware implementing digital predistortion (DPD) technique is the focus of this thesis.

1.2 Overview of Past Research work

With fast development of wireless communications, the requirements of both linearity and efficiency of wireless transmitters rise rapidly. These high demands accelerate the progress of different linearisation techniques, such as feed-forward [1-14], RF feedback [1-15] and DPD. The use of feedback technique limits the gain of PA to the gain of the feedback loop. Also, the delays associated with the feedback loop must be small enough to ensure stability. The main drawback of feed-forward is sensitivity to changes in operating conditions. Moreover, this technique is not adaptive. The DPD is the most cost-effective method [1-16]–[1-19] which minimises the output distortion and reduces spectral re-growth. It has the advantage of unconditional stability and there is no need for an extra PA. These additional PAs that exist in both feed-forward and feedback linearization techniques increase the cost and reduce the stability of implemented techniques. By employing DPD technique for the suppression of distortion in the baseband block, problems like distortion and spectral re-growth can be mitigated. Also, it maximises the power efficiency by digitally preprocessing the input signal in order to achieve a highly linear overall transfer function. However, this results in small bandwidths due to the current limited DSP computational rates.

1.3 Aims and Objectives of the Thesis

The main goal is to develop a novel DPD technique which has potential to jointly compensate I/Q impairments and PA nonlinearity and MIMO impairments (crosstalk effects and CM products) in 4G wireless transmitters. In addition to nonlinear distortion introduced from both I/Q modulator and PA, MIMO wireless transmitters have other side effects that researchers should be aware of. A nonlinear crosstalk specific for multi-

branch MIMO wireless transmitters and CM products that are introduced using concurrent dual-band wireless transmitters will be investigated in details. The overall task during this PhD project is based on: developing low-complexity DPD technique for the joint compensation of I/Q impairments and PA nonlinearity in multi-branch MIMO and concurrent dual-band wireless transmitters.

1.3.1 Aims

The aims of this thesis are:

- Evaluation of undesired effects such as I/Q impairments, PA nonlinearity and crosstalk effects and CM products in multi-branch MIMO and concurrent dual-band wireless transmitters.

- Development a of novel two-box model for multi-branch MIMO wireless transmitters.

- Implementation and experimental validation of the proposed two-box model for dual-branch MIMO wireless transmitters using 4G signals and a real PA.

- Matlab simulation of the proposed two-box model for four-branch MIMO wireless transmitters using 4G signals.

- Development of a novel two-box model for concurrent dual-band wireless transmitters.

- Implementation and experimental validation of the proposed two-box model for concurrent dual-band wireless transmitters using 4G signals and a real PA.

1.3.2 Objectives

The individual research objectives to achieve these aims can be summarised as follows:

- Investigation of behavioural models of I/Q modulators and PAs for the development of a DPD technique.

- Investigation of different adaptation methods to find the best compromise between accuracy and complexity for overcoming degradation that appears in I/Q modulators and PAs.

- Providing a comparative overview of the existing DPD techniques.
- Providing a literature overview of recent advancements in the area of multi-branch MIMO and concurrent dual-band wireless transmitters.
- Setting up the experimental test-bed for developing as well as testing new predistortion methods. Setup contains a real PA (Mini Circuits ZFL-500), Keysight ESG-D Series Signal Generator E4433B, Keysight MXG Vector Signal Generator N5182A, Keysight VSA Series Transmitter Tester and finally, Matlab, ADS, Keysight Signal Studio Toolkit, Keysight DS 89604 and Keysight VSA 89601.
- Creating LAN and GPIB connections between a PC and the instruments: ESG E4433B, MXG N5182A and VSA Series Transmitter Tester for faster offline and online data processing and developing of adaptive system that require all components of experimental test-bed to be connected.
- Developing a new two-box model for multi-branch MIMO wireless transmitters with complexity reduction.
- Experimental verification of this model for dual-branch MIMO wireless transmitters.
- Matlab simulation of this model for four-branch MIMO wireless transmitters.
- Developing a two-box model applicable for concurrent dual-band wireless transmitters.
- Investigating the complexity and linearity of the proposed two-box model for both multi-branch MIMO and concurrent dual-band wireless transmitters.
- Comparative review of this work with the relevant recent works on both multi-branch MIMO and concurrent dual-band wireless transmitters.

1.4 Outline of The Thesis

This section summarises the contents of the thesis for the period from 2012-2015, which is organised into six chapters.

Chapter 2 presents a brief introduction to the background theory relevant to the undertaken research work. It provides an overview of the linearity requirements and the main signal parameters in wireless transmitters. Basic theory about distortion caused by

both I/Q modulator and PA is demonstrated. Also, multi-branch and multi-frequency MIMO wireless transmitters are introduced with attention on the distortion introduced using these techniques. In this chapter, the simulation and experimental results of the nonlinear distortion introduced using multi-frequency MIMO wireless transmitter are presented.

Chapter 3 presents an overview of the most popular DPD techniques together with behavioural models of I/Q modulator and PA. It describes drawbacks and advantages of these techniques. Direct learning architecture (DLA) and indirect learning architecture (ILA) as DPD extraction techniques are introduced. It also demonstrates DPD models for the joint compensation of I/Q impairments and PA nonlinearity and the extensions of the existing DPD models to be applicable for multi-branch MIMO and concurrent dual-band wireless transmitters.

Chapter 4 introduces a two-box model for the joint compensation of I/Q impairments and PA nonlinearity and crosstalk effects for multi-branch MIMO wireless transmitters. The chapter begins with an introduction to the existing DPD models and theirs advantages and drawbacks. Then the realisation of the proposed model is presented. It is shown that cascading rational function (RatF) and real-Volterra (RV) model can lead to the creation of DPD model which improves performance of multi-branch MIMO wireless transmitters and lowers the complexity of the system. Also, it is presented that the nonlinear distortion is compensated gradually. Expanding on this, the chapter finally presents a two-box model which achieves improvements in the adjacent channel power ratio (ACPR), error vector magnitude (EVM) and normalised mean square error (NMSE).

Chapter 5 details an implementation of a two-box model for the joint mitigation of I/Q impairments and PA nonlinearity and CM products for concurrent dual-band wireless transmitters. This chapter gives a brief overview of existing techniques and its disadvantages, followed by an explanation of the implementation of the proposed model for concurrent dual-band wireless transmitters. Experimental results will be provided in order to validate performance. It will be shown that by employing the two-box model, not only its complexity can be reduced, but also better performance can be achieved.

Finally in Chapter 6, the main conclusion of the work presented in this thesis is given alongside a summary of the contribution of this work and suggestions for future work are highlighted.

A list of achievements of the conducted research work and presented in this thesis are summarised here.

1. The thesis presents the development of novel two-box model for joint compensation of I/Q impairments, PA nonlinearity and crosstalk effect for multi-branch MIMO wireless transmitters. Proposed model has been verified through Matlab simulations and experimental verification. It has been shown that the use of proposed two-box model not only improves performance of the multi-branch MIMO wireless transmitters but also reduces complexity of the system.

2. The development of new two-box model for joint compensation of I/Q impairments, PA nonlinearity and CM products for concurrent dual-band wireless transmitters. Experimental verification of the proposed model has been provided. The complexity of modelling process has been significantly minimised while the performance of the system are still at high level.

3. For the first time, the implementation of two-box model based on RatF-RV models has been presented. The main idea is to gradually compensate for the nonlinear distortion that appears in multi-branch and multi-frequency MIMO wireless transmitters.

1.5 References

[1-1] F. Khan, *LTE for 4G Mobile Broadband*, New York: Cambridge University Press, 2009

[1-2] "Cisco Visual Networking Index: Global Mobile Data Traffic Forecast Update 2014-2019," in White Paper, CISCO, Feb. 2015. Available Online: http://www.cisco.com/c/en/us/solutions/collateral/service-provider/visual-networking-index-vni/white_paper_c11-520862.html

[1-3] Y.D. Kim, E.R. Jeong and Y. H. Lee, "Adaptive Compensation for Power Amplifier Nonlinearity in the Presence of Quadratur Modulation/Demodulation Errors," *IEEE Trans. Signal Process.*, vol. 55, no. 9, pp. 4717-4721, Sep. 2007

[1-4] L. Anttila, M. Valkama and M. Renfors, "Frequency-Selective I/Q Mismatch Calibration of Wideband Direct-Conversion Transmitters," *IEEE Transactions on Circuits and Systems II: Express Briefs*, vol. 55, no. 4, pp.359,363, April 2008

[1-5] H. Zareian and V. Vakili, "New Adaptive Method for IQ Imbalance Compensation of Quadrature Modulators in Predistortion Systems", *Eurasip Journal On Advances In Signal Processing*, vol. 2009, no. 1. pp. 1687-6172, 2009

[1-6] Li. Minsheng L. Hoover, K.G Gard and M.B. Steer, "Behavioral Modeling of Quadrature Modulators for Characterization of Nonlinear Distortion," *IEEE MTT-S International Microwave Symposium Digest, ,* vol., no., pp.1117-1120, June 2006

[1-7] P. Zhan, K. Qin and S. Cai, "Nonlinear behavioral model for quadrature modulators and compensators," *IEEE International Conference on Computer Science and Automation Engineering (CSAE)*, vol. 3, no., pp.437-440, June 2011

[1-8] D.R. Morgan, M. Zhengxiang, K. Jaehyeong, M.G. Zierdt and J. Pastalan, "A Generalized Memory Polynomial Model for Digital Predistortion of RF Power Amplifiers," *IEEE Transactions on Signal Processing*, vol.54, no.10, pp. 3852-3860, Oct. 2006

[1-9] K. Jangheon, Y. W. Young, M. Junghwan and K. Bumman, "A New Wideband Adaptive Digital Predistortion Technique Employing Feedback Linearization," *IEEE Transactions on Microwave Theory and Techniques*, vol. 56, no. 2, pp. 385-392, Feb. 2008

[1-10] H. Wang, J. Bao and Z. Wu, "Comparison of the Behavioral Modelings for RF Power Amplifier With Memory Effects," *IEEE Microwave and Wireless Components Letters*, vol. 19, no. 3, pp.179-181, March 2009.

[1-11] J. Qi and S. Aissa, "Analysis and compensation for the joint effects of HPA nonlinearity, I/Q imbalance and crosstalk in MIMO beamforming systems," *IEEE Wireless Communications and Networking Conference (WCNC)*, vol., no., pp.1562-1567, March 2011

[1-12] F Gregorio, J. Cousseau, S. Werner, T. Riihonen and R. Wichman, "Power amplifier linearization technique with IQ imbalance and crosstalk compensation for broadband MIMO-OFDM transmitters," *Eurasip Journal On Advances In Signal Processing*, vol., no., pp: 1687-6172, 2011

[1-13] S. A. Bassam, F. M. Ghannouchi and M. Helaoui, "Multi-Cell Processing Architectures for Modeling and Impairment Compensation in Multi-Input Multioutput Systems," US Patent Application 12/780/455, filed 14 May 2010

[1-14] S.P. Stapleton, "Adaptive feedforward linearization for RF power amplifiers," in *Proc. 55th Automatic RF Techniques Group Conference Digest-Spring*, vol. 37, pp. 1-7, June 2000

[1-15] Y. Y. Woo, J. Kim, J. Yi, S. Hong, I. Kim, J. Moon and B. Kim, "Adaptive digital feedback predistortion technique for linearizing power amplifiers," *IEEE Transactions on Microwave Theory and Techniques*, vol. 55, no. 5, pp. 932-940, May 2007

[1-16] S. Hong, Y. Y. Woo, J. Kim, I. Kim, J. Cha, I. Kim, J. Moon, J. Yi and B. Kim, "Weighted polynomial digital predistortion for low memory effect Doherty power amplifier," *IEEE Transactions on Microwave Theory and Techniques*, vol. 55, no. 5, pp. 925-931, May 2007

[1-17] P. L. Gilabert, A. Cesari, G. Montoro, E. Bertran and J. M. Dilhas, "Multi-lookup table FPGA implementation of an adaptive digital predistorter for linearizing RF power amplifiers with memory effects," *IEEE Transactions on Microwave Theory and Techniques*, vol. 56, no. 2, pp. 372-384, Feb. 2008

[1-18] C. Eun and E. J. Powers, "A new Volterra predistorter based on the indirect learning architecture," *IEEE Transactions Signal Processing*, vol. 45, no. 1, pp. 223–227, Jan. 1997

[1-19] P. Zhan, S.C. Jung, O. Hammi and F. M. Ghannouchi, "Design optimization and DPD linearization of GaN-based unsymmetrical Doherty power amplify ers for 3G multicarrier applications," *IEEE Transactions Microwave Theory and Techniqu*, vol. 57, no. 9, pp. 2105–2113, Sept. 2009

CHAPTER 2
BACKGROUND

Modern wireless designs for the next generation wireless systems are growing in complexity. Emerging mobile radio techniques require wireless transmitters that can support high data rates, throughput and good QoS. Therefore, demands on wireless transmitter for linearity and power efficiency, have increased. This chapter provides an overview of linearity requirements in wireless transmitter. Firstly, linearity requirements and main signal parameters are analysed. Secondly, brief background about distortion that is caused by both, I/Q modulator and PA, is explained. Thirdly, multi-branch and multi-frequency MIMO wireless transmitters are introduced. Also, short background of distortion created by MIMO wireless transmitters is presented.

2.1 Requirements for Linearity in Wireless Transmitters (I/Q modulator and PA)

The block diagram of simplified direct conversion wireless transmitter architecture is shown in Figure 2.1. In this case wireless transmitter has two domains, digital and analogue. Digital domain includes baseband waveform generation, basically digital signal processing and producing complex-valued signal, while analogue domain is responsible for converting that baseband signal to real-valued passband modulated signal at RF frequency and amplification of RF signal to the suitable power level needed for transmitting [2-1].

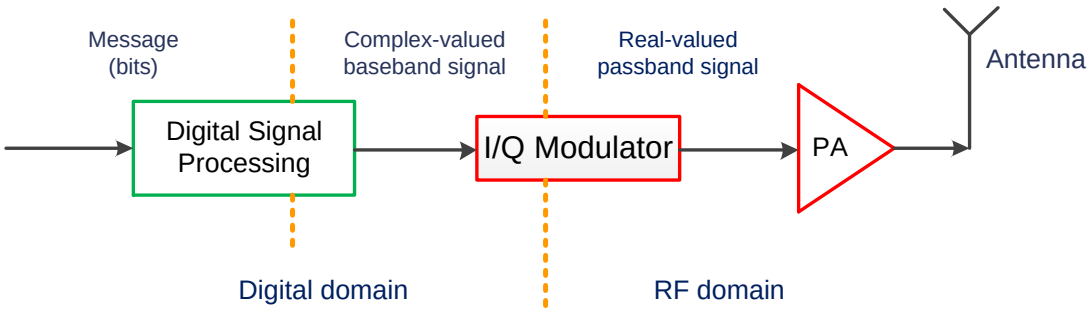

Figure 2.1: Block diagram of simplified wireless transmitter architecture.

The I/Q modulator is responsible for frequency conversion (from baseband frequency to RF frequency) where the complex-valued baseband input signal is divided into real and imaginary part, i.e. in phase (I) and quadrature phase (Q) signals.

Ideal passband signal can be defined as:

$$y(t) = A(t)\cos(\omega_c t + \varphi(t)) \tag{2.1}$$

where $A(t)$ is time-varying envelope of the signal, $\varphi(t)$ is time-varying phase of the signal, and ω_c ($\omega_c = 2\pi f_c t$) is carrier frequency. It can be equivalently written in quadrature form as:

$$y(t) = x_I(t)\cos(\omega_c t) - x_Q(t)\sin(\omega_c t) = 2Re\{x(t)e^{j\omega_c t}\} =$$

$$= x(t)e^{j\omega_c t} + x^*(t)e^{-j\omega_c t} \tag{2.2}$$

where $x_I(t) = A(t)\cos(\varphi(t))$ and $x_Q(t) = A(t)\sin(\varphi(t))$ are I and Q components of the signal, respectively, and $x(t)$ is baseband equivalent signal. Thus, baseband equivalent signal can be written as:

$$x(t) = x_I(t) + jx_Q(t) \tag{2.3}$$

Unfortunately, in real wireless transmitters this cannot be the case since I/Q modulator suffers from imperfect hardware. A simple block diagram of I/Q modulator structure is depicted in Figure 2.2. As illustrated, the I and Q signals are fed to digital to analogue convertors (DACs), which transform the digital signal into an analogue one. During that process nonlinear distortion, as a result of component imperfection, is commonly ensue into the signal and it is manifested as a DC offset. It causes leaking carrier into the passing signal. Subsequently, the analogue signal is passed by reconstruction filter. During this process it is possible to disrupt signal in terms of time delays and phase shift. This distortion often introduces memory effects into signals. Then, analogue signal is fed to an upconverter, which translates baseband signal to RF frequency. Local oscillator (LO) is used to create signals at carrier frequency, which are mixed separately with I and Q signals and combined together to create signal at RF frequency. During this upconversion process imperfections of the signal might occur and they can be manifested as I/Q imbalance and LO leakage. Basically, any differences between amplitude of the I and Q signals will cause distortion which is known as amplitude imbalance. The orthogonality between two branches is often obstructed by error in 90° phase shift, which is commonly known as phase imbalance. Due to imperfection it is common that one part of the LO signal passes through and degrades the quality of signal (LO leakage) [2-1]–[2-2].

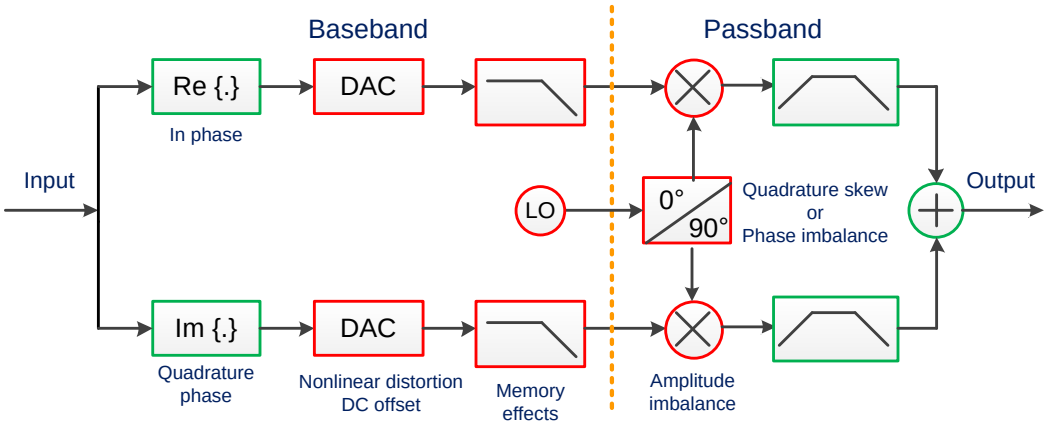

Figure 2.2: Block diagram of simplified I/Q modulator structure.

I/Q modulator induces impairments to the signal and they can be manifested as additional components due to LO leakage, DC offset and I/Q imbalance. These distortions must not be disregarded since they affect transmitted signal and will further introduce distortion when passing through nonlinear component such as PA.

Figure 2.3 depicts I/Q imbalanced model of I/Q modulator, since perfect analogue I/Q mixing is not achievable in real wireless transmitters. The variables d_I and d_Q denote DC offset components for I and Q branches, respectively. Also, imperfection of analogue components leads to deviations from both, the desired 90° phase shift (θ_I and θ_Q represent phase imbalance or quadrature skew) and the desired equal amplitude in I and Q branches (g_I and g_Q represent amplitude imbalance). Functions $h_I(t)$ and $h_Q(t)$ denote the impulse responses of low-pass filters for I and Q branches, respectively.

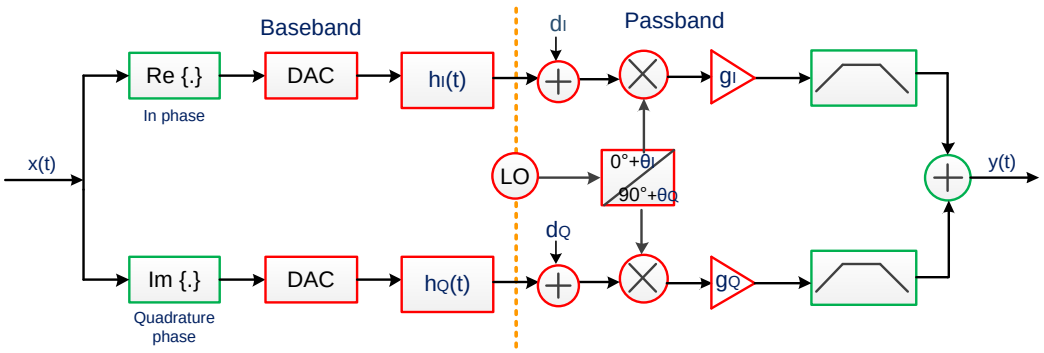

Figure 2.3: I/Q imbalnced model of I/Q modulator.

The corrupted RF signal can be expressed as:

$$y(t) = (x_I(t) + d_I)g_I\cos(\omega_c t + \theta_I) * h_I(t) - (x_Q(t) + d_Q)g_Q\sin(\omega_c t + \theta_Q) * h_Q(t)$$

$$= x(t) * k_1(t) + x^*(t) * k_2(t) + D(t) \qquad (2.4)$$

where the * and subscript $(.)^*$ symbol denote convolution and complex conjugation operators, respectively, $k_1(t) = \frac{1}{2}\left(g_I e^{-j\theta_I} h_I(t) + g_Q e^{-j\theta_Q} h_Q(t)\right)$ and $k_2(t) = \frac{1}{2}\left(g_I e^{j\theta_I} h_I(t) - g_Q e^{j\theta_Q} h_Q(t)\right)$, and $D(t)$ denotes term caused by DC offset. The desired term is distorted by self-distortion $k_1(t)$. Additionaly, the quality of the signal is degraded by both mirror-image distortion $k_2(t)$ and DC offset ($D(t)$). In case where $g_I \neq g_Q$, $\theta_I \neq 0$ and $\theta_Q \neq 0$ amplitude and phase imbalance occurs. Moreover, relative difference between $h_I(t)$ and $h_Q(t)$ will increase frequency-dependent I/Q imbalance. Contrary, in ideal case $g_I = g_Q$ and $\theta_I = \theta_Q \neq 0$ and $h_I(t) = h_Q(t)$ and $D(t) = 0$, which will lead to $y(t) = x(t)e^{j\omega_c t} + x^*(t)e^{-j\omega_c t}$.

Apart from I/Q modulator, a PA stands for one of the most critical components in the wireless transmitter. As the major power consuming block, it has the greatest impact on overall wireless transmitter efficiency. In other words, an efficient PA will reduce the cost of power consumption and increase the battery life of wireless transmitter. This means that the PA should work in saturation region. However, the increase in efficiency will lead to degradation of linearity. Thus, a trade-off between efficiency and linearity needs to be considered during designing process.

Figure 2.4 shows typical input-output amplitude characteristic of PA. As it can be seen, real PA response does not have linear characteristic as ideal. The unavoidable thing is that PA characteristic in real systems becomes saturated and PA gain declines. Moreover, PA introduces memory effects in wireless transmitters, since its response is not constant over time. In other words, when signal with wide bandwidth passes through PA, it exhibits memory effects. The causes of the memory effects can be attributed to the thermal constants of the components in the biasing network that have frequency-dependent behaviour. As a result, the PA output not only depends on the instantaneous input, but also on the past input values. Distortion introduced by PA can be classified as: nonlinear distortion catalyzed manly from DC characteristic and memory effects caused by non-ideal bias networks, temperature dependence, trapping effects, time delays, phase shift and etc.

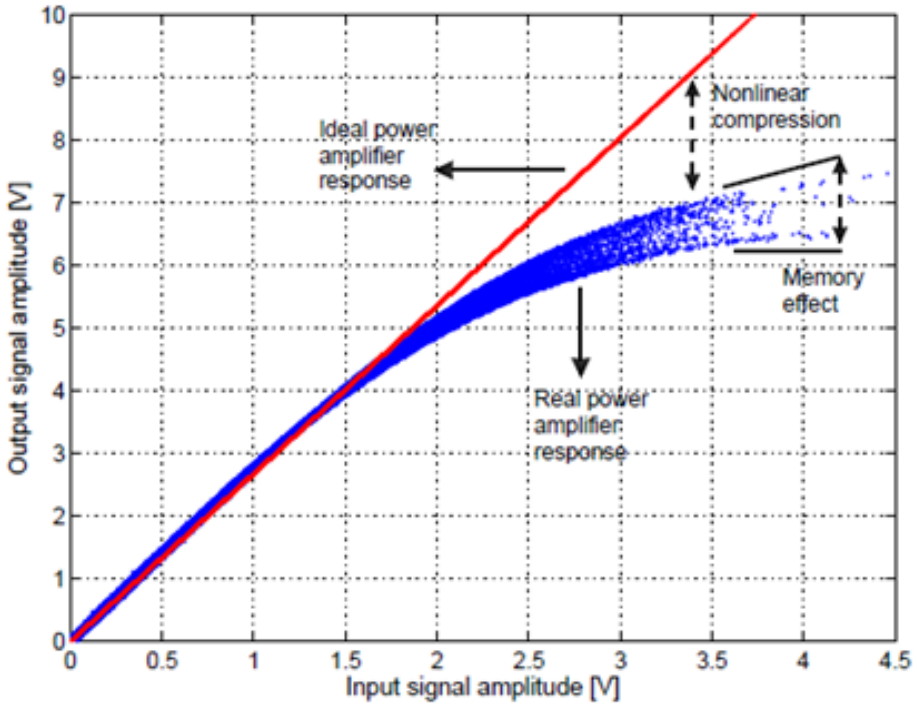

Figure 2.4: Input-output characteristics of an ideal and real PA [2-2].

Categorisation of memory effects that are induced by PA can be classified into two groups: electrical and thermal. The electrical memory effects are dominant in wideband systems and they are produced by poor gate and drain decoupling in field-effect transistor and base and collector decoupling in bipolar junction transistor. Also, they are generated by non-constant, frequency-dependent envelope impedances within frequency bands. These memory effects result in the frequency-dependent gain and phase shifts of the signal passing through the PA. Hence, the memory effects cause distortion of the output signal and result in intermodulation distortion (IMD) asymmetry [2-1].

2.2 Wireless Transmitter System Parameters

In the following section main system parameters are briefly explained [2-1]–[2-3].

2.2.1 PA system parameters

Gain:

The gain of a PA is defined as ratio of the output power to the input power. Also, it is usually expressed in decibels (dB) as follows [2-1]:

$$G(dB) = 10 \log \frac{P_{out}}{P_{in}} \quad (2.5)$$

where P_{in} is the input power and P_{out} is the output power.

Bandwidth:

The range of frequencies for which the PA gives acceptable performance is called the bandwidth. The acceptable performance is different for different applications. Additionally, as shown in Figure 2.5, the bandwidth of PA is often defined as the difference between lower and higher half power points, which is known as a 3 dB bandwidth. Half power point is a frequency where power of a PA decrease by the half of its peak value [2-1].

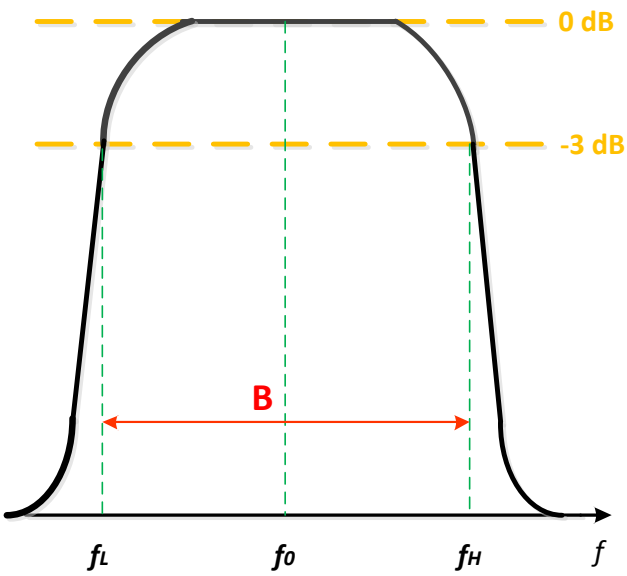

Figure 2.5: 3 dB bandwidth of a PA.

Power efficiency:

Power efficiency is a metric that quantifies the ability of a system to transform the given input power to useful output power. The PA as a most power-consuming component of a wireless transmitter is responsible for determining the overall power efficiency. The three different definitions of PA efficiency exist in the literature, which are the total efficiency, the drain efficiency, and the power added efficiency.

Total efficiency is defined as [2-1]:

$$\eta_t = \frac{P_{out}}{P_{dc}+P_{in}} \tag{2.6}$$

where η_t is the total efficiency of the PA, P_{dc}, P_{in} and P_{out} are the DC and RF powers at the input and output of the PA, respectively.

Drain efficiency is defined as [2-1]:

$$\eta_{D\ trans.} = \frac{P_{RF\ Drain}}{P_{dc\ Drain}} \tag{2.7}$$

where $P_{dc\ Drain}$ and $P_{RF\ Drain}$ are the DC and RF powers, at the drain level of the transistor.

Power added efficiency is defined as [2-1]:

$$\eta_{PAE} = \frac{P_{out}-P_{in}}{P_{dc}} \tag{2.8}$$

where η_{PAE} is the total power added efficiency of the PA, P_{dc}, P_{in} and P_{out} are the DC and RF powers at the input and output of the PA, respectively.

P1dB compression point (P1dB):

Figures 2.6 and 2.7 show input-output and gain characteristics of a PA respectively. The 1dB compression point (P1dB) is a measure of PA linearity. The gain of an amplifier compresses when the output signal level enters the compression region before it reaches saturation. Higher output power corresponds to a higher compression point. P1dB is an input (or output) power for which the gain of the PA is 1 dB less than the small-signal gain (ideal linear gain) [2-1].

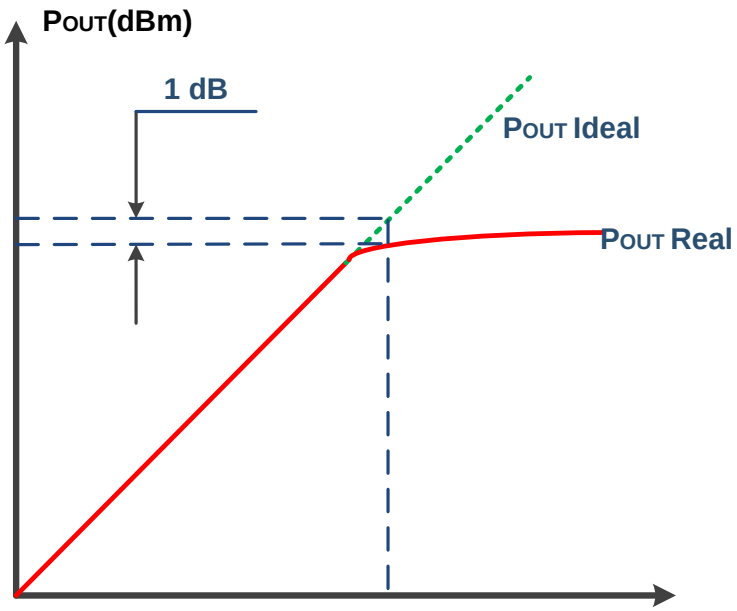

Figure 2.6: The input-output characteristic of a PA.

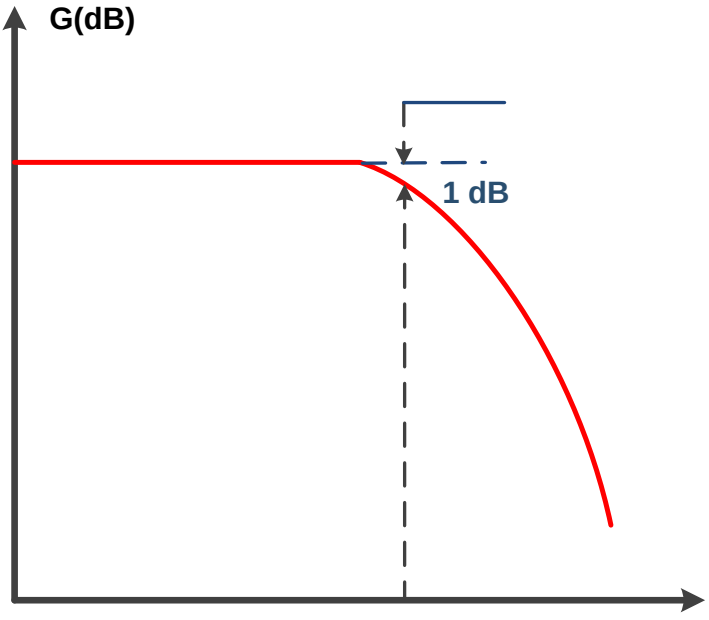

Figure 2.7: The gain characteristic of a PA.

The maximum saturation point corresponds to the point where the PA reaches its output maximum power. This maximum power is called the saturation power $P_{sat[max]}$. The 3 dB saturation power $P_{sat[dB]}$ corresponds to the power for which the gain of the PA is 3 dB less than the small-signal gain. To avoid intermodulation (IM) problems and distortion, the output power needs to be reduced below the P1dB.

Third order intercept point (IP3):

Graphical derivation of second and third order intercept points is depicted in Figure 2.8. The third order intercept point (IP3) is a widely used metric in PAs, which gives information about the linearity of a PA. A higher IP3 means better linearity and lower distortion generation. It is a theoretical point at which the desired output signal and third-order IM (undesired) signal are equal in levels considering an ideal linear gain for the PA. The theoretical input point is the input IP3 (IIP3) and the output point is the output IP3 (OIP3) [2-1].

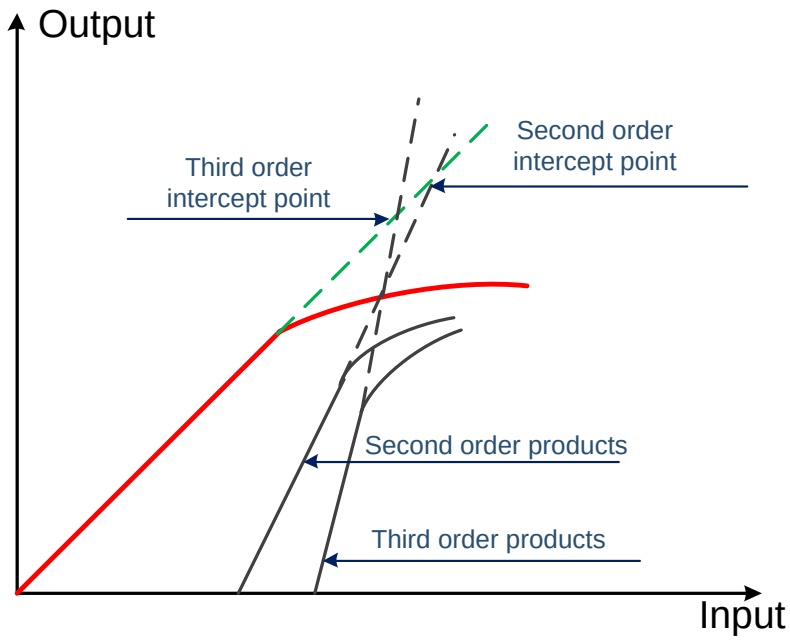

Figure 2.8: The second and third order intercepts points.

Power back-off:

An amplifier appears linear for sufficiently small departures from its bias conditions. The power back-off is defined as the ratio between the PA's saturation power to the RF signal's mean power. There are two types of power back-off: input power back-off and output power back-off. The back-off at the input of the PA *(IBO)* is obtained by:

$$IBO(dB) = P_{i,sat} - P_{i,mean} \tag{2.9}$$

where $P_{i,sat}$ and $P_{i,mean}$ are the saturation power and mean signal power at the input of the PA, respectively. Similarly, the back-off at the output *(OBO)* of the PA is given by:

$$OBO(dB) = P_{o,sat} - P_{o,mean} \quad (2.10)$$

where $P_{o,sat}$ and $P_{o,mean}$ are the saturation power and mean signal power at the output of the PA, respectively. Moreover, there is the peak back-off *(PBO)* is given as follows [2-2]:

$$PBO(dB) = P_{o,sat} - P_{o,peak} \quad (2.11)$$

This is the ratio of saturated output power ($P_{o,sat}$) to peak output power ($P_{o,peak}$).

Figure 2.9 graphically illustrates two types of power back-off (PBO and OBO) that are described above.

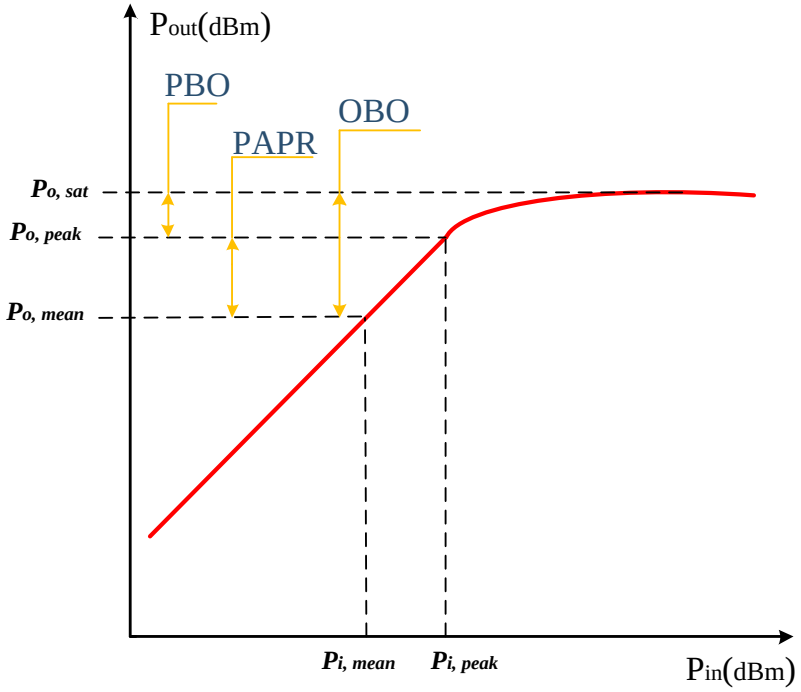

Figure 2.9: The output back-off, peak back-off and peak-to-average power ratio for PAs.

Peak-to-average power ratio (PAPR):

The peak-to-average power ratio (PAPR) is the ratio between the peak power P_{peak} (related to peak amplitude) and the average power P_{mean} (related to mean amplitude) of a signal. It presents a valuable signal parameter in terms of linearity. Also, PAPR is called the crest factor and it is defined as:

$$PAPR(dB) = 10\log\left(\frac{max(|x(t)|^2)}{mean(|x(t)|^2)}\right) = 10\log\left(\frac{P_{peak}}{P_{mean}}\right) \quad (2.12)$$

As presented in Figure 2.9, when the power is logarithmically transformed in dBm, the PAPR is a difference between signal peak and average powers.

2.2.2 Signal Quality Parameters

The spectrum regrowth or out-of-band distortion represents undesired expansion of the output spectrum of a signal into adjacent channel due to nonlinear distortion. Linear components do not result in spectrum regrowth. Basically, the nonlinear components in wireless transmitters create counterfeit energy near the fundamental and harmonics of the carrier frequency that spreads into adjacent channels. The spectrum regrowth is measured in decibels relative to the carrier (dBc). Typically, it is measured at the offset frequency from the carrier equal to the modulated signal's bandwidth, or sometimes 1.5 times the signal bandwidth. The spectrum regrowth improvements on the output of PA at lower and upper adjacent bands are graphically demonstrated in Figure 2.10.

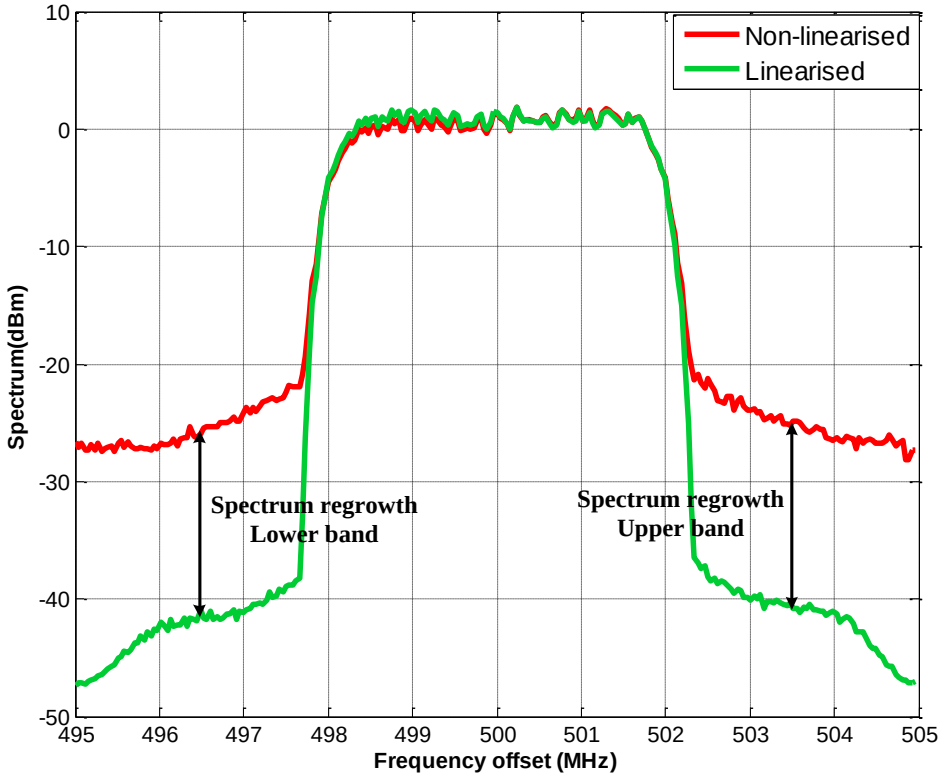

Figure 2.10: Improvements in spectrum regrowth in lower and upper adjacent channels.

Error Vector Magnitude (EVM):

The in-band signal quality can be analysed based on its EVM measurement in time domain. The EVM is a common metric for the fidelity of the symbol constellation. In other words, EVM is a measure of how far the actual (measured) points are from the ideal locations.

The EVM is the ratio of the power of the error vector to the power of the reference vector related to the ideal constellation and it can be defined in dB [2-1]:

$$EVM(dB) = 10\log_{10}\left(\frac{P_{error}}{P_{ideal}}\right) = 10\log_{10}\left(mean\left(\frac{(I_{actual}-I_{ideal})^2+(Q_{actual}-Q_{ideal})^2}{I_{ideal}^2+Q_{ideal}^2}\right)\right) \quad (2.13)$$

or in percentage (%) [2-1]:

$$EVM(\%) = \sqrt{\frac{P_{error}}{P_{ideal}}} * 100\% \quad (2.14)$$

where P_{error} and P_{ideal} are the power of the error vector and highest power point in the reference signal constellation, I_{ideal} and Q_{ideal} are the ideal I and Q signals, and I_{actual} and Q_{actual} are the transmitted I and Q signals. Also, the EVM is a measure of the quality of the allocated part of the signal.

2.2.3 Evaluating Performance of Wireless Transmitters

This chapter describes the metrics used for evaluation of amount of distortion created by the imperfect hardware, (mainly I/Q modulator and PA). In other words, these metrics are developed to show how well wireless transmitter operates. A mean squared error (MSE), a normalised mean squared error (NMSE) and an adjacent channel power ratio (ACPR) are typically used for the quantitative measure of an accuracy of the behavioural modelling, [2-4]. MSE and NMSE are used as accuracy metrics in time domain, whereas ACPR is used in frequency domain.

Mean Squared Error

The simplest metric used to show how well the wireless transmitter performs is MSE. It is defined as**:**

$$MSE_{dB} = 10\log_{10}\left(\frac{1}{K}\sum_{n=1}^{K}|y_{meas}(n) - y_{est}(n)|^2\right) \quad (2.15)$$

where y_{meas} and y_{est} are the measured and estimated output waveforms, respectively, and K is the number of samples of the output waveform.

Normalised Mean Squared Error

Metric MSE is not suitable for comparing systems with different power levels. Therefore, normalised MSE (NMSE) is commonly used for these cases. Hence, the second time-domain metric is NMSE and is defined as:

$$NMSE_{dB} = 10\log_{10}\left(\frac{\sum_{n=1}^{K}|y_{meas}(n)-y_{est}(n)|^2}{\sum_{n=1}^{K}|y_{meas}(n)|^2}\right) \quad (2.16)$$

where, similarly as in MSE, $y_{meas}$and y_{est} are the measured and estimated output waveforms, and K is the number of samples of the output waveform.

Adjacent channel power ratio (ACPR)

NMSE is considered as in-band measure for the wireless transmitter. There is a need for metric that will be used for measuring out-of-band power. Thus, the ACPR is used to measure the amount of power leaked into adjacent channel. It is a measure of spectral regrowth and appears in the signal sidebands. ACPR is defined as the ratio of power in a bandwidth adjacent to the main channel to the power within the main signal bandwidth. The ACPR for the right side of the power spectral density (PSD) is defined as:

$$ACPR(right) = \frac{\int_{f_c+\Delta f-\frac{B}{2}}^{f_c+\Delta f+\frac{B}{2}} PSD(f)df}{\int_{f_c-\frac{B}{2}}^{f_c+\frac{B}{2}} PSD(f)df} \quad (2.17)$$

Similarly, the ACPR for the left side of the PSD can be is defined as:

$$ACPR(left) = \frac{\int_{f_c-\Delta f-\frac{B}{2}}^{f_c-\Delta f+\frac{B}{2}} PSD(f)df}{\int_{f_c-\frac{B}{2}}^{f_c+\frac{B}{2}} PSD(f)df} \quad (2.18)$$

where f_c is the carrier frequency, B is the bandwidth of the modulated signal, and $PSD(f)$ is the power spectral density at frequency f.

2.3 OFDM Modulation-Basic Principle

Orthogonal frequency-division multiplexing (OFDM) has been chosen as the downlink modulation scheme for the third generation partnership project (3GPP) Long-Term Evolution (LTE) as 4G and is also used for several other radio technologies, e.g. worldwide interoperability for microwave access and the digital video broadcasting broadcast technologies. OFDM presents digital multicarrier scheme that uses a large number of closely spaced subcarriers to carry data and control information. To be more precise it uses a fast Fourier transform (FFT) at the receiver and an inverse FFT operation (IFFT) at the transmitter side, to move between time and frequency domain representation. The key advantage of OFDM is its ability to perform well through low quality channel. It also contains a cyclic prefix (CP) for protecting transmitting information.

Moving from time to frequency domain is depicted in Figure 2.11 below using FFT [2-1]–[2-5].

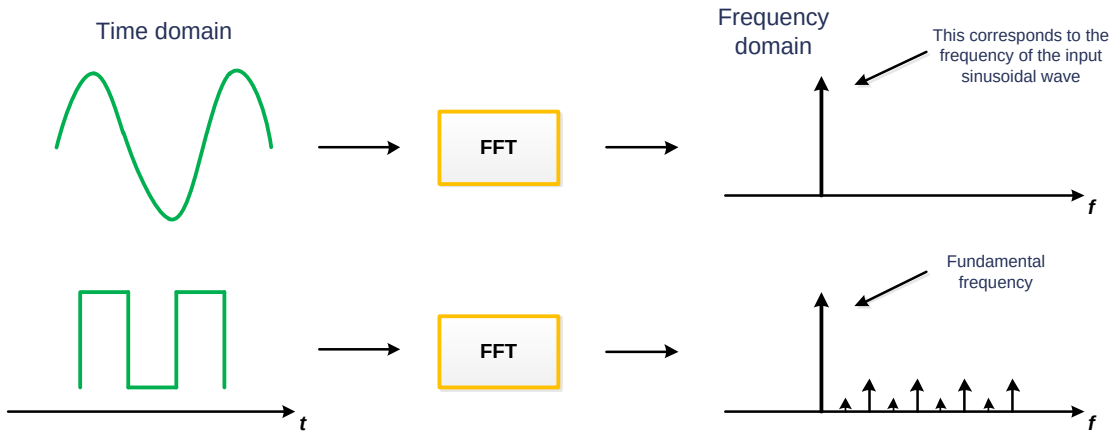

Figure 2.11: Moving from time to frequency domain using FFT.

The basic principle of OFDM system is to use narrow, mutually orthogonal subcarriers. Each subcarrier can be modulated using quadrature amplitude modulation (QAM) scheme or phase shift keying (PSK). Spacing between subcarriers is 15 kHz regardless of the total transmission bandwidth. Thus, symbol rate is 66.7 µs in LTE systems. In this way, peaks and nulls of subcarriers line up perfectly at any frequency of subcarrier. Each subcarrier is defined in frequency domain by a vector, which represents the amplitude and phase of the data symbol that has been mapped to it. After modulation process, signal is fed to serial-to-parallel conversion and further to the IFFT block. Then, each subcarrier is converted to time domain waveforms using an IFFT. Each

input for the IFFT block corresponds to the input representing a particular subcarrier (or particular frequency component of the time domain signal) and can be modulated independently of the other subcarriers. At this point the CP is inserted for each waveform and then waveforms are vector-summed to produce the composite waveform for transmission, as shown in Figure 2.12.

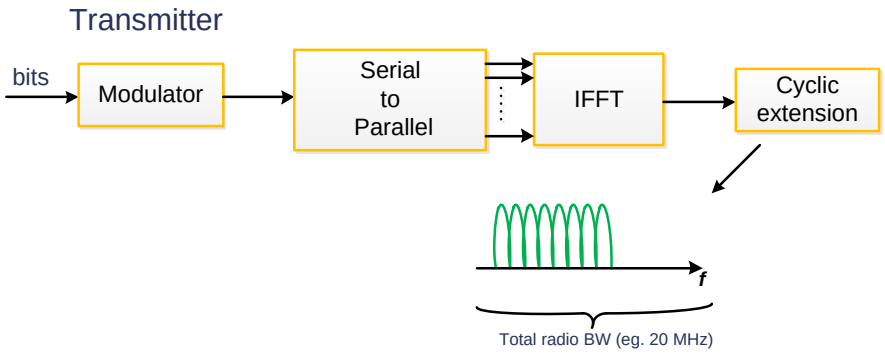

Figure 2.12: Simplified block diagram of OFDM wireless transmitter.

Moreover, as subcarriers are orthogonal there is no interference between them. However, inter-symbol interference (ISI) is caused by dispersive effects of the transmission channel. Therefore, cyclic extension is added to compensate for ISI. CP as one of the possible cyclic extension implies adding redundancy by repetition of the signal. Basically, this process is based on copying the end of the OFDM symbol and placing that copy at the beginning of the symbol, for every symbol. The length of the CP depends on the impulse response of the wireless channel. In the cellular systems the choice of CP depends on the propagation conditions and cell size. For LTE the standard CP is set to 4.69 μs.

Therefore, the centre frequencies of the overlapping channels are:

$$f_n = f_c + nB_N n = 0, \ldots . N - 1 \tag{2.19}$$

where f_c is carrier frequency. The data rate for each substream is N times lower than data rate of initial stream. The modulated signal related to all subcarriers is presented as:

$$s(t) = \sum_{i=0}^{N-1} s_i g(t) \cos(2\pi f_i t + \varphi_i) \tag{2.20}$$

where $g(t)$ is the pulse-shaping filter, s_i is the complex symbol associated with ith subcarrier, and φ_i is the phase of the ith carrier. The subcarriers $\cos(2\pi(f_c + i/T_N)t + \varphi_i)$ provide a set of orthogonal basis function over the interval $[0, T_N]$.

2.4 LTE Technology

The LTE radio transmission and reception specifications for the UE and the eNodeB RBS are documented in [2-6].

Operating bands:

LTE must support the international wireless market and regional spectrum regulations and spectrum availability. The specifications include variable signal bandwidths selectable from 1.4 to 20 MHz, with subcarrier spacing of 15 kHz. Subcarrier spacing is constant regardless of the signal bandwidth. 3GPP has defined the LTE radio interface to be adaptable to different signal bandwidths with minimum impact on system operation [2-7]. Also, LTE support both paired and unpaired bands, which requires flexibility in the duplex arrangement. Therefore, LTE supports both frequency division duplex (FDD) and time division duplex (TDD) modes.

Release 8 of the 3GPP specifications for LTE includes fifteen frequency bands for FDD and eight for TDD. The paired bands for FDD operation are numbered from 1 to 14 and 17 as shown in Table 2.1 [2-8]. The unpaired bands for TDD operation are numbered from 33 to 40 as shown in Table 2.1. It should be noted that by definition of frequency bands does not ensue its availability.

Table 2.1 shows the currently defined LTE frequency bands, together with the corresponding duplex mode (FDD or TDD). The band numbers 15 and 16 are skipped since those numbers were used in European telecommunications standard institute (ETSI) specifications [2-8].

E-UTRA operating band	**Uplink (UL) operating band** **RBS receive** **UE transmit** $F_{UL\_low} - F_{UL\_high}$	**Downlink (DL) operating band** **RBS transmit** **UE receive** $F_{DL\_low} - F_{DL\_high}$	**Duplex mode**
1	1920MHz - 1980MHz	2110MHz - 2170MHz	FDD
2	1850MHz - 1910MHz	1930MHz - 1990MHz	FDD
3	1710MHz - 1785MHz	1805MHz - 1880MHz	FDD
4	1710MHz - 1755MHz	2110MHz - 2155MHz	FDD

5	824MHz - 849MHz	869MHz - 894MHz	FDD
6	830MHz - 840MHz	875MHz - 885MHz	FDD
7	2500MHz - 2570MHz	2620MHz - 2690MHz	FDD
8	880MHz - 915MHz	925MHz - 960MHz	FDD
9	1749.9 MHz - 1784.9MHz	1844.9 MHz - 1879.9MHz	FDD
10	1710MHz - 1770MHz	2110MHz - 2170MHz	FDD
11	1427.9MHz - 1447.9MHz	1475.9MHz - 1495.9MHz	FDD
12	698MHz - 716MHz	729MHz - 746MHz	FDD
13	777MHz - 787MHz	746MHz - 756MHz	FDD
14	788MHz - 798MHz	758MHz - 768MHz	FDD
⋮			
17	704MHz - 716MHz	734MHz - 746MHz	FDD
⋮			
33	1900MHz - 1920MHz	1900MHz - 1920MHz	TDD
34	2010MHz - 2025MHz	2010MHz - 2025MHz	TDD
35	1850MHz - 1910MHz	1850MHz - 1910MHz	TDD
36	1930MHz - 1990MHz	1930MHz - 1990MHz	TDD
37	1910MHz - 1930MHz	1910MHz - 1930MHz	TDD
38	2570MHz - 2620MHz	2570MHz - 2620MHz	TDD
39	1880MHz - 1920MHz	1880MHz - 1920MHz	TDD
40	2300MHz - 2400MHz	2300MHz - 2400MHz	TDD

Table 2.1: E-UTRA operating bands.

Channel bandwidths:

One of the properties of the OFDM modulation scheme upon which universal mobile telecommunication system has been based on, it is the ability to scale its channel bandwidth linearly without changing the underlying properties of the physical layer; these being the subscriber spacing and symbol length. LTE was designed to support six different channel bandwidths: 1.4 MHz, 3 MHz, 5 MHz, 10 MHz, 15 MHz and 20 MHz with 15 kHz subcarrier spacing, which depicts a more deployment flexibility of the system [2-7].

The smallest amount of resource that can be allocated in the uplink or downlink is called a resource block (RB). The transmission bandwidth configuration is defined in RBs and represents the maximum number of RBs that can be transmitted for any channel bandwidth, as given in Table 2.2, [2-7]. An RB is 180 kHz wide and lasts for one 0.5 ms timeslot. Therefore, for LTE, a RB includes 12 subcarriers (since frequency spacing is 15 kHz). The maximum number of RBs supported by each transmission bandwidth and the minimum total power dynamic range of different LTE signals are given in Table 2-2. The PAPR of the signal is one half of its dynamic range and directly depends on the signal bandwidth and the number of allocated resource blocks [2-8].

Channel bandwidth $BW_{Channel}$ [MHz]	1.4	3	5	10	15	20
Transmission bandwidth configuration(RB)	6	15	25	50	75	100

Table 2.2: Transmission bandwidth configuration.

2.5 Multi-branch and Multi-frequency MIMO Wireless Transmitters

The MIMO as an emerging technique will provide higher data rate, better reliability and improve capacity in wireless system. The input data is transmitted using M_T antennas and after passing through the wireless channel it is received by M_R receiving antennas. This way, the capacity of wireless system using MIMO technique is increased by the number of antennas that are used on the transmitter and receiver sides without increasing the average transmit power or frequency bandwidth [2-1].

Additionally, MIMO is often referred as a system where multiple modulated signals are simultaneously transmitted through a single or multiple branches of RF front end. These

modulated signals can be separated in frequency or space domain. On the one hand, MIMO systems with modulated signals separated in space domain correspond to wireless topologies with multiple branches of RF front-ends. In these multi-branch MIMO systems all branches are simultaneously involved in signal transmission. On the other hand, MIMO systems with modulated signals separated in frequency domain refer to systems where multiple signals modulated in different carrier frequencies are concurrently transmitted through a single branch RF front-end, named multi-frequency MIMO systems. One of the most common examples of these systems are concurrent dual-band and multi-carrier transmitters [2-9].

2.6 Distortion in Multi-branch MIMO Wireless Transmitters

As expected, implementing multi-branch MIMO wireless transceivers induce several challenges. These challenges can be categorised into two groups. The first one consists of issues related to general transceiver design, such as transmitter linearity, receiver dynamic range, and imbalance and leakages in mixers, and there are not specific to MIMO systems [2-10]. These problems are similar to the challenges that single input single output (SISO) systems introduce.

A simplified block diagram of a dual-branch MIMO wireless transmitter as an example of a multi-branch MIMO system is shown in Figure 2.13, where two transmitter chains exist. As mentioned before, in the direct conversion transmitter, I/Q modulator and PA are the most challenging blocks. In this up-converting process impairments such as amplitude and phase imbalance, DC offset and nonlinear distortion are unavoidable. As a highly nonlinear component, PA will introduce in-band and out-of-band distortion to the signal. These will degrade bit error rate at the receiver side and increase inter-channel interference (ICI).

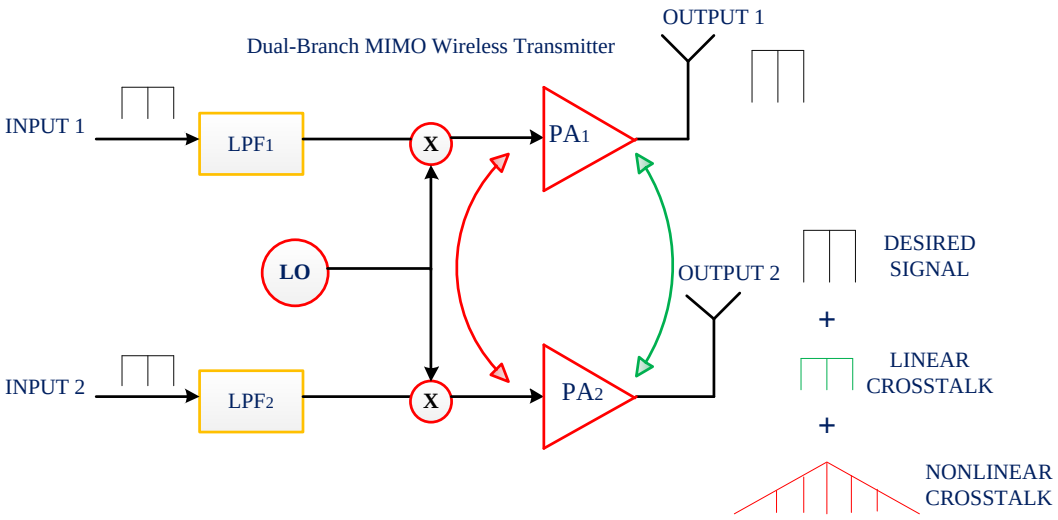

Figure 2.13: Simplified block diagram of dual-branch MIMO wireless transmitter.

The second group is specific to MIMO transceivers, where multiple transmission/reception paths are implemented on the same chipset. Hence, there are inevitable interactions and correlations between different signals in a MIMO system, called crosstalk effect [2-11]–[2-12]. Speaking generally, crosstalk effect can be categorised into two groups: linear and nonlinear. The basic difference is the place of origin. If crosstalk affects signal before it passes through nonlinear component, then it is nonlinear crosstalk, otherwise is linear. Linear crosstalk can be modelled as a linear function of the interference and desired signal. On the other hand, the nonlinear crosstalk produces undesired signal at the output of the dual-branch MIMO wireless transmitter. The sources of nonlinear crosstalk may be interference in the chipsets between the different paths of the MIMO transceiver and leakage of RF signals through the common local oscillator path.

It can be concluded that these crosstalk effect considerably degrade the performance of the MIMO system. Linear crosstalk can be easily eliminated at the receiver side using matrix inversion algorithm, [2-13]–[2-14]. Contrary, nonlinear crosstalk cannot be eliminated or reduced with conventional signal processing algorithms applied to SISO systems. Therefore, it must be taken into account during linearisation process.

In order to quantify contributions of undesired effects in multi-branch MIMO wireless transmitters, the four-branch MIMO baseband equivalent wireless transmitter model is introduced. It is applied for analysing 64-QAM OFDM signal in multi-branch MIMO wireless transmitter [2-15].

Simulation parameters

The system level simulation was performed in Matlab. Signal was generated and passed through dual-branch MIMO and four-branch MIMO wireless transmitters. OFDM signals with 300 data subcarriers and 512 FFT size, were created. All data subcarriers of OFDM signals were modulated with the 64-QAM. In these simulations, different bit streams were sent in every of two/four signal paths. Therefore, spatially multiplexed dual-branch MIMO and four-branch MIMO wireless transmitters had been analysed. Taylor series PA model for real Mini-Circuits ZHL-1042J power amplifier was extracted experimentally using test bed [2-16] and this model was used in simulations.

Simulation results

In the present simulations, 5% amplitude imbalance and 5° phase imbalance, and amount of -15 dB nonlinear crosstalk (three branches in four-branch MIMO wireless transmitter have the same crosstalk impact on the simulated branch) are introduced in dual-branch MIMO and four-branch MIMO wireless transmitters. Plots in Figures 2.14, 2.15, 2.16, 2.17 and 2.18 illustrate the constellation diagrams of 64-QAM OFDM signal of dual-branch MIMO and four-branch MIMO wireless transmitter for different cases: input signal in ideal case without impairments, signal at the PA output without additional impairments, signal at the PA output with I/Q imbalance, dual-branch MIMO signal at the PA output with I/Q imbalance and nonlinear crosstalk, four-branch MIMO signal at the PA output with I/Q imbalance and nonlinear crosstalk. Moreover, in order to mathematically quantify level of nonlinear distortion that appears in dual-branch and four-branch MIMO wireless transmitters, EVM is calculated and presented for four different cases in Table 2.3.

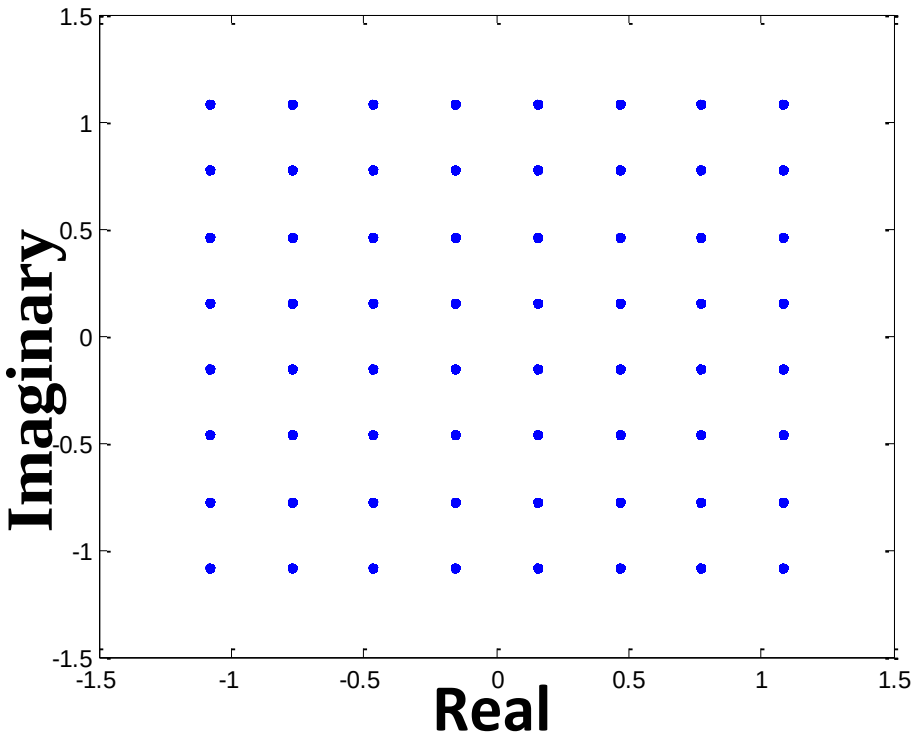

Figure 2.14: The constellation diagram of signal in ideal case.

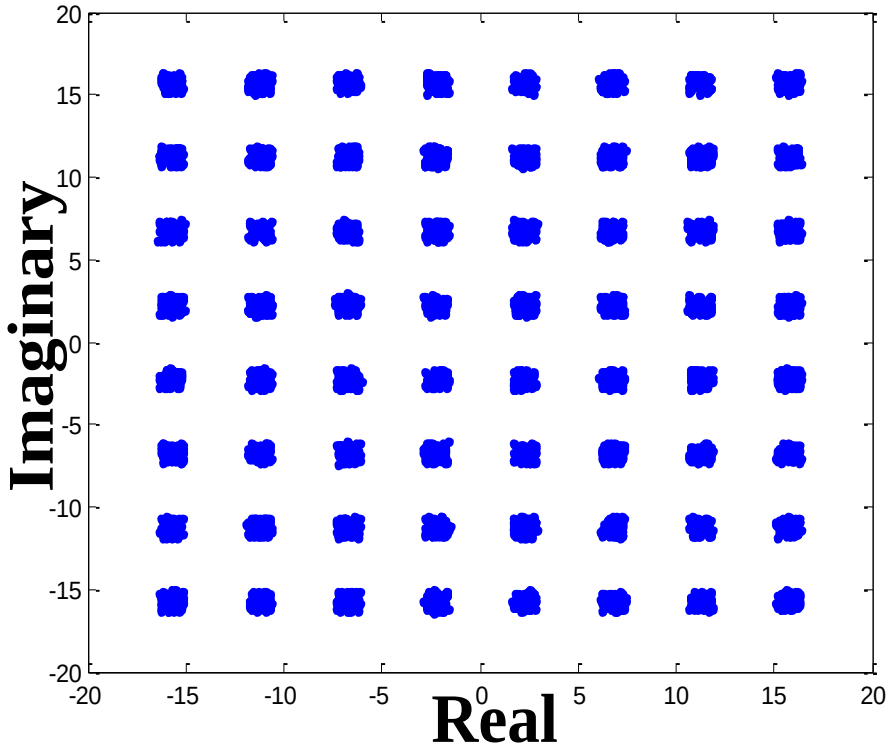

Figure 2.15: The constellation diagram of signal at the PA output.

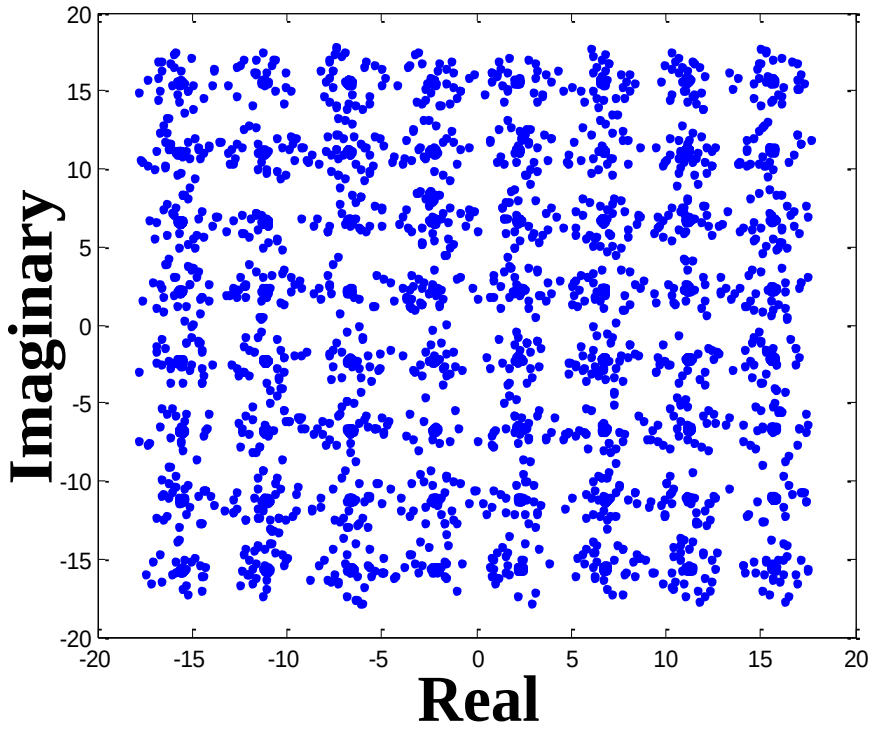

Figure 2.16: The constellation diagram of signal at the PA output with I/Q imbalance.

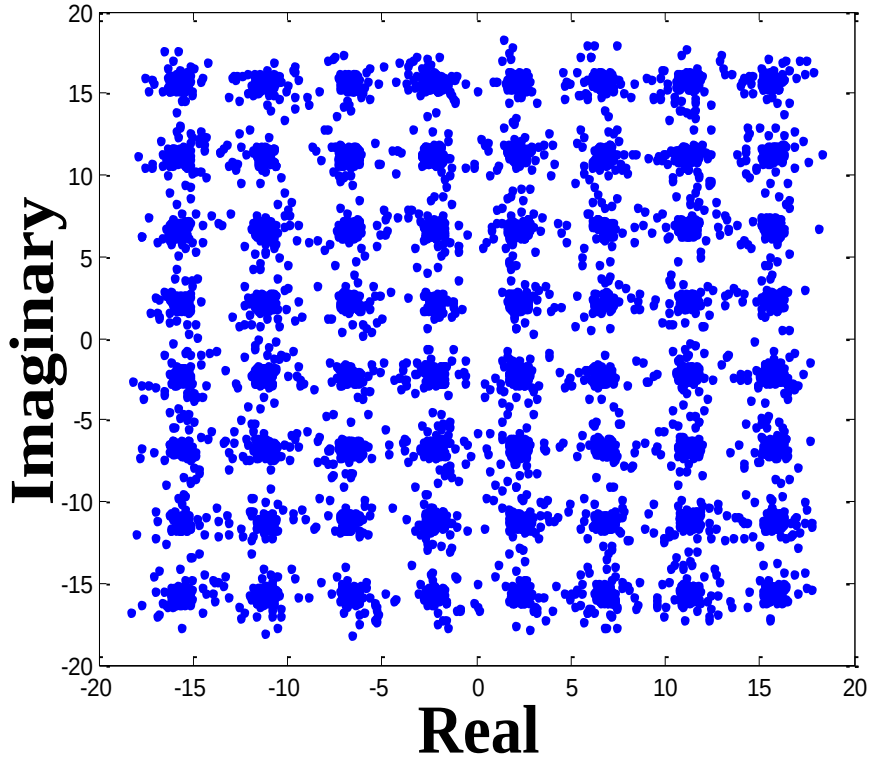

Figure 2.17: The constellation diagram of dual-branch MIMO signal at the PA output with I/Q imbalance and nonlinear crosstalk.

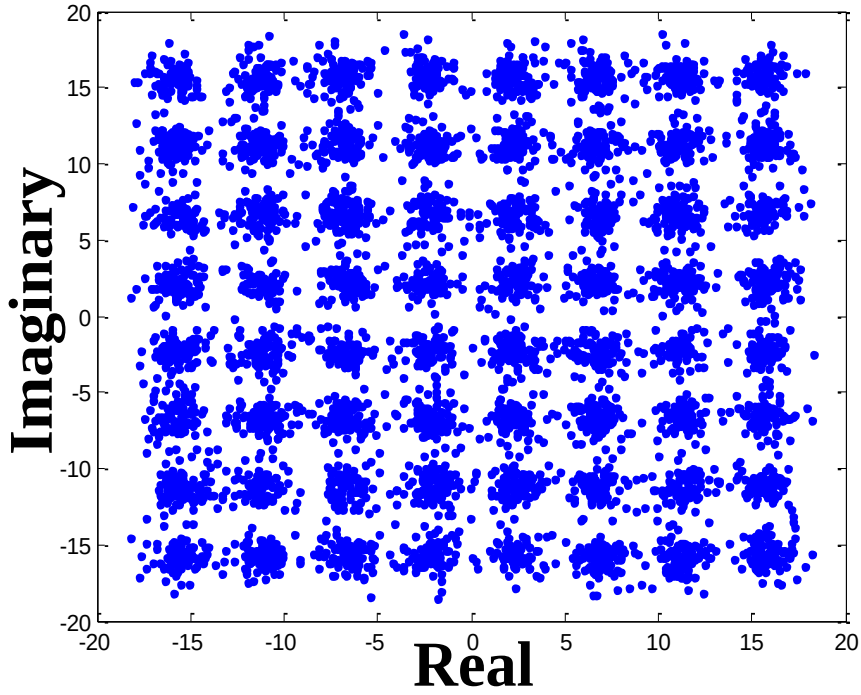

Figure 2.18: The constellation diagram of four-branch MIMO signal at the PA output with I/Q imbalance and nonlinear crosstalk.

Undesired effects	EVM [%] for MIMO	
	dual-branch	four-branch
PA nonlinearity	14.8560	14.8561
I/Q imbalance and PA nonlinearity	15.7654	16.3359
I/Q imbalance and -15 dB nonlinear crosstalk and PA nonlinearity	18.9952	20.2689

Table 2.3: EVM for LTE signal using dual-branch and four-branch MIMO wireless transmitter.

Plot in Figure 2.15 shows the effects of PA nonlinearities, where EVM is 14.8%. Also, I/Q imbalance has great impact on signal constellation (Figure 2.16); consequently it is difficult to distinguish each constellation (EVM is about 15.7% and 16.3% for dual- and four-branch cases respectively). When I/Q imbalance is simulated together with nonlinear crosstalk effect of dual-branch and four-branch MIMO wireless transmitters, it is almost impossible to demodulate the transmitted signal, (Fig. 2.17 and 2.18) and EVM is further degraded.

The measurement setup is consisted of two signal generators, MXG N5182A and ESG E4433B, used to emulate dual-branch MIMO wireless transmitter. General-purpose interface bus (GPIB) was used to connect these generators with personal computer (PC). The signals were created in Matlab and downloaded to MXG using Agilent Signal Studio Toolkit and to ESG using Advanced Design System (ADS) assistance. The coupler was utilised in order to model the crosstalk effect that appears in the paths of MIMO wireless transmitters. The coupled signal was passed through real PA model Mini-Circuits ZFL-500 (P1dB compression point +9 dBm), which represented Device Under Test (DUT). During the measurements, the PA was biased to work in hard compression region. The output signals from the PA were down-converted with Vector Signal Analyzer (VSA) 4406A and captured by VSA Distortion Suite (DS) 89604A software running on PC. Connection between the PC and VSA E4406A was established via GPIB interface. Finally, the captured signals were passed by VSA 89601A-ADS link into ADS for signal analysis.

Experimental results:

First experimental measurement was performed with two identical two-tone signals with 5 MHz frequency offset. These signals were generated on MXG and ESG generators (ESG was used for crosstalk emulation) for fundamental, second and third harmonic frequency analysis. Experiment was accomplished for four different cases of PA output signals: without impairments, when affected with nonlinear crosstalk, with I/Q imbalance and with both, I/Q imbalance and nonlinear crosstalk. In all four cases the two-tone signals with the same input power were used. Experimental results are shown in Figure 2.19. As noticed, the same power is differently divided between components. This is the reason why initial tones get smaller power compared to harmonics and IMD. IMD ratio decreases correspondently with the presence of additional impairments. The analyses of impairments for conventional SISO wireless transmitters which use IMD and harmonics injection DPD techniques have been carried out in previous papers, (for instance [2-16]). The problem is that existing analyses cannot be used in MIMO wireless transmitters because of the variation of unwanted products (IMD and harmonics). Those variations are caused by additional impairments, such as I/Q imbalance and crosstalk effect.

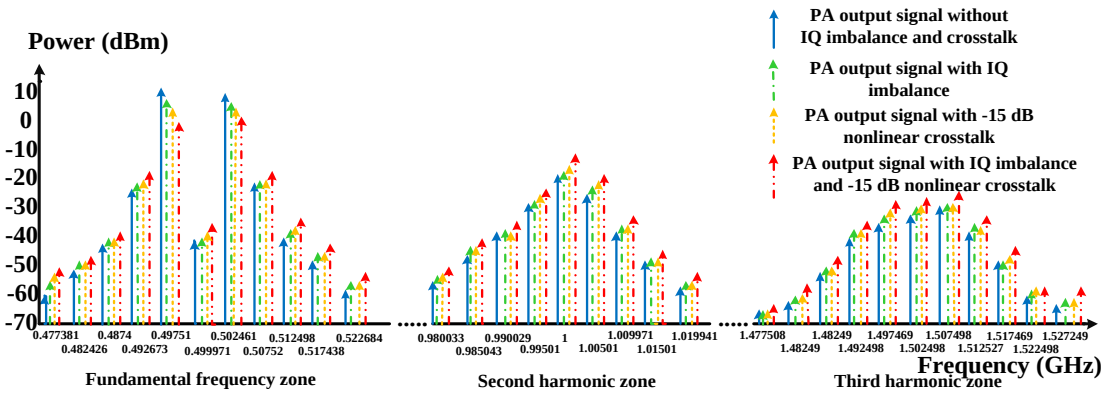

Figure 2.19: Two-tone measurement results of a dual-branch MIMO wireless transmitter.

Second experimental measurement was performed with two identical wideband code division multiple access (WCDMA) signals. These signals were sent from MXG N5182A and ESG E4433B signal generators on the same frequency and with the same power, so the effect of nonlinear crosstalk is realised. The amount of this crosstalk was -15 dB. Additional distortion to the WCDMA signals was introduced with 5% imbalance in amplitude and 5° imbalance in phase. Spectrum of WCDMA signals are shown in Figure 2.20 for five different cases: input signal without impairments, output PA signal, output PA signal with I/Q imbalance, with nonlinear crosstalk and with both effects, respectively. As depicted in Figure 2.20, I/Q imbalance combined with nonlinear crosstalk introduced about 20 dB out-of-band distortion to the spectrum. That is about 10 dB more distortion then in conventional SISO wireless transmitters without I/Q imbalance.

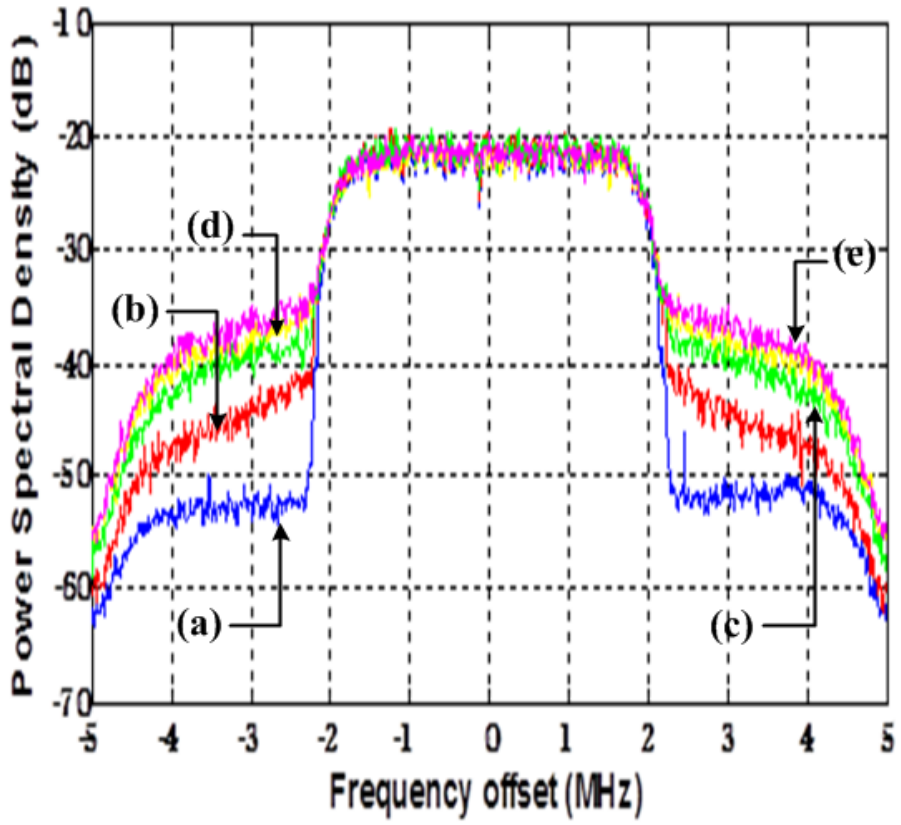

Figure 2.20: Power spectrum of the WCDMA signal (a) at the PA input; (b) at the PA output; (c) at the PA output with I/Q imbalance; (d) at the PA output with nonlinear crosstalk; (e) at the PA output with I/Q imbalance and nonlinear crosstalk.

2.7 Distortion in Multi-frequency MIMO Wireless Transmitters

Figure 2.21 depicts simplified block diagram of concurrent dual-band wireless transmitter where two modulated signals at different operating frequencies are transmitted simultaneously. This implies use of PAs that accommodate concurrent signals at different frequency bands. The nonlinear behaviour of the dual-band PA is more emphasized than in the single band. Moreover, the existence of complex I/Q modulators ensues generating and processing the I and Q channel inputs separately. Any differences between these two real components cause imperfections, which must be taken into account during compensation process. IM products in concurrent dual-band transmitters are also unavoidable. They can be categorised into three major groups.

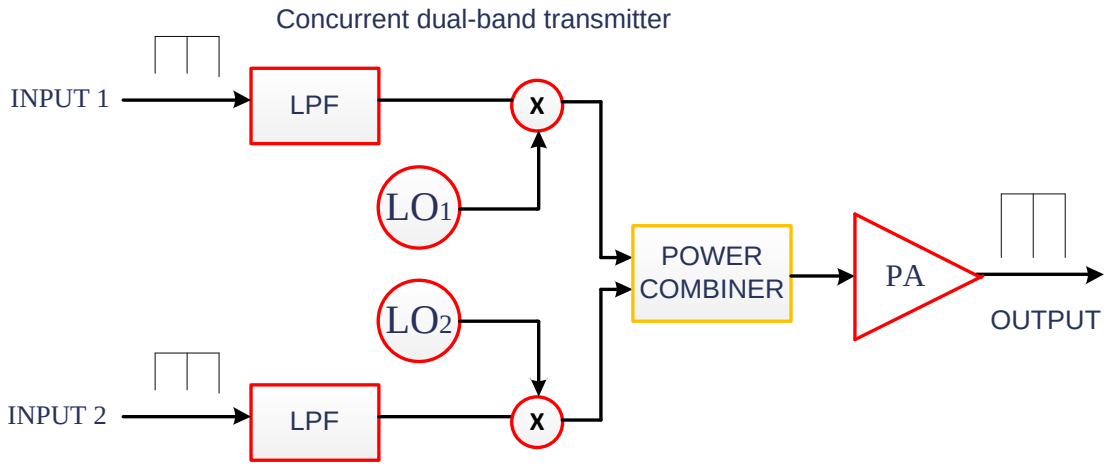

Figure 2.21: Simplified block diagram of concurrent dual-band MIMO wireless transmitter.

The first one is known as in-band IM, consisting of IM products around each carrier frequency, which are solely due to the IM between the signal elements within each band.

The second group includes CM products, which appear within the same frequency range as the in-band IM, resulting in IM products between signals in both frequency bands.

Third group, known as out-of-band IM, represents IM products between the two signals in both frequency bands. However, these products are located far away from the desired signals in the lower and upper frequency bands and they are easy to compensate using filters.

These three types of IM products, which appear in concurrent dual-band transmitters using two-ton signals, are shown in Figure 2.22.

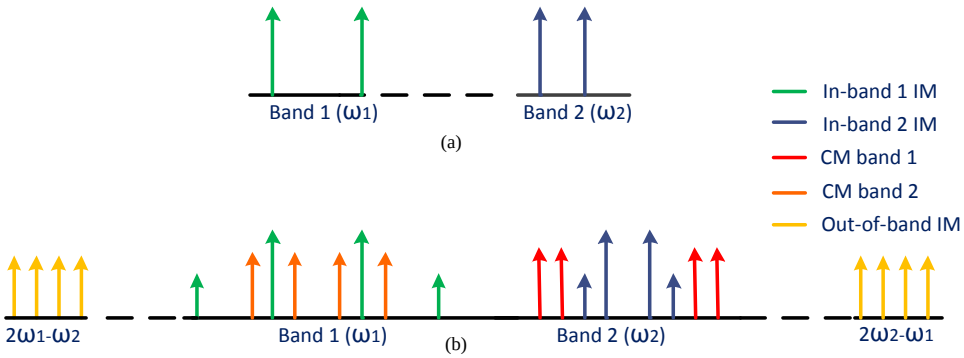

Figure 2.22: Power spectrum of the signal at (a) the input; (b) the output of concurrent dual-band wireless transmitter.

There are difficulties in the implementation of conventional DPD techniques when it comes to compensation of the in-band IM and CM distortion. The use of single digital

predistorter (PD) requires capturing the whole dual-band signal spectrum at the output of the nonlinear PA. A problem can occur with sampling rate limitation of the analogue-to-digital convertors (ADCs) and digital-to-analogue converters (DACs). Since the effect of cross-modulation products is not considered, it is not appropriate to use two independent conventional DPDs for compensation of distortion in each carrier frequency [2-17].

2.8 Summary

In this chapter an overview of linearity requirements and main signal parameters in wireless transmitters have been briefly explained. Also, distortion caused by both, I/Q modulator and PA has been described. As demands on wireless transmitter for linearity and power efficiency have increased, the industry has developed multi-branch and multi-frequency MIMO wireless transmitters. Therefore, short background on distortion created by MIMO wireless transmitters is presented with the individual impacts of PA nonlinearity, I/Q imbalance and crosstalk and CM effects for multi-branch and multi-frequency MIMO wireless transmitters. Hence, all these impairments must be considered carefully during the process of designing of MIMO wireless transmitters and appropriate distortion compensators.

2.9 References

[2-1] A. Mohammadi and F. M. Ghannouchi, *RF Transceiver Design for MIMO Wireless Communications*, New York: Springer, 2012

[2-2] A. S. Tehrani, "Behavioral modeling of wireless transmitters for distortion mitigation", PhD thesis, Chalmers University of Technology, Gothenburg, Sweden, 2012

[2-3] D. Bondar, "Advanced Digital Predistortion of Power Amplifiers for Mobile and Wireless Communications", PhD Thesis, University of Westminster, London, UK, 2009

[2-4] O. Hammi, M. Younes, and F. M. Ghannouchi, "Metrics and Methods for Benchmarking of RF Transmitter Behavioral Models With Application to the Development of a Hybrid Memory Polynomial Model," *IEEE Transactions on Broadcasting*, vol. 56, no. 3, pp. 350-357, Sept. 2010.

[2-5] E. Dahlman, S. Parkvall, J. Sköld and P. Beming ,*3G Evolution HSPA and LTE for Mobile Broadband*, Linacre House, Jordan Hill, Oxford, Second edition, 2008

[2-6] "ETSI TS 136 106 V8.3.0 (2009-10) Technical Specification". Available Online :http://www.etsi.org/deliver/etsi_ts/136100_136199/136106/08.03.00_60/ts_136106v080300p.pdf

[2-7] "3GPP Long Term Evolution. System Overview, Product Development, and Test Challenges," Agilent Technologies, Palo Alto, CA, USA, Application Note 5991-2556EN, July 2013. Available Online: http://cp.literature.agilent.com/litweb/pdf/5991-2556EN.pdf

[2-8] "3GPP Technical Specification", TS 36.104 V8.4.0. Available Online: http://www.3gpp.org/ftp/Specs/latest/Rel-8/36_series/

[2-9] S. A. Bassam, F. M. Ghannouchi and M. Helaoui, "Multi-Cell Processing Architectures for Modeling and Impairment Compensation in Multi-Input Multioutput Systems," US Patent Application 12/780/455, filed 14 May 2010

[2-10] A. Luzzatto and G. Shirazi, *Wireless Transceiver Design*, New York: John Wiley & Sons, 2007

[2-11] Y. Palaskas, A. Ravi, S. Pellerano, B. R. Carlton, M. A. Elmala, R. Bishop, G. Banerjee, R. B. Nicholls, S. K. Ling, N. Dinur, S. S. Taylor and K. Soumyanath, "A 5-GHz 108-Mb/s 2x2 MIMO transceiver RFIC with fully integrated 20.5-dBm power amplifiers in 90-nm CMOS," *IEEE J. Solid-State Circuits*, vol. 41, no. 12, pp. 2746–2756, Dec. 2006

[2-12] W.-C. Hua, P.-T. Lin, C.-P. Lin, C.-Y. Lin, H.-L. Chang, C. W. Liu, T.-Y. Yang and G.-K. Ma, "Coupling effects of dual SiGe power amplifiers for 802.11n MIMO applications," in *IEEE Radio Frequency Integrated Circuits (RFIC) Symposium*, vol., no., pp. 4, June 2006

[2-13] S.A Bassam, M. Helaoui and F.M. Ghannouchi, "Crossover Digital Predistorter for the Compensation of Crosstalk and Nonlinearity in MIMO Transmitters," *IEEE Transactions on Microwave Theory and Techniques*, vol.57, no.5, pp.1119-1128, May 2009

[2-14] M. Cabarkapa, M. Bozic, N. Neskovic, A. Neskovic and D. Budimir, "Compensation of Undesired Effects in MIMO Wireless Transceivers", *IEEE International Symposium on Antennas and Propagation and CNC/USNC/URSI National Radio Science Meeting (APS2012)*, Chicago, Illinois, USA, vol., no., pp. 1-2, July 2012

[2-15] M. Bozic, M. Cabarkapa, D. Budimir, N. Neskovic and A. Neskovic "Evaluation of Nonlinear Distortion in MIMO Transmitters", *IEEE European Microwave Conference*, vol., no., pp. 908-911, Nov 2012

[2-16] D. Bondar and D. Budimir, "A Digital Predistorter for Wireless Transmitters", *International Journal of RF and Microwave Computer*, vol. 19, no 4, pp. 453 – 459, April 2009

[2-17] S. A. Bassam, M. Helaoui, and F. M. Ghannouchi, "2-D digital predistortion (2-D-DPD) architecture for concurrent dual-band transmitters," *IEEE Trans. Microw. Theory Tech.*, vol. 59, no. 10, pp. 2547–2553, Oct. 2011.

CHAPTER 3

BEHAVIOURAL MODELLING OF WIRELESS TRANSMITTERS AND DESCRIPTION OF DIGITAL PREDISTORTION TECHNIQUES

3.1 Introduction

The nonlinear behaviour of wireless transmitters can significantly degrade the overall performance of modern wireless systems. They include complex I/Q modulators, which inherently have I/Q impairments. These impairments must be compensated in advance. Otherwise, they will limit performance of the compensation technique. The high spectral efficiency is achieved when nonlinear component operates near its maximum output level, where it exhibits strong nonlinear behaviour. Thus, the presence of nonlinear distortion caused by both I/Q modulator and PA cannot be avoided. In recent years, more and more attention is shifted towards developing compensation techniques which jointly mitigate I/Q impairments and PA nonlinearity. The DPD is one of the most popular techniques used for compensating nonlinear distortion that appears in a wireless transmitter chain. Figure 3.1 depicts a block diagram of the basic principle using DPD technique. This technique is based on adding digital PD in the baseband block, which creates inverse nonlinear function to reduce nonlinearity. In other words, the cascade of PD and nonlinear components will result in a linear system and power efficiency will increase significantly [3-1]–[3-3]. Also placing PD block after nonlinear component, should result in linear system. Unfortunately, this type of DPD implementation cannot give the same level of linearity as placing PD in the baseband block before nonlinear component. The level of nonlinear distortion at the PA output is considerably high and using DPD coefficient after nonlinear component cannot compensate for the undesirable effects. Also it is easier to manipulate with dpd

coefficients and input signal, which is not distorted than dpd coefficients and output signal. Implementation of DPD before nonlinear block gives better results.

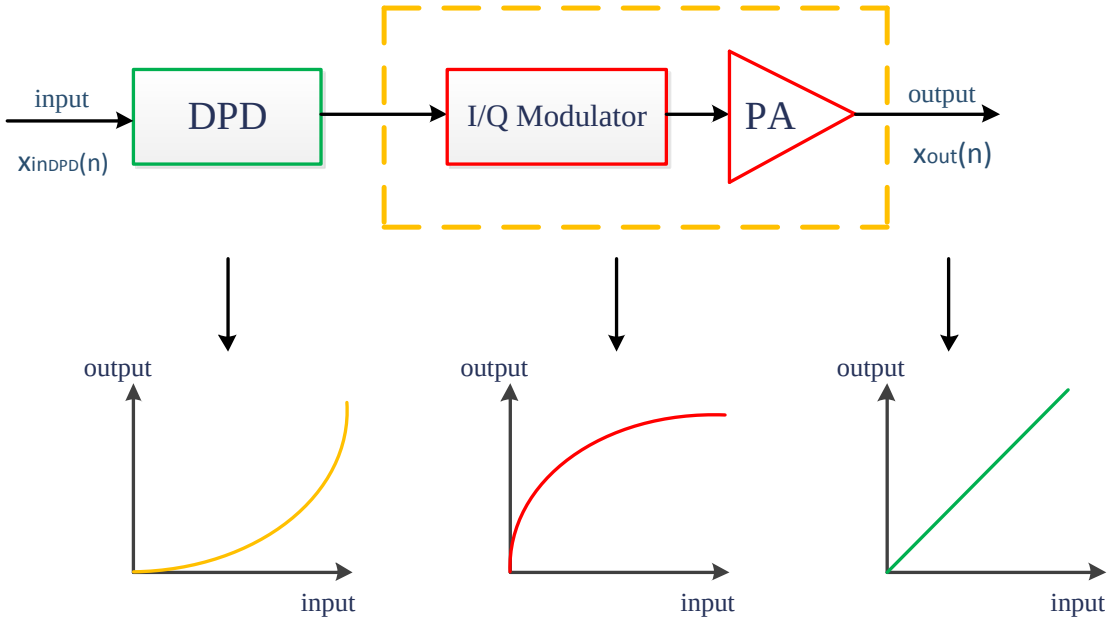

Figure 3.1: Block diagram of basic principle of DPD technique.

In this chapter, an overview of the most popular DPD techniques implemented to increase the performance of wireless transmitters is provided, together with a description of the advantages and the drawbacks of the presented models.

3.2 Behavioural Modelling Process

The DPD technique is based on creating an inverse transfer function of a nonlinear component (such as I/Q modulator and PA). Accordingly, a cascade of digital PD and nonlinear component will behave as a linear system. Fundamental part of DPD is behavioural modelling process which will determine behaviour of the nonlinear component. During that process there are no requirements about a deep knowledge of the RF circuit physics and functionality. The key idea is that a component of an RF circuit, known as a DUT, is considered as a black box. The relationship between input and output is described using mathematical formulations. Therefore, the DPD technique can be seen as a behavioural modelling problem.

The performance of behavioural modelling depends on the observation and the formulation. The observation relates to the accurate assessment of signals characteristics at the input and output of the DUT. The formulation refers to the process of choosing adequate mathematical formulation that would describe all crucial interactions between the signals at the input and output of the DUT.

As can be seen from Figure 3.1, the signal at the input of the digital PD ($x_{in_{DPD}}(n)$) can be derived from the signal at the PA output ($x_{out}(n)$) in the case of linear amplification system according to:

$$x_{in_{DPD}}(n) = \frac{x_{out}(n)}{G} \tag{3.1}$$

where $x_{out}(n)$ is the output waveform and G is the gain of the linearised PA. The behavioural modelling process is based on finding $f_{DUT}\left(x_{in}(n)\right) = x_{out}(n)$, while the DPD process is based on the estimation $f_{DPD}(x_{out}(n)/G) = x_{in}(n)$. The steps of the process are summarised in Figure 3.2. The propagation delay through the DUT will introduce a mismatch between the data samples used to calculate the instantaneous amplitude modulation to amplitude modulation (AM/AM) and amplitude modulation to phase modulation (AM/PM) characteristics of the DUT. This mismatch will translate into dispersion in the AM/AM and AM/PM characteristics that can be wrongly considered as memory effects. Therefore, the captured PA output signal must be time-aligned with the captured input signal. The time-aligned input and output waveforms are then used to identify the behavioural model/digital PD of the DUT as well as its performance [3-2].

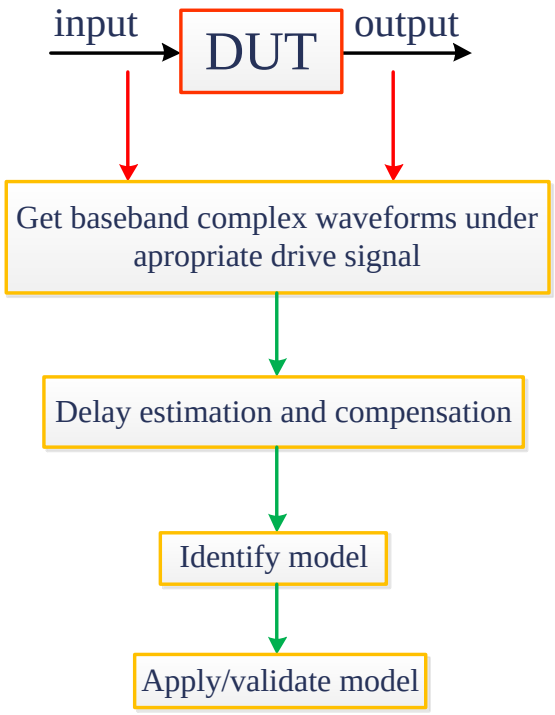

Figure 3.2: Behavioural model extraction procedure.

In order to define the behavioural model and the DPD of wireless transmitters, prolific mathematical models have been proposed. In this chapter, some commonly used formulations, such as memoryless look-up table, nested look-up table, Volterra, memory polynomial, generalised memory polynomial, Wiener, and Hammerstein, will be presented.

3.3 Commonly Used Models for PA Modelling

Look-up table model

Look-up table (LUT) model introduced in [3-4] presents the basic behavioural model for memoryless AM/AM and AM/PM nonlinearities. The AM/AM and AM/PM characteristics are used to create LUTs. In those tables the complex gain is stored. Therefore, the output signal of DUT, that is modelled using LUT, is defined as:

$$x_{out}(n) = G(|x_{in}(n)|)x_{in}(n) \tag{3.2}$$

where $G(|x_{in}(n)|)$ is the instantaneous complex gain of the DUT. The AM/AM and AM/PM characteristic of the DUT can be obtained from the measured data using the averaging or polynomial fitting techniques. The main advantage of this technique is that it enables a faster response to changes in the PA characteristics. Therefore, the LUT is still used as a model for static nonlinearity in two- and three-box-based behavioural models and digital PD [3-2] - [3-4].

Nested look-up table:

Conventional LUT model only takes into account the static nonlinearity while excludes the memory effects. Thus, a nested LUT is proposed to augment the existing model. For ths purpose, the instantaneous gain of the DUT is a function of the actual input sample and the $M-1$ preceding samples (where M is memory depth for the DUT). Accordingly, the output signal can be modelled using a nested LUT as:

$$x_{out}(n) == G(|X_{in}(n)|)x_{in}(n) \tag{3.3}$$

where input vector $X_{in}(n) = [x_{in}(n), x_{in}(n-1), \dots x_{in}(n-M)]$ (M is the memory), $G(|X_{in}(n)|)$ is the instantaneous complex gain of the DUT. This model does not require any curve fitting of the measured data. Also, the complex gain values are derived from the measurement after an accurate time delay alignment [3-2].

Volterra model:

Volterra model is the most comprehensive and the most general model for dynamic nonlinear systems. It consists of a sum of multidimensional convolutions. The output signal modelled using the Volterra model is defined as:

$$x_{out}(n) = \sum_{k=1}^{K} \sum_{i_1=0}^{M} \dots \sum_{i_p=0}^{M} h_p(i_1, \dots i_p) \prod_{j=1}^{k} x_{in}(n - i_j) \qquad (3.4)$$

where $h_p(i_1, \dots i_p)$ are the parameters of the Volterra model, K is the nonlinearity order and M is the memory depth of the model. On the one hand, this model has a high accuracy in modelling highly nonlinear systems. On the other hand, the number of parameters increases exponentially with the increase of nonlinearity order and memory depth. This makes Volterra model useful only in weakly nonlinear systems with low memory. Therefore, several models are proposed to simplify the Volterra model. These include the pruning techniques and the dynamic reduction deviation technique, [3-5] - [3-6].

To overcome the limitation of the classical Volterra series, a new approach, called a modified Volterra series or dynamic Volterra series is developed. Using this model the input/output relationship for nonlinear system with memory is described as a memoryless nonlinear term plus a purely dynamic contribution. This was based on introducing the dynamic deviation function:

$$e(n, i) = x(n - i) - x(n) \qquad (3.5)$$

which represents the deviation of the delayed input signal $x(n - i)$ with respect to the current input signal $x(n)$. The modification of (3.4) using dynamic deviation function will lead to:

$$y(n) = \sum_{k=1}^{K} \sum_{i_1=0}^{M} \dots \sum_{i_p=0}^{M} h_p(i_1, i_2, \dots, i_p) \prod_{j=1}^{k} [x(n) + e(n, i_j)] \qquad (3.6)$$

Now the following representation of the Volterra series is derived as in [3-5]:

$$y(n) = \sum_{p=1}^{P} h_{p,0}(0, \dots .0) x^p(n) +$$
$$\sum_{p=1}^{P} \left\{ \sum_{r=1}^{p} \left[x^{p-r}(n) \sum_{i_1=1}^{M} \dots \sum_{i_{r=}\, i_{r-1}}^{M} h_{p,r}(0 \dots 0, i_1 \dots i_r) \prod_{j=1}^{r} x(n - i_j) \right] \right\} \qquad (3.7)$$

where $h_{p,r}(0 \dots 0, i_1 \dots i_r)$ represents the pth order Volterra kernel where the first $p-r$ indices are "0", corresponding to the input item $x^{p-r}(n)x(n-i_1), \dots x(n-i_r)$. In this representation, r is the possible number of product terms of the delayed inputs in the input items. Compared to the Volterra model, extraction is much simpler.

Memory polynomial model:

Memory polynomial (MP) model is widely used for behavioural modelling and digital predistortion of PAs exhibiting memory effects. MP model is a simplified structure of the Volterra model and it is also known as parallel Hammerstein (PH) in literature. It represents a parallelisation of a nonlinear function followed by a linear memory. In comparison with the Volterra model, only diagonal terms are kept. The output waveform of the model is:

$$y(n) = \sum_{m=0}^{M-1} \sum_{k=1}^{K} a_{k,m} |x(n-m)|^k x(n-m) \tag{3.8}$$

where K is the polynomial order, M is the memory depth and $a_{k,m}$ are the model coefficients [3-2], [3-7].

Also, several variations of the memory polynomial model have been proposed in literature, which include the envelope memory polynomial [3-2], the generalised memory polynomial model [3-8] and the orthogonal memory polynomial model [3-9].

Generalised memory polynomial model:

Generalised memory polynomial (GMP) behavioural model extends the MP model by including more cross-terms. The kth MP component in (3.8) can be written in general form as:

$$y(n) = \sum_{m=0}^{M-1} \sum_{k=1}^{K} b_{km} x(n)\, x(n-m)^k \tag{3.9}$$

where a delay of m samples between the signal and its exponentiated envelope is inserted. Taking multiple such delayed version of (3.9) using both positive and negative cross-term time shifts and combining with (3.8) results in GMP model.

The GMP output waveform is written:

$$y(n) = \sum_{k=0}^{K_a-1} \sum_{l=0}^{L_a-1} a_{kl} x(n-l)\, |x(n-l)|^k + \sum_{k=1}^{K_b} \sum_{l=0}^{L_b-1} \sum_{m=1}^{M_b} b_{klm} x(n-l)|x(n-l-m)|^k + \sum_{k=1}^{K_c} \sum_{l=0}^{L_c-1} \sum_{m=1}^{M_c} c_{klm} x(n-l)|x(n-l+m)|^k \tag{3.10}$$

where $K_a L_a$ are the number of coefficients for aligned signal and envelope (memory polynomial), $K_b L_b M_b$ are the number of coefficients for signal and lagging envelope, and $K_c L_c M_c$ are the number of coefficients for signal and leading envelope. Model adds an extra degree of freedom in coefficients that corresponds to the amount of memory in the lagging and leading terms. The merit of this cross-term model is that the coefficients appear in a linear form. Therefore, all of the coefficients can be estimated using any least square (LS) method. This has great impact on algorithm stability and computational complexity. Also, it includes "even order" power terms [3-2], [3-8].

Wiener model:

Wiener model is a special case of the general Volterra model, which is composed of linear filter (h) followed by a nonlinear function. It is known as a two-box model and is written in the form:

$$y(n) = \sum_{k=1}^{K} a_k [\sum_{m=0}^{M-1} h(m) x(n-m)]^k \qquad (3.11)$$

where a_k are polynomial coefficients of nonlinearity, $h(m)$ are coefficients of the linear finite impulse response (FIR), $x(n)$ is the input signal and $y(n)$ is the output signal. This model is one of the most manageable ways to combine nonlinearity and memory effects. However, Wiener model nonlinearly depends on coefficients $h(m)$, which makes their estimation more complicated than for the models with linear parameters. Thus, this model is not widely used for modelling highly nonlinear and efficient PAs, [3-2], [3-8], [3-10].

Hammerstein model:

Hammerstein model is another simplified form of the Volterra model, which consists of nonlinearity followed by a linear filter (g). The Hammerstein model is written:

$$y(n) = \sum_{m=0}^{M-1} g(m) \sum_{k=1}^{K} a_k x^k (n-m). \qquad (3.12)$$

This is a very simple memory nonlinearity, which has been studied for general applications but is of limited effectiveness for PD. It has linear parameters $g(m)a_k$ if they are considered as a two-dimensional array over m and k.

It can be noticed that the Hammerstein and Wiener models can form mutual inverses if their linear filters have stable inverses and if their nonlinear polynomials are one-to-one inverses over the range of interest [3-2], [3-8], [3-10].

Wiener-Hammerstein model:

In order to better represent linear memory, a new model is developed by combining the Wiener and Hammerstein models. In this way, a cascade of linear filter (h), memoryless nonlinearity and another linear filter (g) is formed. Wiener-Hammerstein model is written:

$$y(n) = \sum_{m_2=0}^{M-1} g(m_2) \sum_{k=1}^{K} a_k \times \left[\sum_{m_1=0}^{M-1} h(m_1) x(n - m_1 - m_2)\right]^k \qquad (3.13)$$

As can be seen, this model is more general in comparison with the Wiener and Hammerstein models. However, it is still nonlinear in the parameters $h(m_1)$, [3-8].

Figure 3.3 illustrates Wiener, Hammerstein and Wiener-Hammerstein models.

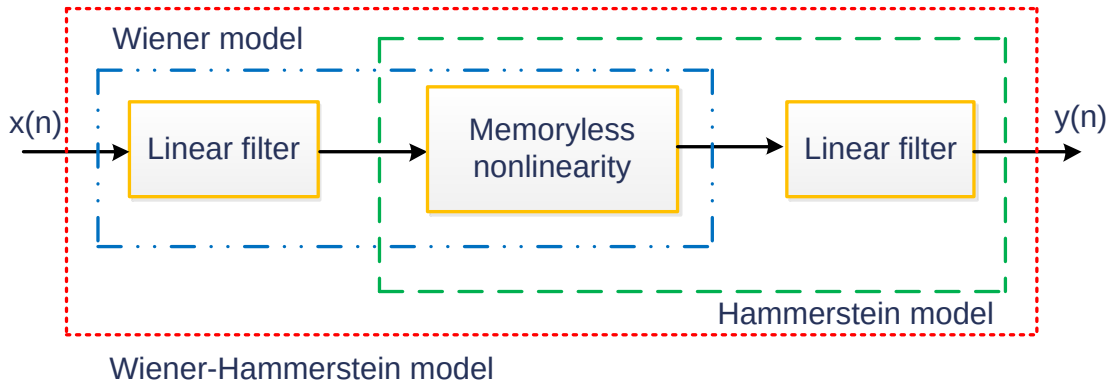

Figure 3.3: Block diagram of Wiener, Hammerstein and Wiener-Hammerstein models.

3.4 Commonly Used Models for I/Q Modulator Modelling

Direct-conversion architecture is seen as one of the most popular architectures in wireless system due to small-size and low cost. As this structure is reconfigurable, it can easily generate RF signals in different frequency bands. Also, fewer components are needed for implementation in comparison with super-heterodyne convertors. However, direct conversion transmitters inevitably suffer from imperfections that exist in I/Q modulator. These imperfections can be considered frequency-independent for narrowband signals. On the other hand, for wideband signals this cannot be the case since they exhibit frequency-dependent behaviour due to both reconstruction filters and analogue modulators. I/Q modulator suffers as well from nonlinear distortion.

Modelling and compensation of impairments which exist in I/Q modulator have been categorised in different ways. Categorisation has been based on the physical location of

the modelling and compensation (either at the transmitter and receiver side separately [3-11]–[3-14] or jointly for both transmitter and receiver impairments at the receiver side [3-15]–[3-16]); the data type needed for modelling and compensation (data-aided techniques that utilise pilot symbols [3-17]–[3-18] or blind statistical techniques that use properties like correlation between I and Q branch for modelling [3-14]), whether they are frequency independent [3-19] or dependent [3-20]–[3-24] and whether they can model and compensate for linear [3-11]–[3-12] or both linear and nonlinear impairments [3-25]–[3-28]. Furthermore, techniques in [3-29]–[3-31] are proposed for joint mitigation of I/Q impairments and PA nonlinearity at the transmitter side.

In this thesis, I/Q impairments modelling is categorised into linear and nonlinear I/Q impairments models in transmitters.

Also, this thesis is based on a technique that jointly mitigates I/Q impairments and PA nonlinearity at the wireless transmitter side.

Linear I/Q Imbalance:

As mentioned before, direct conversion wireless transmitters are sensitive to mismatch between the I and Q branches. In other words, these mismatches are unavoidable in any practical implementation and they can severely degrade the performance of DPD technique. Therefore, the effects of I/Q imbalance must be compensated (for example by using DSP).

In [3-11] it was shown that using matrix notation, I/Q imbalance can be modelled as:

$$\begin{bmatrix} w_I[n] \\ w_Q[n] \end{bmatrix} = m \begin{bmatrix} z_I[n] \\ z_Q[n] \end{bmatrix}, m = \begin{bmatrix} 1 & -g_m \sin \varphi_m \\ 0 & g_m \cos \varphi_m \end{bmatrix} \tag{3.14}$$

where $w[n] = w_I[n] + jw_Q[n]$ is the complex baseband representation of the I/Q modulator and $z_I[n]$ and $z_Q[n]$ are I and Q component of the baseband input signal respectively and g_m and φ_m are amplitude and phase imbalance respectively.

In [3-12], simple detector diode is used for estimation and compensation of I/Q imbalance and DC offset. Implementation of this method is easy, since there is no need to know the characteristics of the detector diode. This allows the usage of a power detector which is often integrated in PAs in the feedback loop. The benefit comes at the expense of the need for a dedicated test signal for the I/Q impairments estimation.

These techniques are suitable for narrowband signals, since the amplitude and phase imbalance can be considered frequency-independent. Conversely, for wideband signals, amplitude and phase imbalance (I/Q imbalance) exhibits frequency-dependent behaviour. It comes from frequency-dependent behaviour of the analogue components in the I and Q paths. Hence, models which take into account frequency-dependent I/Q imbalance are developed.

Model based on a parametric method of frequency-dependent I/Q imbalance compensation using the spectrum measurement of an RF signal is proposed in [3-21]. This model empirically estimates the frequency-dependent parameters using only the magnitude of the frequency spectrum of the RF signal. Modelling process of frequency-dependent I/Q imbalance is accomplished using frequency-dependent circuit parameters.

In [3-23], an efficient pre-distortion scheme is developed for frequency-selective I/Q mismatch calibration. This technique utilises an internal feedback signal. Also, it is a widely linear (WL) predistortion structure, with two different filter estimation schemes (second-order statistics of complex random signals and WL LS).

The above methods only consider the linear distortions while the nonlinear distortions are not taken into account. Thus, new models which take into account linear and nonlinear I/Q imbalances are developed and presented below.

Nonlinear I/Q Imbalance:

In [3-25], model of the nonlinear response of an I/Q modulator is developed. This model is used to investigate impact of the I/Q modulator nonlinearity on spectral regrowth of signals. It is based on using complex power series to separately model nonlinear characteristic of the I and Q channels. The initial assumption is that the nonlinearity of the I and Q channels is isolated. Therefore, it can be modelled as two independent bandpass nonlinearities. Consequently, I/Q modulator output signal is defined as:

$$z_{RF} = G_I[z_I(t)] + jG_Q[z_Q(t)] \tag{3.15}$$

where $z_{RF}e^{j\omega_c t} = G_I[z_I(t)]e^{j\omega_c t} + jG_Q[z_Q(t)]e^{j(\omega_c t + \pi/2)}$, ω_c is the carrier frequency, and G_I and G_Q are the complex nonlinear transfer characteristics of the I and Q channel

respectively. These G_I and G_Q transfer characteristics are described as envelope complex power series:

$$G_I[z_I(t)] = \sum_{n=0}^{N} a_{I,2n+1} z_I^{2n+1} \tag{3.16}$$

$$G_Q[z_Q(t)] = \sum_{n=0}^{N} a_{Q,2n+1} z_Q^{2n+1} \tag{3.17}$$

where $a_{I,2n+1}$ and $a_{Q,2n+1}$ are the complex power-series coefficients and $2N+1$ is the highest order of the nonlinearities. Coefficients are defined as:

$$a_{I,2n+1} = b_{I,2n+1} \frac{2^{2n} n!(n+1)!}{(2n+1)!} \tag{3.18}$$

$$a_{Q,2n+1} = b_{Q,2n+1} \frac{2^{2n} n!(n+1)!}{(2n+1)!} \tag{3.19}$$

where $b_{I,2n+1}$ and $b_{Q,2n+1}$ are the complex power series which relate the complex envelope of the input to the complex envelope of the output at the carrier frequency. They are extracted by fitting a complex polynomial to AM/AM and AM/PM measurements of the I and Q channels separately.

Another type of modelling the nonlinear characteristic of the I and Q channels of the I/Q modulator can be presented as a sum of two bandpass nonlinearities that are described as the sum of two complex power series [3-27]. The model result is the envelope of the modulator RF output, which can be obtained by the quadrature summation of the envelopes of the I and Q channel outputs:

$$\tilde{z}_{RF}(t) = \tilde{z}_I(t) + j\tilde{z}_Q(t) \tag{3.20}$$

The nonlinear behavioural model [3-25] was extended to be able to accurately capture both nonlinear distortion and linear static errors. The DC offset and amplitude/phase imbalance are modelled as three add-on coefficients: $a_{I,0}/a_{Q,0}$, δ and θ, which are added into the two complex power series, as shown in (3.18) and (3.19).

$$\tilde{z}_I(t) = \tilde{G}_I[I(t)] = a_{I,0} + \tilde{a}_{I,1} I + \sum_{\substack{n=3 \\ odd}}^{N} \tilde{a}_{I,n} I^n \tag{3.21}$$

$$\tilde{z}_Q(t) = \tilde{G}_Q[Q(t)] = a_{Q,0} + \tilde{a}_{Q,1} \delta e^{j\theta} Q + \sum_{\substack{n=3 \\ odd}}^{N} \tilde{a}_{Q,n} Q^n \tag{3.22}$$

where $\tilde{a}_{I,n}$ and $\tilde{a}_{Q,n}$ are the complex power-series coefficients characterising the non-linear response of the I and Q channels. These coefficients were extracted by an offset

single-tone sinusoid AM/AM and AM/PM measurement and LS curve fitting [15]. The coefficients $a_{I,0}/a_{Q,0}$, δ and θ characterise the DC offset, amplitude imbalance and phase imbalance between the I and Q channels respectively.

In [3-28], dual-input nonlinear model based on real valued Volterra (RV) series is proposed for the modelling and compensation of the nonlinear frequency-dependent I/Q imbalance. This model can be used for modelling both linear and nonlinear as well as frequency-dependent I/Q imbalance. The frequency-independent I/Q imbalance can be characterised using amplitude and phase error mismatch and compensated using Gram-Shmidt procedure. Therefore, the ordinary Volterra series are extended to a dual-input Volterra series with the real and imaginary part of the output signal. The model is defined as following:

$$RV\{x(n)^I, x(n)^Q\} = \sum_{m_1}^{M} \boldsymbol{h}_{m_1}^T \boldsymbol{x}_{m_1} + \sum_{m_1=0}^{M} \sum_{m_2=m_1}^{M} \boldsymbol{h}_{m_1 m_2}^T \left(\boldsymbol{x}_{m_1} \otimes \boldsymbol{x}_{m_2}\right) + \\ \dots \sum_{m_1=0}^{M} \dots \sum_{m_K=m_{K-1}}^{M} \boldsymbol{h}_{m_1 \dots m_K}^T (\boldsymbol{x}_{m_1} \otimes \boldsymbol{x}_{m_2} \dots \otimes \boldsymbol{x}_{m_K}) \quad (3.23)$$

where $\boldsymbol{h}_{m_1 \dots m_K}$ and $k \in K$ (and $m_k \in M$) are the model coefficients determined in step 2, K is the nonlinear order, M is the memory depth and $\boldsymbol{x}_{m_K}$is the input of the step 2. Symbol $\otimes$ is used to denote Kronecker product. Also, vectors $\boldsymbol{h}$ and $\boldsymbol{x}$ are defined as:

$$\boldsymbol{h}_{m_1 \dots m_p} = [h_{m_1 \dots m_p,1} \; h_{m_1 \dots m_p,2} \; , \dots h_{m_1 \dots m_p,2^p}]^T \quad (3.24)$$

and

$$\boldsymbol{x}_{m_p} = \begin{bmatrix} x^I(n - m_p) \\ x^Q(n - m_p \end{bmatrix} \quad (3.25)$$

3.5 Identification of DPD Functions

There are two different ways to deploy DPD. The first approach is known as DLA and the second as ILA. These two architectures are used to create a DPD in the baseband block.

Direct Learning Architectures:

DLA implies synthesizing a model of the wireless transmitter and then inverting this model to determine DPD function (Figure 3.4). This architecture enables inverse function of the wireless transmitter behavioural model to be used directly to construct

DPD. Also, to minimise the error, DLA commonly utilises iterative optimisation procedure for the DPD parameter. In addition, determining the inverse of nonlinear PA function is complicated, especially when memory of the component is involved, [3-32]–[3-34].

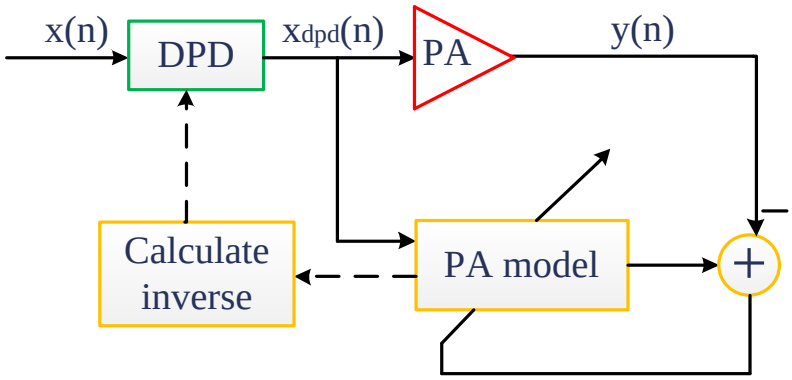

Figure 3.4: Block diagram of DLA.

Indirect Learning Architectures:

The second approach is based on identifying DPD function directly from the input and output waveforms of the DUT, which are computed with the measured input and output waveforms of the DUT (Figure 3.5). This way, it is possible to avoid the modelling process and parameter estimation of wireless transmitter components. Moreover, it has been shown that when good a behavioural model is obtained, a good inverse model ensues. This method will be used in this thesis for parameter identification [3-34]–[3-35].

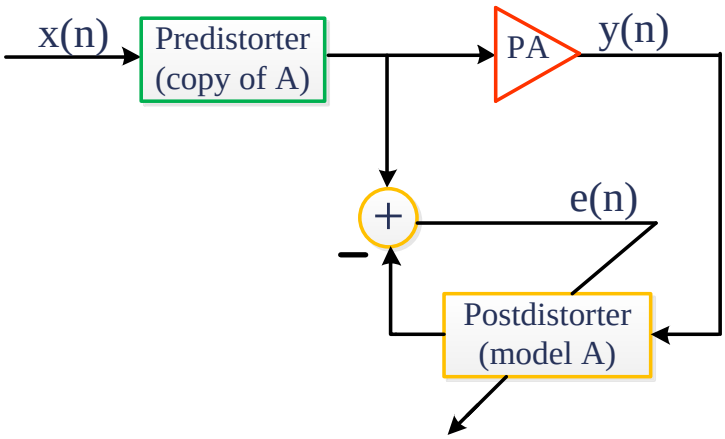

Figure 3.5: Block diagram of ILA.

A large number of DPD are based on ILA. In implementing ILA, post-inverse coefficients are first identified and then copied to work as a PD. This post-compensator models the output into the desired input and after that, it can be used as a pre-inverting model for the DPD. In other words, a postdistorter first derives a postinverse of the nonlinear model without any PD and then the postdistorter is used as a PD [3-34]–[3-35].

3.6 Joint Mitigation of I/Q Impairments and PA Nonlinearity Using DPD Techniques

As discussed in previous chapters, I/Q impairments can significantly degrade the linearisation performance of DPD. Therefore, I/Q impairments should be considered in the DPD system.

This section describes DPD technique which jointly compensates for I/Q impairments and PA nonlinearity in wireless transmitters.

Parallel Hammerstein model:

In [3-29], the PD is based on an extended PH structure, yielding a DPD that is fully linear in the parameters. This structure is completely parallel, enabling one-step joint estimation of all PD parameters using linear LS techniques and without any extra RF hardware. Thus, the PA PD is given by polynomials:

$$\psi_p(x_n) = \sum_{k\in I_p} u_{k,p}|x_n|^{k-1}\, x_n,\ p \in I_p \tag{3.26}$$

with P denoting the polynomial order, I_P denoting the set of used polynomial orders and $u_{k,p}$ denoting the polynomial weights. Furthermore, the subset of I_P in which orders only up to p are retained is denoted by I_p. The filters $H_p(z)$ are usually FIR filters. The PH model has been shown to be a versatile tool for inverse. The statistically orthogonal polynomials are adopted and the polynomial weights for x_n are:

$$u_{k,p} = (-1)^{(p-k)/2}\frac{\sqrt{\frac{(p+1)}{2}}}{\left[\frac{(k+1)}{2}\right]!}\underbrace{\binom{\frac{(p-1)}{2}}{\frac{(k-1)}{2}}}_{b} \tag{3.27}$$

where b is the binomial coefficient.

Figure 3.6 depicts the proposed PD structure.

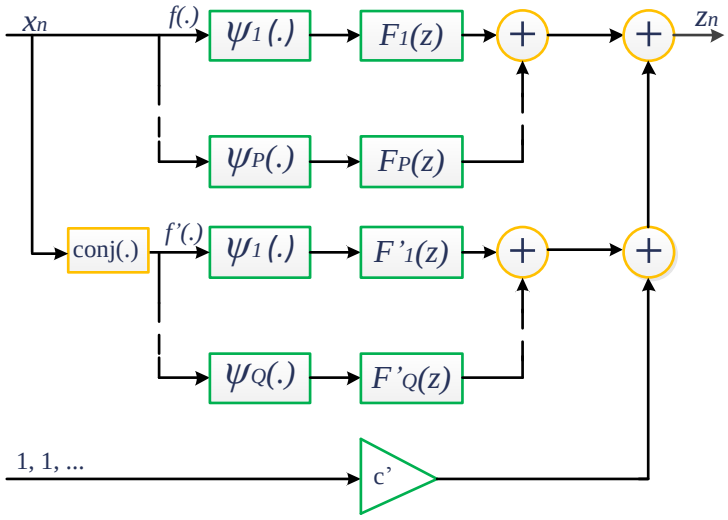

Figure 3.6: Block diagram of DPD based on PH structure.

In this model, the conjugate and non-conjugate parts of PD structure are split, which results in parallel connection of two PH PDs with outputs:

$$f(x_n) = \sum_{p=1}^{P} f_{p,n} * \psi_p(x_n) \tag{3.28}$$

$$\bar{f}(x_n{}^*) = \sum_{q=1}^{Q} \bar{f}_{q,n} * \psi_q(x_n{}^*) \tag{3.29}$$

where $f_{p,n}$ and $\bar{f}_{q,n}$ denote the impulse response of $F_p(z)$ and $\bar{F}_q(z)$ respectively and $*$ denotes convolution. It should be noted that:

$$F_p(z) = H_p(z)G_1(z) \tag{3.30}$$

$$\bar{F}_q(z) = H_q{}^*(z)G_2(z) \tag{3.31}$$

where $G_1(z)$ and $G_2(z)$ are filters for the original and conjugated signals used for I/Q modulator PD.

Finally, taking into account the DC offset compensator c', the output of the complete PD can be written:

$$z_n = f(x_n) + \bar{f}(x_n{}^*) + c' \tag{3.32}$$

For the parameter estimation stage, ILA is utilised. Therefore, postdistorter output signal can be written in a vector-matrix notation as:

$$\hat{z}_n = \sum_{p\in I_P} \boldsymbol{\psi}_{p,n}^T \boldsymbol{f}_p + \sum_{q\in I_Q} \overline{\boldsymbol{\psi}}_{q,n}^T \bar{\boldsymbol{f}}_q + c' \tag{3.33}$$

where $\hat{z}_n$ is the postdistorter output signal. The filter impulse response vectors are given as:

$$\boldsymbol{f}_p = \left[f_{p,0}\, f_{p,1} \ldots f_{p,L_p-1}\right]^T \; p \in I_P \tag{3.34}$$

$$\bar{\boldsymbol{f}}_q = \left[\bar{f}_{q,0}\, \bar{f}_{q,1} \ldots \bar{f}_{q,\bar{L}_q-1}\right]^T \; q \in I_Q \tag{3.35}$$

And the filter input vectors are obtained as:

$$\boldsymbol{\psi}_{p,n} = \left[\psi_p(s_n)\ \psi_p(s_{n-1}) \ldots \psi_p\left(s_{n-L_p+1}\right)\right]^T, p \in I_P \tag{3.36}$$

$$\overline{\boldsymbol{\psi}}_{\boldsymbol{q,n}} = \left[\psi_q(s^*{}_n)\ \psi_q(s^*{}_{n-1}) \ldots \psi_q\left(s^*{}_{n-\bar{L}_q+1}\right)\right]^T, q \in I_Q \tag{3.37}$$

Notice that $\boldsymbol{f}_1$ and $\bar{\boldsymbol{f}}_1$ are the linear filters of the PD, with respective lengths L_1 and $\bar{L}_1$, while $\boldsymbol{f}_p$ and $\bar{\boldsymbol{f}}_q$ are the polynomial filters. The output vectors of the pth nonconjugate and qth conjugate PD branches are:

$$\boldsymbol{z}_p = \boldsymbol{\psi}_p \boldsymbol{f}_p \tag{3.38}$$

$$\bar{\boldsymbol{z}}_q = \overline{\boldsymbol{\psi}}_q \bar{\boldsymbol{f}}_q \tag{3.39}$$

Here $\boldsymbol{\psi}_p$ is the nonconjugate polynomial basis matrix of order p and it is given by:

$$\boldsymbol{\psi}_p = \begin{bmatrix} \psi_p(s_0) & 0 & 0 & \cdots & 0 \\ \psi_p(s_1) & \psi_p(s_0) & 0 & \cdots & 0 \\ \psi_p(s_2) & \psi_p(s_1) & \psi_p(s_0) & \cdots & 0 \\ \vdots & \vdots & \vdots & & \vdots \\ \psi_p(s_{N-1}) & \psi_p(s_{N-2}) & \psi_p(s_{N-3}) & \cdots & \psi_p\left(s_{N-L_p}\right) \\ 0 & \psi_p(s_{N-1}) & \psi_p(s_{N-2}) & \cdots & \psi_p\left(s_{N-L_p+1}\right) \\ 0 & 0 & \psi_p(s_{N-2}) & \cdots & \psi_p\left(s_{N-L_p+2}\right) \\ \vdots & \vdots & \vdots & & \vdots \\ 0 & 0 & 0 & \cdots & \psi_p(s_{N-1}) \end{bmatrix} \tag{3.40}$$

while $\overline{\boldsymbol{\psi}}_q$ is the conjugate polynomial basis matrix of order q, constructed in a similar manner. The matrix $\boldsymbol{\psi}_p$ has dimension $\left(N + L_p - 1\right) \times L_p$, $\overline{\boldsymbol{\psi}}_q$, where N is the number

of samples. Zeros rows are add to the bottom of these matrices to make them equal in height. By collecting all the polynomials basis matrices into a single block matrix and appending it with a vector of all 1's, denoted by $\mathbf{1}$, to account for the LO leakage, it is obtained:

$$\boldsymbol{\psi} = \left[\boldsymbol{\psi}_1\ \boldsymbol{\psi}_2\ \ldots \boldsymbol{\psi}_P\ \bar{\boldsymbol{\psi}}_1\ \bar{\boldsymbol{\psi}}_2 \ldots \bar{\boldsymbol{\psi}}_Q\ 1\right] \tag{3.41}$$

Finally, stacking the filter impulse response and the LO leakage compensator coefficients into a single vector as:

$$\boldsymbol{f} = \left[\boldsymbol{f}_1^T\ \boldsymbol{f}_2^T\ \ldots \boldsymbol{f}_P^T\ \bar{\boldsymbol{f}}_1^T \boldsymbol{f}_2^T\ \ldots \boldsymbol{f}_Q^T\ c'\right]^{\boldsymbol{T}}, \tag{3.42}$$

It is possible to write the complete postdistorter vector as:

$$\hat{\boldsymbol{z}} = \boldsymbol{\psi f}. \tag{3.43}$$

Now, PD coefficients $\boldsymbol{f}$ can be calculated using the LS parameter estimation techniques as follows:

$$\boldsymbol{f} = (\boldsymbol{\psi}^{\boldsymbol{H}}\boldsymbol{\psi})^{-1}\boldsymbol{\psi}^{\boldsymbol{H}}\boldsymbol{z}. \tag{3.44}$$

Joint compensation model for memory PA and frequency-dependent I/Q impairments:

The model in [3-30] is depicted in Figure 3.7. it follows the ILA structure, which obtains the post-compensator first and then regards the post-compensator as the pre-compensator.

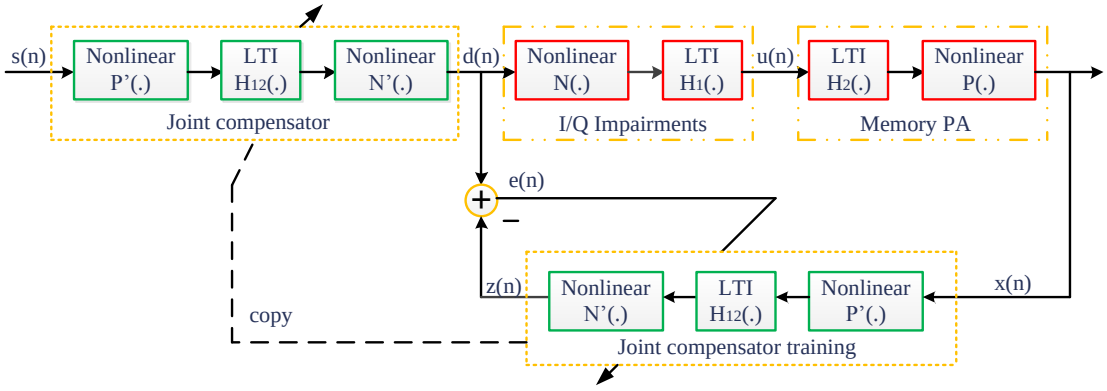

Figure 3.7: Block diagram of DPD based on joint compensation model.

On one hand, the frequency-dependent nonlinear I/Q impairments of the upconversion circuit are modelled as a static nonlinear I/Q model followed with a linear time invariant (LTI) system. On the other hand, the memory PA is modelled as a Wiener model, which is represented as an LTI system followed with a memoryless nonlinear system. It should be noted that the two LTI systems (H_1 and H_2) can be merged, so only one LTI system H_{12} is required in the joint compensator. Based on the ILA, the cascade of the nonlinear system P' and LTI system H_{12} makes up a Hammerstein model and they use the simpler MP model to replace the Hammerstein model, which can be described as:

$$y(n) = H_{12}\left(P'\left(x(n)\right)\right) = \sum_{q=0}^{M-1}\sum_{k=1}^{N} a_{kq}|x(n-q)|^{k-1}x(n-q), \qquad (3.45)$$

where N and M denote the order and the memory depth respectively and a_{kq} denotes the complex coefficients. For simplicity, only the odd-order terms of the memory polynomial model are used. The static nonlinear I/Q compensator proposed in [5] is modelled as:

$$z(n) = N'\left(y(n)\right) = c_0 + c_1 y_i(n) + c_2 y_i^2(n) + c_3 y_i^3(n) + c_4 y_q(n) + c_5 y_q^2(n) + c_6 y_q^3(n) + c_7 y_i(n) y_q(n) + c_8 y_i^2(n) y_q(n) + c_9 y_i(n) y_q^2(n) \qquad (3.46)$$

where $y(n) = y_i(n) + j y_q(n)$ and the coefficients c_i ($i = 0 \ldots .9$) is a complex number. Substituting (3.45) into (3.46), the different time-delay cross terms can be cut off, which have a less impact on the model and then the simplified new joint compensation model can be written as follows:

$$z(n) = c_0 + \sum_{q=0}^{M-1}\sum_{k=1}^{N}\sum_{l=0}^{k} c_{qkl} I(n-q)^{k-l} Q(n-q)^{l} = \sum_{q=0}^{M-1}\sum_{k=0}^{N}\sum_{l=0}^{k} c_{qkl} I(n-q)^{k-l} Q(n-q)^{l} \qquad (3.47)$$

where N and M denote the order and the memory depth of the joint compensation model respectively and c_{qkl} denotes the complex coefficient. It should be noted that the model should contain both odd-order and even-order terms. Finally, based on the ILA, parameters of the joint compensator can be obtained by using the recursive least-mean square (RLS) algorithm.

Rational function based model:

The model in [3-31] is based on rational function (RatF) and it is defined as:

$$y(n) = \frac{\sum_{i=0}^{I} a_i x^i(n)}{\sum_{j=0}^{J} b_j x^j(n)} \tag{3.48}$$

where i and j are the order of the numerator and denominator respectively, a_i and b_j are the coefficients of the model and $x(n)$ is the input of the system. The above representation does not take into account the memory of the system which cannot be ignored in the real system. Thus, with incorporation of the memory effects and consideration of the stability of the system, the output signal is defined as:

$$y(n) = \frac{\sum_{i=0}^{I} \sum_{m=0}^{M} a_{i,m} x(n-m)|x(n-m)|^i}{1+\sum_{j=1}^{J} b_j x(n)|x(n)|^j} \tag{3.49}$$

where m is the memory depth and $a_{i,m}$ and b_j are the coefficients of the model. In matrix notation, the above equation can be written as:

$$\boldsymbol{Y} = \boldsymbol{H}\boldsymbol{\theta} \tag{3.50}$$

where $\boldsymbol{H}$ is the matrix which takes into account the input signal $x(n)$ and the output samples $y(n)$. For the mitigation of PA nonlinearity and I/Q imbalance, the $\boldsymbol{H}$ matrix can be written as:

$$\boldsymbol{H} = [\boldsymbol{h_1} \vdots \boldsymbol{h_1^*}] \tag{3.51}$$

To account for I/Q compensation, $\boldsymbol{h_1^*}$ has been appended to the $\boldsymbol{h_1}$ matrix. The $\boldsymbol{h_1}$ is defined as:

$$\boldsymbol{h_1} = \begin{pmatrix} X_{i,0}(1) \dots X_{i,M}(1) - y(1)x(1)|x(1)| \dots - y(1)x(1)|x(1)|^J \\ X_{i,0}(2) \dots X_{i,M}(2) - y(2)x(1)|x(2)| \dots - y(2)x(2)|x(2)|^J \\ \vdots \\ X_{i,0}(N) \dots X_{i,M}(N) - y(N)x(N)|x(N)| \dots - y(N)x(N)|x(N)|^J \end{pmatrix} \tag{3.52}$$

Also, the complex input vector is expressed as:

$$X_{i,M}(N) = [x(N-m) \dots x(N-m)|x(N-m)|^i]. \tag{3.53}$$

Hence, the coefficients can be determined using the LS approach:

$$\boldsymbol{\theta} = (\boldsymbol{H^T H})^{-1}\boldsymbol{H^T Y}. \tag{3.54}$$

3.7 Joint Mitigation of I/Q Impairments and PA Nonlinearity Using DPD Techniques in Multi-branch and Multi-frequency MIMO Wireless Transmitters

As indicated in chapter 2, the main challenge in designing wireless transmitters is the need for highly linear system with high data rates while spending as little power as possible. Therefore, wireless transmitters which support multi-branch and multi-frequency MIMO technique are developed. However, there are side effects, such as crosstalk effect and CM products, which cannot be compensated for using techniques developed for SISO wireless transmitters.

This section describes DPD techniques which jointly compensates for I/Q impairments and PA nonlinearity and additional side effects introduced from multi-branch or multi-frequency MIMO wireless transmitters.

Multi-branch MIMO:

Multi variables memory polynomial model:

The usage of multi-branch MIMO techniques introduces many problems similar to those encountered in SISO wireless transmitters, such as I/Q impairments and PA nonlinearity [3-36]. In addition to the nonlinearity induced by the existing PAs, linear and nonlinear memory effects and imperfections in the I/Q modulator, other issues specific to multi-branch MIMO wireless transmitters must be taken into account which are the crosstalk effects between the multiple input paths due to the interference between signals of different paths.

The joint model for I/Q modulator's I/Q imbalance and PA's nonlinearity modelling in the case of multi-branch MIMO wireless transmitter is based on the MP model. The multi-branch MIMO wireless transmitter studied herein is a dual-input dual-output transmitter. To model the coupling effect, each output of the transmitter includes nonlinear cross terms between the two input signals. Furthermore, the modelling of the I/Q imbalance in the I/Q modulator is based on the modelling of the cross coupling channels between the I and Q components of the input signal of the I/Q modulator. These cross coupling terms can be introduced in the model by using the conjugate of the two input signals as described by (3.55).

The whole multi-branch MIMO wireless transmitter shown in Figure 3.8 is considered as a nonlinear system with four inputs (x_1,x_2, x_1^*, x_2^*) and two outputs (y_1 y_2) .

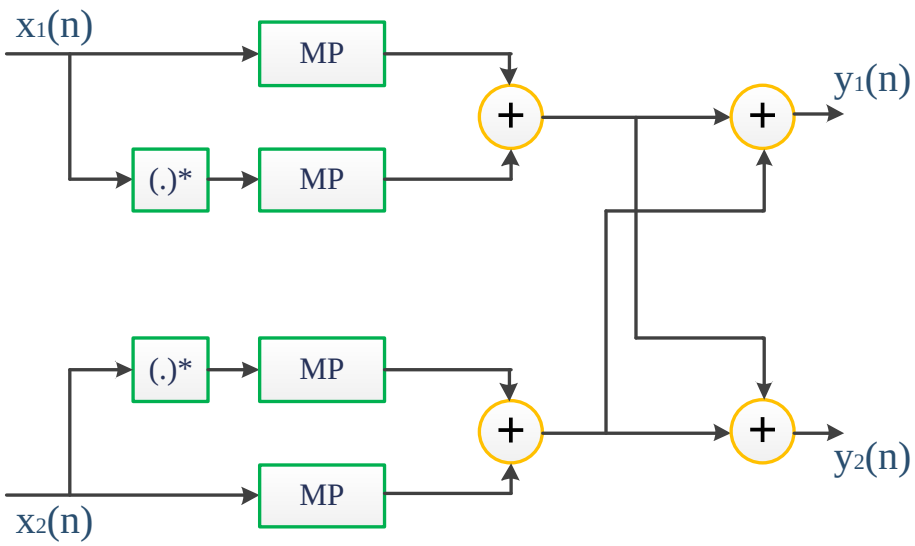

Figure 3.8: Block diagram of DPD based on MP model.

The relation between the inputs and outputs is expressed in matrix form as follows:

$$[y_1\ y_2] = W[x_1 x_2\ x_1^*\ x_2^*]^T \tag{3.55}$$

where W is a nonlinear matrix function representing the behaviour of the wireless transmitter, including the PA nonlinearity, I/Q imbalance and the nonlinear crosstalk.

The multi-branch polynomial model is used to characterise the static and dynamic (memory effect) nonlinear behaviour of the wireless transmitter. The closed form expression relating the complex envelope signals at the input and output of the nonlinear transmitter can be written as follows (see [3-36] ref therein):

$$y(n) = \sum_{q=0}^{Q}\sum_{k=1}^{K} h_{k,q}|x(n-q)|^{k-1}x(n-q) \tag{3.56}$$

where $x(n)$ and $y(n)$ are the input and output complex signal envelops, $h_{k,q}$ are the polynomial coefficients of the qth filter tap, and K and Q are the maximum polynomial order and memory depth respectively.

Equation (3.56) can be expressed in the matrix form as:

$$\vec{y} = A_{\vec{x}}\vec{h} \tag{3.57}$$

where:

- $\vec{y} = [y(1) \ \dots \ y(N)]^T$ is $N \times 1$ a vector representing N samples of the output signal,
- $\vec{h} = \left[h_{1,0} \ h_{2,0} \ \dots \ h_{K,0} \ \dots \ h_{1,Q} \ h_{2,Q} \ \dots \ h_{K,Q}\right]$ is a $K(Q+1)$ vector of the polynomial coefficients,
- $A_{\vec{x}} = \left[\beta_{\vec{x}}^0 \ \dots \ \beta_{\vec{x}}^q \ \dots \ \beta_{\vec{x}}^Q\right]$ is an $N \times K(Q+1)$ matrix,
-

$$\beta_{\vec{x}}^q = \begin{bmatrix} 0_{1xq} & 0_{1xq} & \dots & 0_{1xq} \\ \beta_1(x(1)) & \beta_2(x(1)) & \dots & \beta_K(x(1)) \\ & \vdots & & \\ \beta_1(x(N-q)) & \beta_2(x(N-q)) & \dots & \beta_K(x(N-q)) \end{bmatrix}$$ is a $N \times K$ matrix and $\beta_k(x(n))$ is defined as $\beta_k(x(n)) = x(n)^{k-1}x(n)$,

- $\vec{x} = [x(1) \ \dots \ x(N)]^T$ is a $N \times 1$ vector representing N samples of the input signal.

The coefficients $h_{k,q}$ can be determined by pseudoinversing matrix $A_{\vec{x}}$ as follows:

$$\vec{h} = \left(A_{\vec{x}}{}^H A_{\vec{x}}\right)^{-1} A_{\vec{x}}{}^H \vec{y}. \tag{3.58}$$

The aforementioned model can be extended for the dual-branch MIMO case, where there are two input and two output ports, in the presence of I/Q imbalance. The expression in equation (3.57) can be extended to the dual-input dual-output system as follows:

$$[y_1 \ y_2] = \left[\vec{A}_{\vec{x}_1} \ \vec{A}_{\vec{x}_2} \ \vec{A}_{\vec{x}_1^*} \ \vec{A}_{\vec{x}_2^*}\right] \begin{bmatrix} \vec{H}_{1,1} & \vec{H}_{2,1} \\ \vec{H}_{1,2} & \vec{H}_{2,2} \\ \vec{H}^*{}_{1,1} & \vec{H}^*{}_{2,1} \\ \vec{H}^*{}_{1,2} & \vec{H}^*{}_{2,2} \end{bmatrix} \tag{3.59}$$

where $\vec{A}_{\vec{x}_1}$, $\vec{A}_{\vec{x}_2}$, $\vec{A}_{\vec{x}_1^*}$, $\vec{A}_{\vec{x}_2^*}$ are the matrices defined for inputs $\vec{x}_1$, $\vec{x}_2$, $\vec{x}_1^*$, $\vec{x}_2^*$ and $\vec{H}_{i,j}$ are the polynomial coefficients between input $\vec{x}_j$ and output $\vec{y}_i$. Therefore the polynomial coefficients for the dual-branch MIMO model will be:

$$\begin{bmatrix} \vec{H}_{1,1} & \vec{H}_{2,1} \\ \vec{H}_{1,2} & \vec{H}_{2,2} \\ \vec{H}^{*}_{1,1} & \vec{H}^{*}_{2,1} \\ \vec{H}^{*}_{1,2} & \vec{H}^{*}_{2,2} \end{bmatrix} = pinv([\vec{A}_{\vec{x}_1}\ \vec{A}_{\vec{x}_2}\ \vec{A}_{\vec{x}_1^*}\ \vec{A}_{\vec{x}_2^*}])[y_1\ y_2] \quad (3.60)$$

where $pinv$ is the Moore-Penrose pseudo-inverse of matrix.

Parallel memory polynomial DPD:

The drawback of the proposed MP DPD for the compensation of I/Q impairments and PA nonlinearity in multi-branch MIMO wireless transmitters is the high computational complexity involved in the DPD coefficient estimation technique (inversion of a large matrix). A parallel MP PD proposed in [3-37], compensates for PA nonlinearity, I/Q imbalance and crosstalk effect. Also, it reduces computational complexity. The DPD coefficients are estimated using an ILA. In this structure, the DPD parameters are estimated and copied to the PD avoiding the inverse model calculation required for DLA. However, upon several advantages, ILA is affected by measurement noise at the PA output. The DPD structure is depicted in Figure 3.9, where each block $P_{l,i}$ denotes the memory polynomial of the branch i.

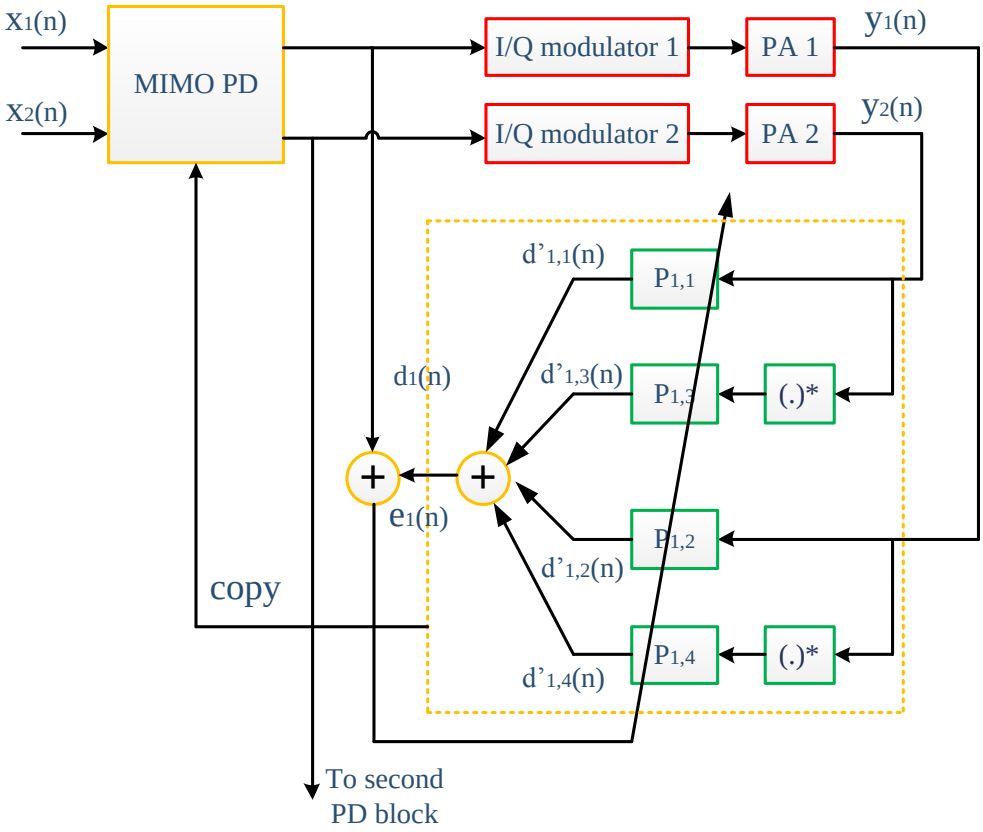

Figure 3.9: Block diagram of DPD based on parallel MP model.

Based on this model, the DPD output associated to antenna l can be written:

$$\hat{d}_l(n) = \sum_{p=0}^{P_{l1}-1}\sum_{k=0}^{M_{l1}} \theta_{pk}^{(l,1)}(n)\,\psi_{1p}^{*}(n-k) + \sum_{p=0}^{P_{l2}-1}\sum_{k=0}^{M_{l2}} \theta_{pk}^{(l,2)}(n)\,\psi_{1p}(n-k) + \sum_{p=0}^{P_{l3}-1}\sum_{k=0}^{M_{l3}} \theta_{pk}^{(l,3)}(n)\,\psi_{2p}^{*}(n-k) + \sum_{p=0}^{P_{l4}-1}\sum_{k=0}^{M_{l4}} \theta_{pk}^{(l,4)}(n)\,\psi_{2p}(n-k) = \hat{d}_{l,1}(n) + \hat{d}_{l,2}(n) + \hat{d}_{l,3}(n) + \hat{d}_{l,4}(n) \quad (3.61)$$

where $\theta_{pk}^{(l,1)}$ and $\theta_{pk}^{(l,3)}$ are the MP coefficients associated with the input signal and its conjugate respectively. $\theta_{pk}^{(l,2)}$ and $\theta_{pk}^{(l,4)}$ are the coefficients associated with the crosstalk signal and its conjugate. The basis function are defined as $\psi_{1p} = y_1(n)|y_1(n)|^{2p}$ and $\psi_{2p} = y_2(n)|y_2(n)|^{2p}$. P_{li} and $M_{li}$are the polynomial order and the memory depth of the branch i respectively.

By defining the coefficients vector:

$$\boldsymbol{\theta}_l(n) = \left[\theta^{(l,1)^T}(n)\ \theta^{(l,2)^T}(n)\ \theta^{(l,3)^T}(n)\ \theta^{(l,4)^T}(n)\right] \quad (3.62)$$

where

$$\theta^{(l,i)} = \left[\theta_{10}^{(l,i)}(n), \ldots\ \theta_{P_{lo}0}^{(l,i)}(n), \ldots\ \theta_{1M_{li}}^{(l,i)}(n), \ldots \theta_{P_{li}M_{li}}^{(l,i)}(n)\right]^T \quad (3.63)$$

with $i = 1, \ldots 4$ and by defining

$$\psi^{(l,1)}(n) = \left[\psi_{1_0}(n), \ldots\ \psi_{1_{P_{l1}}}(n)\right]^T$$

$$\psi^{(l,2)}(n) = \left[\psi_{2_0}(n), \ldots\ \psi_{2_{P_{l2}}}(n)\right]^T$$

$$\psi^{(l,3)}(n) = \left[\ \psi_{1_0}^{*}(n), \ldots\ \psi_{1_{P_{l1}}}^{*}(n)\right]^T$$

$$\psi^{(l,4)}(n) = \left[\psi_{2_0}^{*}(n), \ldots\ \psi_{2_{P_{l2}}}^{*}(n)\right]^T \quad (3.64)$$

with $i = 1, \ldots 4$ and the basis function vector can be written as:

$$\boldsymbol{\psi}_l(n) =$$

$$\left[\psi^{(l,1)^T}(n) \ldots \ \psi^{(l,1)^T}(n-M_{l1}) \ \psi^{(l,2)^T}(n) \ldots \psi^{(l,2)^T}(n-M_{l2}) \psi^{(l,3)^T}(n) \ldots \ \psi^{(l,3)^T}(n-M_{l3}) \psi^{(l,4)^T}(n) \ldots \psi^{(l,4)^T}(n-M_{l4})\right]^T \quad (3.65)$$

Finally, branch l DPD output can be written as:

$$\hat{d}_l(n) = \boldsymbol{\theta}_l^H(n)\boldsymbol{\psi}_l(n). \quad (3.66)$$

Multi-frequency MIMO:

Recently, a two-dimensional (2D) MP model [3-38], its low complexity version [3-39] and augmented Hammerstein [3-40] have been proposed for concurrent dual-band DPD. However, these DPD techniques are focused towards concurrent dual-band PA linearisation utilising an ideal modulator.

Multi-frequency MIMO wireless transmitters need to simultaneously accommodate multiple standards of signal formats. The dual-band PAs for the RF front end have been successfully designed and is able to transmit dual-band signals concurrently. Accordingly, the overall efficiency of the wireless transmitter, which is mostly affected with the PA efficiency, is increased. However, the nonlinear behaviour of the dual-band PA is not the same as in the single band, it is more emphasised. I/Q impairments show CM effects between signals in two bands, which seriously affects the performance of the DPD technique. Therefore, during the DPD development presence of I/Q impairments must be taken into account.

2D-DPD for I/Q

In [3-41], joint PD for both the I/Q impairments and PA nonlinearity is proposed based on the 2D-DPD technique. Figure 3.10 illustrates the basic concept of construction for the joint PD, where LB is the lower band and UB is the upper band.

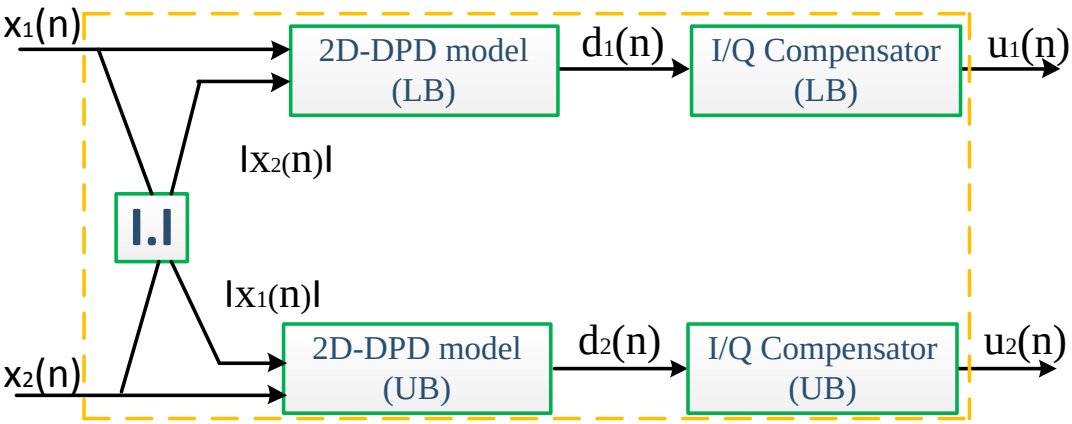

(a)

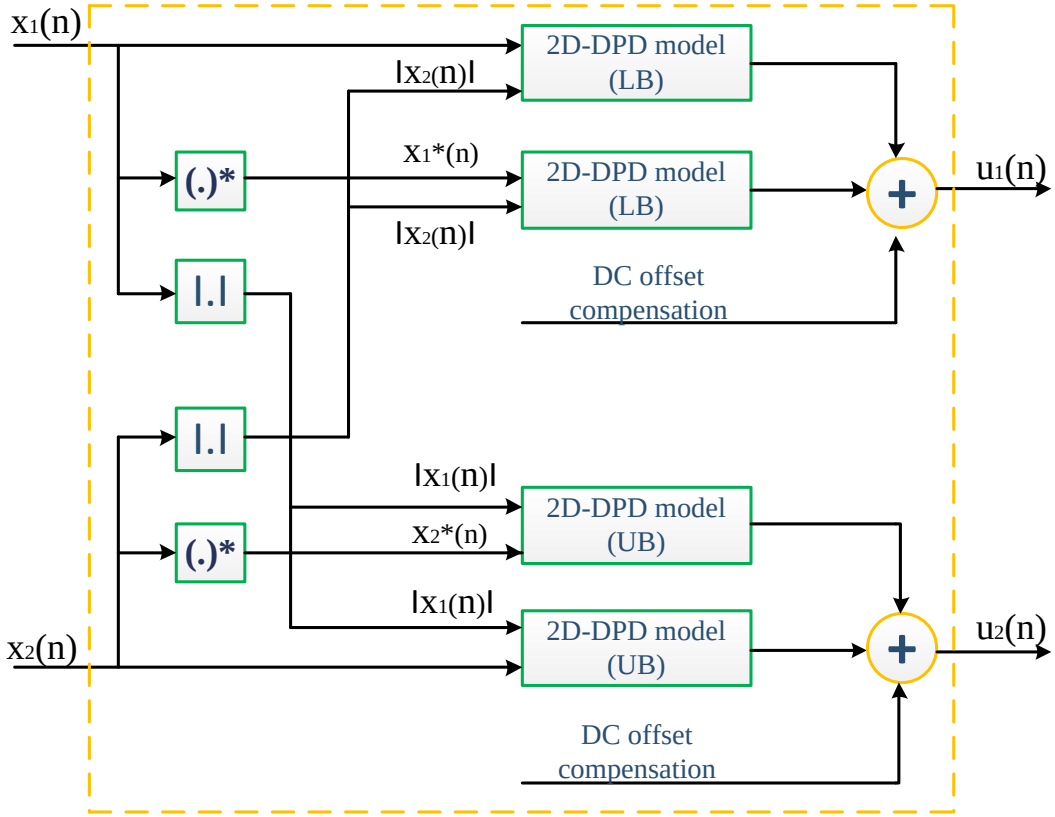

(b)

Figure 3.10: Block diagram of joint predistortion technique based on 2D-DPD technique.

First, when compensating the I/Q impairments and PA nonlinearity in a separate manner, two I/Q compensators are cascaded after the 2D-DPD blocks, as shown in Figure 3.9 (a). The I/Q compensators can be represented as the following model to give the final PD signals as

$$u_i(n) = \alpha_i d_i(n) + \beta_i d_i^*(n) + \gamma_i \qquad (3.67)$$

where $i = 1,2$ correspond to the LB and the UB respectively. The α_i and β_i are the compensation coefficients for I/Q imbalance and γ_i are that for DC offset. Joint PD model based on 2D-DPD technique can be written:

$$u_1(n) = \sum_{q=0}^{Q-1}\sum_{k=0}^{K}\sum_{j=0}^{k} A_{k,j,q}^{(1)} x_1(n-q)|x_1(n-q)|^{k-j}\,|x_2(n-q)|^{j} + \sum_{q=0}^{Q-1}\sum_{k=0}^{K}\sum_{j=0}^{k} B_{k,j,q}^{(1)} x_1^*(n-q)|x_1(n-q)|^{k-j}\,|x_2(n-q)|^{j} + \gamma_1 \quad (3.68)$$

$$u_2(n) = \sum_{q=0}^{Q-1}\sum_{k=0}^{K}\sum_{j=0}^{k} A_{k,j,q}^{(2)} x_2(n-q)|x_2(n-q)|^{k-j}\,|x_1(n-q)|^{j} + \sum_{q=0}^{Q-1}\sum_{k=0}^{K}\sum_{j=0}^{k} B_{k,j,q}^{(2)} x_2^*(n-q)|x_2(n-q)|^{k-j}\,|x_1(n-q)|^{j} + \gamma_2 \quad (3.69)$$

where ($A_{k,j,q}^{(i)}$, $B_{k,j,q}^{(i)}$, γ_i) ($i = 1,2$) are the model coefficients. And the model structure is shown in Figure 3.9 (b), which actually consists of four 2D-DPD blocks by considering both the desired signals ($x_1(n)$, $x_2(n)$) and their image signals ($x_1^*(n)$, $x_2^*(n)$). One can easily use the LS algorithm for the extraction of coefficients since the output of the model is linear with respect to its coefficients.

The pruned joint 2D-MP model:

In [3-42], a method to prune the joint 2D-DPD model for concurrent dual-band transmitter where I/Q imbalance and LO leakage often exist is proposed. The phenomenon of over-compensation of the DPD model is found if too many terms in the DPD model are adopted. Thus redundant polynomial terms are removed in order to solve this problem and to reduce the model complexity. In other words, it was found that the conjugate signal is typically tens of decibels smaller than the direct signal, so there exist possible redundant terms which can be eliminated. Following this line of thought, the unnecessary high order terms of the conjugate signal can be removed, without causing serious negative influence on the performance. Thus the pruned new model is expressed as:

$$z_1(n) = \sum_{l=0}^{L}\sum_{k=1}^{K}\sum_{j=0}^{k-1} a_{l,k,j}^{(1)} x_1(n-l)|x_1(n-lq)|^{k-l-j}\,|x_2(n-l)|^{j} + \sum_{l=0}^{L}\sum_{p=1}^{P}\sum_{j=0}^{k-1} b_{l,p,j}^{(1)} x_1^*(n-l)|x_1(n-l)|^{p-l-j}\,|x_2(n-l)|^{j} + e_1 \quad (3.70)$$

$$z_2(n) =$$
$$\sum_{l=0}^{L}\sum_{k=1}^{K}\sum_{j=0}^{k-1} a_{l,k,j}^{(2)} x_2(n-l)|x_2(n-lq)|^{k-l-j}\,|x_2(n-l)|^{j} +$$
$$\sum_{l=0}^{L}\sum_{p=1}^{P}\sum_{j=0}^{k-1} b_{l,p,j}^{(2)} x_2^*(n-l)|x_2(n-l)|^{p-l-j}\,|x_1(n-l)|^{j} + e_2 \qquad (3.71)$$

By carefully choosing the orders P and K ($P < K$), typically $K - P \geq 4$ or more, the number of coefficients and the model complexity can be effectively reduced. By cutting off redundant terms of the joint 2D-DPD for I/Q model as expressed in equations (3.70) and (3.71), computational load can be decreased. Moreover, the numerical instability of model identification process can be mitigated.

The radially-pruned multidimensional Volterra model:

In [3-43], a radially-pruned multidimensional Volterra model for the modelling and linearisation of concurrent dual-band transmitters is developed. The general Volterra series for SISO transmitters, truncated to nonlinearity order P, representing a causal, discrete-time system of memory depth L is given by:

$$y(n) = \sum_{p=1}^{P}\sum_{i_1=0}^{L}\dots\sum_{i_p=0}^{L} H_p\,(i_1,\dots i_p)\prod_{q=1}^{p} x(n-i_q) \qquad (3.72)$$

where $x(n)$ and $y(n)$ are the RF input and output signals of the PA respectively and $H_p(i_1,\dots i_p)$ are the passband Volterra kernels. For a dual-band PA, $x(n)$ is:

$$x(n) = x_{m,1}(n) + x_{m,2}(n) \qquad (3.73)$$

$$x(n) =$$
$$\frac{1}{2}\left(\tilde{x}_{m,1}(n)e^{j\omega_1 nT_s} + \tilde{x}_{m,1}^*(n)e^{-j\omega_1 nT_s}\right) + \frac{1}{2}\left(\tilde{x}_{m,2}(n)e^{j\omega_2 nT_s} + \tilde{x}_{m,2}^*(n)e^{-j\omega_2 nT_s}\right) \qquad (3.74)$$

where T_s is the period of sampling. Also, $\tilde{x}_{m,1}(n)$ and $\tilde{x}_{m,2}(n)$ are defined as:

$$\tilde{x}_{m,1}(n) = \beta_1\tilde{x}_1(n) + \beta_2\tilde{x}_1^*(n) \qquad (3.75)$$

$$\tilde{x}_{m,2}(n) = \beta_3\tilde{x}_2(n) + \beta_4\tilde{x}_2^*(n) \qquad (3.76)$$

These signals present the baseband representations of the impaired input signals considering the effects of the I/Q imperfections, where β_1, β_2, β_3 and β_4 present I/Q impairments and they are defined as:

$$\beta_1 = \frac{1}{2}[(\alpha_1\cos\theta_1 + \alpha_2\cos\theta_2) + j(\alpha_1\sin\theta_1 + \alpha_2\sin\theta_2)]$$

$$\beta_2 = \frac{1}{2}[(\alpha_1 \cos\theta_1 - \alpha_2 \cos\theta_2) + j(\alpha_1 \sin\theta_1 - \alpha_2 \sin\theta_2)]$$

$$\beta_3 = \frac{1}{2}[(\alpha_3 \cos\theta_3 + \alpha_4 \cos\theta_4) + j(\alpha_3 \sin\theta_3 + \alpha_4 \sin\theta_4)]$$

$$\beta_4 = \tfrac{1}{2}[(\alpha_3 \cos\theta_3 - \alpha_4 \cos\theta_4) + j(\alpha_3 \sin\theta_3 - \alpha_4 \sin\theta_4)] \qquad (3.77)$$

The substitution of (3.75) and (3.76) in (3.74) results in:

$$x(n) = \tfrac{1}{2} \times \big[(\beta_1 \tilde{x}_1(n) + \beta_2 \tilde{x}_1^*(n))e^{j\omega_1 nT_s} + (\beta_1^* \tilde{x}_1^*(n) + \beta_2^* \tilde{x}_1(n))e^{-j\omega_1 nT_s} + (\beta_3 \tilde{x}_2(n) + \beta_4 \tilde{x}_2^*(n))e^{j\omega_2 nT_s} + (\beta_3^* \tilde{x}_2^*(n) + \beta_4^* \tilde{x}_2(n))e^{-j\omega_2 nT_s}\big] \qquad (3.78)$$

Then by substituting $x(n)$ given by (3.78) in (3.72), and regrouping the terms around the fundamental frequencies, ω_1 and ω_2, the baseband representation of the full dual-band Volterra model around ω_1 is:

$$\tilde{y}_1(n) = \sum_{\substack{p=1 \\ odd}}^{N} \sum_{\substack{s=1 \\ odd}}^{p} \sum_{\boldsymbol{l}_p=0}^{\boldsymbol{L}_p} h_{ps}^{(1)}(\boldsymbol{l}_p)\tilde{x}_1(n-l_1)\psi_{p,s,l_p}[\tilde{x}_1(n), \tilde{x}_2(n)] + \sum_{\substack{p=1 \\ odd}}^{N} \sum_{\substack{s=1 \\ odd}}^{p} \sum_{\boldsymbol{l}_p=0}^{\boldsymbol{L}_p} \bar{h}_{ps}^{(1)}(\boldsymbol{l}_p)\tilde{x}_1^*(n-l_1)\psi_{p,s,l_p}[\tilde{x}_1(n), \tilde{x}_2(n)] \qquad (3.79)$$

where

$$\psi_{p,s,l_p}[\tilde{x}_1(n), \tilde{x}_2(n)] = \prod_{q=1}^{(s-1)/2} \tilde{x}_1(n-l_{2q})\tilde{x}_1^*(n-l_{2q+1}) \times \prod_{q=(s+1)/2}^{(p-s)/2} \tilde{x}_2(n-l_{2q})\tilde{x}_2^*(n-l_{2q+1})$$

The selection of the radial directions can be performed along the diagonals of this cube; (see ref [16] in [3-43]). Selecting the radial directions, forces all cross terms to have a delay of either 0 or l, and ignores all the different delays in between. The importance of these terms diminishes moving away from the origin. This becomes more evident in a dual-band model, since the effect of the input at the second band on the output of the first band decreases more when moving away from the origin with respect to each radial direction. Therefore, retaining only the most relevant terms in each direction considerably reduces the complexity of the model in (3.79).

Real valued time delayed neural networks:

In [3-44], a concurrent dual-band DPD scheme for the joint mitigation of I/Q impairments and PA nonlinearity using a real valued feedforward neural network is proposed. Figure 3.11 shows the proposed real valued focused time delay neural network (RVFTDNN) topology for concurrent dual-band PA modelling.

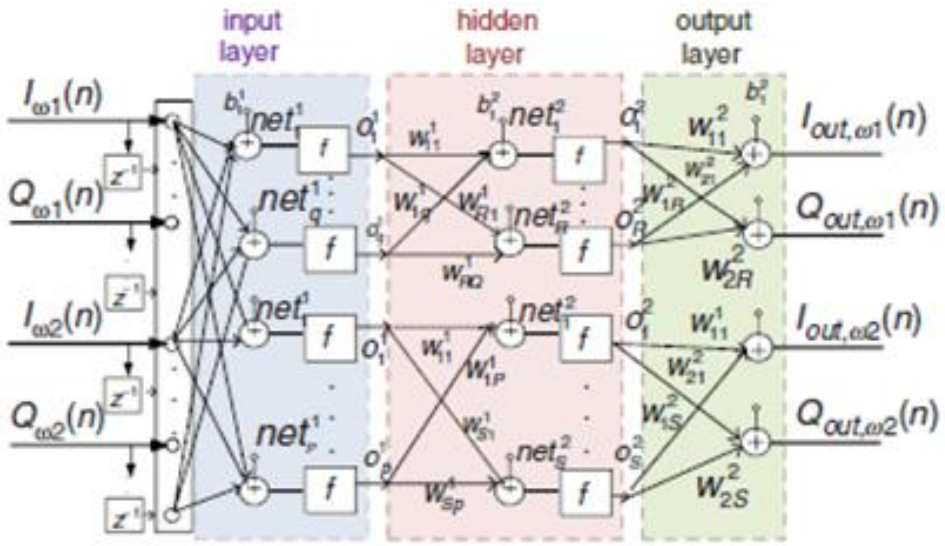

Figure 3.11: RVFTDNN model for concurrent dual-band wireless transmitters [3-44].

As it can be seen from Figure 3.11, the neural network (NN) takes both signal components and their previous samples as the input and individually models them to the PA output. Nonlinear activation function f is a hyperbolic tangent function, which maps each input into a range of $[-1, 1]$. Weights are selected randomly in the range $[-0.8, 0.8]$ to avoid saturation of the neuron at 1 or -1. (The detailed description of feedforward NNs can be found in ref [5] of [3-44].) The backward-propagation weight adjustment is done in batch mode to adjust the synaptic weights and biases at each layer according to the Levenberg-Marquardt algorithm:

$$\Delta \boldsymbol{X} = [J^T(\boldsymbol{X})J(\boldsymbol{X}) + \mu \boldsymbol{I}]^{-1} J^T(\boldsymbol{X})\boldsymbol{e}(\boldsymbol{X}) \tag{3.80}$$

where $J(\boldsymbol{X})$ is the Jacobian matrix calculated over the error matix, $\boldsymbol{e}(\boldsymbol{X})$, with respect to $\boldsymbol{X}$, where

$$\boldsymbol{X} = [w_{11}^l, w_{12}^l, \dots w_{nR}^l, w_{1R}^l, \dots w_{Rn}^l, b_1^l, \dots b_n^l] \tag{3.81}$$

$$\boldsymbol{e}(\boldsymbol{X}) = [\varepsilon_1(1) \dots \varepsilon_n(N)] \tag{3.82}$$

N denotes the total number of training samples, l denotes the present layer, R denotes the succeeding layer and 1n is the error term calculated for the nth neuron of layer l. According to the notations used in Figure 3.11, the number of neurons in each layer were $q = 5, R = 7$ for the lower band NN operating at $\omega 1$ and $p = 5, S = 5$ for the upper band NN operating at $\omega 2$. The number of neurons in the outer layer was 2 for both NNs and memory depth is 1.

3.8 Summary

This chapter is focused on explaining of different PA and I/Q behavioural models in order to understand how they work. Also, basic principle of DPD technique is extensively presented with explanation of two different architectures used to identify DPD function (DLA and ILA). Moreover, DPD techniques which jointly mitigate I/Q impairments and PA nonlinearity are described. DPD techniques applicable in multi-branch and multi-frequency MIMO wireless transmitters are delineated as well.

3.9 References

[3-1] M. Rumeny, *LTE and Evolution to 4G Wireless Design and Measurement Challenges*, Second edition, reprinted for Agilent Technologies: John Wiley & Sons, 2009

[3-2] F. M. Ghannouchi and O. Hammi, "Behavioral modeling and predistortion," *IEEE Microwave Magazine*, vol. 10, no. 7, pp. 52-64, Dec. 2009.

[3-3] A. S. Tehrani, "Behavioral modeling of wireless transmitters for distortion mitigation", PhD thesis, Chalmers University of Technology, Gothenburg, Sweden, 2012

[3-4] J. K. Cavers, "Amplifier linearization using a digital PD with fast adaptation and low memory requirements," *IEEE Transactions on Vehicular Technology*, vol. 39, no. 4, pp. 374–382, Nov. 1990.

[3-5] A. Zhu, J. C. Pedro and T. J. Brazil, "Dynamic deviation reduction-based behavioral modeling of RF power amplifiers," *IEEE Transactions on Microwave Theory and Techniques*, vol. 54, no. 12, pp. 4323–4332, Dec. 2006.

[3-6] A. Zhu, J. Pedro and T. Cunha, “Pruning the Volterra series for behavioral modeling of power amplifiers using physical knowledge,” *IEEE Transactions on Microwave Theory and Techniques*, vol. 55, no. 5, pp. 813–821, May 2007.

[3-7] A.S. Tehrani, C. Haiying, S. Afsardoost, T. Eriksson, M. Isaksson and C. Fager, "A Comparative Analysis of the Complexity/Accuracy Tradeoff in Power Amplifier Behavioral Models," *IEEE Transactions on Microwave Theory and Techniques*, vol.58, no.6, pp.1510-1520, June 2010

[3-8] D. Morgan, Z. Ma, J. Kim, M. Zierdt and J. Pastalan, “A generalized memory polynomial model for digital predistortion of RF power amplifiers,” *IEEE Transactions Signal Processing*, vol. 54, pp. 3852–3860, Oct. 2006.

[3-9] R. Raich, H. Qian, and G. T. Zhou, “Orthogonal polynomials for power amplifier modeling and PD design,” *IEEE Transactions Vehicular Technolgy*, vol. 53, pp. 1468–1479, Sept. 2004.

[3-10] M. Isaksson, D. Wisell and D. Ronnow, "A comparative analysis of behavioral models for RF power amplifiers," *IEEE Transactions on Microwave Theory and Techniques*, vol. 54, no. 1, pp. 348-359, Jan. 2006

[3-11] H.assan Zareian and V. T. Vakili , “New adaptive method for IQ imbalance compensation of quadrature modulators in predistortion systems” *EURASIP Journal on Advances in Signal Processing*, Aug. 2009

[3-12] S. Burglechner, G. Hueber and A. Springer, "On the estimation and compensation of IQ impairments in direct conversion transmitters," *European Conference on Wireless Technology, EuWiT*, vol., no., pp. 69-72, Oct. 2008

[3-13] M. Valkama, M. Renfors and V. Koivunen, "Compensation of frequency-selective I/Q imbalances in wideband receivers: models and algorithms," *IEEE Third Workshop on Signal Processing Advances in Wireless Communications, 2001. (SPAWC '01).* , vol., no., pp. 42-45, 2001

[3-14] M. Windisch and G. Fettweis, "On the performance of standard-independent I/Q imbalance compensation in OFDM direct-conversion receivers," *13th European in Signal Processing Conference,* , vol., no., pp.1-5, Sept. 2005

[3-15] A. Tarighat and A.H. Sayed, "Joint compensation of transmitter and receiver impairments in OFDM systems," *IEEE Transactions on Wireless Communications*, vol. 6, no. 1, pp. 240-247, Jan. 2007

[3-16] G. Xing, M. Shen and H. Liu, "Frequency offset and I/Q imbalance compensation for OFDM direct-conversion receivers," *IEEE International Conference on in Acoustics, Speech, and Signal Processing, 2003. Proceedings. (ICASSP '03).*, vol. 4, no., pp. IV-708-11, April 2003

[3-17] E. Lopez-Estraviz, S. De Rore, F. Horlin and L. Van der Perre, "Optimal Training Sequences for Joint Channel and Frequency-Dependent IQ Imbalance Estimation in OFDM-based Receivers," *IEEE International Conference on in Communications, 2006. ICC '06.*, vol.10, no., pp.4595-4600, June 2006

[3-18] L. Anttila, M. Valkama and M. Renfors, "Efficient Mitigation of Frequency-Selective I/Q Imbalance in OFDM Receivers," *IEEE 68th in Vehicular Technology Conference, VTC 2008-Fall.*, vol., no., pp. 1-5, Sept. 2008

[3-19] R. Marchesani, "Digital precompensation of imperfections in quadrature modulators," *IEEE Transactions on Communications*, vol. 48, no. 4, pp. 552-556, April 2000

[3-20] J. Tuthill and A. Cantoni, "Efficient compensation for frequency-dependent errors in analog reconstruction filters used in IQ modulators," *IEEE Transactions on Communications*, vol. 53, no. 3, pp. 489-496, March 2005

[3-21] K. Minseok, Y. Maruichi and J. Takada, "Parametric Method of Frequency-Dependent I/Q Imbalance Compensation for Wideband Quadrature Modulator," *IEEE Transactions on Microwave Theory and Techniques*, vol. 61, no. 1, pp. 270-280, Jan. 2013

[3-22] L. Ding, M. Zhengxiang, D.R. Morgan, M. Zierdt and G.T. Zhou, "Compensation of Frequency-Dependent Gain/Phase Imbalance in Predistortion Linearization Systems," *IEEE Transactions on Circuits and Systems I: Regular Papers*, vol. 55, no. 1, pp. 390-397, Feb. 2008

[3-23] L. Anttila, M. Valkama and M. Renfors, "Frequency-Selective I/Q Mismatch Calibration of Wideband Direct-Conversion Transmitters," *IEEE Transactions*

on Circuits and Systems II: Express Briefs, vol. 55, no. 4, pp. 359-363, April 2008

[3-24] L. Ding, M. Zhengxiang, D.R. Morgan, M. Zierdt and G.T. Zhou "Frequency-dependent modulator imbalance in predistortion linearization systems: modeling and compensation," *Conference Record of the Thirty-Seventh Asilomar Conference on Signals, Systems and Computers*, vol.1, no., pp. 688-692, Nov. 2003

[3-25] M. Li, L. Hoover, K.G. Gard and M.B. Steer, "Behavioral Modeling of Quadrature Modulators for Characterization of Nonlinear Distortion," *IEEE MTT-S International in Microwave Symposium Digest*, vol., no., pp. 1117-1120, June 2006

[3-26] A. Cantoni and J. Tuthill, "Digital Compensation of Frequency Dependent Imperfections in Direct Conversion I-Q Modulators," *IEEE International Symposium on Circuits and Systems, ISCAS*, vol., no., pp. 269-272, May 2007

[3-27] M. Li, L. Hoover, K.G. Gard and M.B. Steer, "Behavioural modelling and impact analysis of physical impairments in quadrature modulators," *IET in Microwaves, Antennas & Propagation*, vol. 4, no. 12, pp. 2144-2154, Dec. 2010

[3-28] C. Haiying A.S. Tehrani, C. Fager, T. Eriksson and H. Zirath, "I/Q Imbalance Compensation Using a Nonlinear Modeling Approach," *IEEE Transactions on Microwave Theory and Techniques*, vol. 57, no. 3, pp. 513-518, March 2009

[3-29] L. Anttila, P. Handel and M. Valkama, "Joint Mitigation of Power Amplifier and I/Q Modulator Impairments in Broadband Direct-Conversion Transmitters," *IEEE Transactions on Microwave Theory and Techniques*, vol. 58, no. 4, pp.730-739, April 2010

[3-30] P. Zhan, K. Qin, and S. Cai, "Joint compensation model for memory power amplifier and frequency-dependent nonlinear IQ impairments," *Electronics Letters*, vol. 47, no. 25, pp. 1382-1384, December 2011

[3-31] M. Aziz, M. Rawat and F.M. Ghannouchi, "Rational Function Based Model for the Joint Mitigation of I/Q Imbalance and PA Nonlinearity," *IEEE Microwave and Wireless Components Letters*, vol. 23, no. 4, pp. 196-198, April 2013

[3-32] Y. H. Lim, Y. S. Cho, I. W. Cha, and D. H. Youn, “An adaptive nonlinear prefilter for compensation of distortion in nonlinear systems,” *IEEE Transaction on Signal Processing*, vol. 46, no. 6, pp. 1726-1730, Jun. 1998.

[3-33] D. Zhou and V. E. DeBrunner, “Novel adaptive nonlinear PDs based on the direct learning algorithm,” *IEEE Transaction on Signal Processing*, vol. 55, no. 1, pp. 120–133, Jan. 2007.

[3-34] H. Paaso and A. Mammela, “Comparison of Direct Learning and Indirect Learning Predistortion Architectures”, *IEEE International Symposium on Wireless Communication Systems*, vol., no., pp. 309-313, Oct. 2008

[3-35] R. Marsalek, P. Jardin, and G. Baudoin, “From post-distortion to predistortion for power amplifiers linearization,” *IEEE Communications Letters*, vol. 7, no. 7, pp. 308–310, Jul. 2003.

[3-36] D. Saffar, N. Boulejfen, F. Ghannouchi, M. Helaoui and A. Gharssalah, "Behavioral modeling of MIMO transmitters exhibiting nonlinear distortion and hardware impairements," *European Microwave Integrated Circuits Conference (EuMIC)*, vol., no., pp. 486-489, Oct. 2011

[3-37] F. Gregorio, J. Cousseau, S. Werner, T. Riihonen and R. Wichman, "Compensation of IQ imbalance and transmitter nonlinearities in broadband MIMO-OFDM," *IEEE International Symposium on Circuits and Systems (ISCAS)*, vol., no., pp. 2393-2396, May 2011

[3-38] S.A. Bassam, M. Helaoui, and F.M. Ghannouchi, "2-D digital predistortion (2-D-DPD) architecture for concurrent dual-band transmitters," *IEEE Transactions on Microwave Theory and Techniques*, vol. 59, no. 10, pp. 2547-2553, Oct. 2011.

[3-39] Y.J. Liu, J. Zhou, W. Chen, B. Zhou and F.M. Ghannouchi, "Low-complexity 2D behavioural model for concurrent dual-band power amplifiers," *Electronics Letters*, vol. 48, no. 11, pp. 620-621, May 2012.

[3-40] Y.-J. Liu, W. Chen, B. Zhou, J. Zhou, and F.M. Ghannouchi, "2D augmented Hammerstein model for concurrent dual-band power amplifiers," *Electronics Letters*, vol. 48, no. 19, pp. 1214-1216, Sept. 2012.

[3-41] You-Jiang Liu; Wenhua Chen; Jie Zhou; Bang-Hua Zhou; Yi-Nong Liu, "Joint predistortion of IQ impairments and PA nonlinearity in concurrent dual-band transmitters," *42nd European Microwave Conference (EuMC)*, vol., no., pp. 132-135, Oct. -Nov. 2012

[3-42] L. Li, F. Liu, G. Yang and H. Wang, "A pruning method of joint 2D digital predistortion model for nonlinearity and I/Q imperfections in concurrent dual-band transmitters," *IEEE/ACIS 13th International Conference on Computer and Information Science (ICIS)*, vol., no., pp. 71-74, June 2014

[3-43] M. Younes and F.M. Ghannouchi, "Behavioral Modeling of Concurrent Dual-Band Transmitters Based on Radially-Pruned Volterra Model," *IEEE Communications Letters*, vol. 19, no. 5, pp. 751-754, May 2015

[3-44] M. Rawat, K. Rawat, M. Younes and F. Ghannouchi, "Joint mitigation of nonlinearity and modulator imperfections in dual-band concurrent transmitter using neural networks," *Electronics Letters*, vol. 49, no. 4, pp. 253-255, Feb. 2013

CHAPTER 4

COMPENSATION OF NONLINEAR DISTORTION FOR MULTI-BRANCH MIMO WIRELESS TRANSMITTERS USING TWO-BOX MODEL

4.1 Introduction

In this chapter, a novel two-box model for the joint compensation of nonlinear distortion introduced from both I/Q modulator and PA for multi-branch MIMO wireless transmitters is proposed [4-1]. Many models have already been proposed in literature [4-2]–[4-4]. A joint predistorter based on PH model is developed for the compensation of both I/Q impairments and PA nonlinearity [4-2]. The main problem using this model is the high complexity. Also, the RatF [4-3] characterises PA nonlinearity and linear I/Q impairments. As a universal approximator and good extrapolator RatF provides more accurate results in comparison with MP model. The only problem is that memory needs to be incorporated in the real system, which will result in an increased model complexity. Furthermore, the dual-input nonlinear model based on the RV series for frequency-dependent linear and nonlinear I/Q impairments is proposed in [4-4]. This RV model as a simplified Volterra structure is still quite impractical in real systems because the number of parameters increases exponentially with higher nonlinear order and memory depth. All three algorithms are developed for SISO transmitters. These algorithms will be extended for multi-branch MIMO applications. Due to the aforementioned drawbacks of the models, a new two-box model for I/Q impairments and PA nonlinearity for multi-branch MIMO wireless transmitter is proposed. The nonlinear distortion is compensated by implementing PD in two phases, where each phase is identified separately and modelled by a lower order of implemented functions (RatF-RV). The proposed two-box model relies on the idea to gradually compensate the nonlinear distortion. It will be shown that by employing the two-box model not only its complexity can be reduced, but also better performance can be achieved. The performance of the proposed model is evaluated through simulations and measurements,

in terms of ACPR, EVM and NMSE improvements using four 3 MHz LTE signals and two WCDMA signals respectively.

4.2 Proposed Approach for Multi-branch MIMO Wireless Transmitters

Multi-branch MIMO wireless transmitters enable increasing both the coverage of wireless transmitters and the capacity without increasing the frequency bandwidth or average transmit power. Therefore, multi-branch MIMO wireless transmitters are becoming one of the most popular designs for wireless communication systems. The simplified block diagram of a dual-branch MIMO wireless transmitter as an example of multi-branch MIMO wireless transmitter is shown in Figure 4.1.

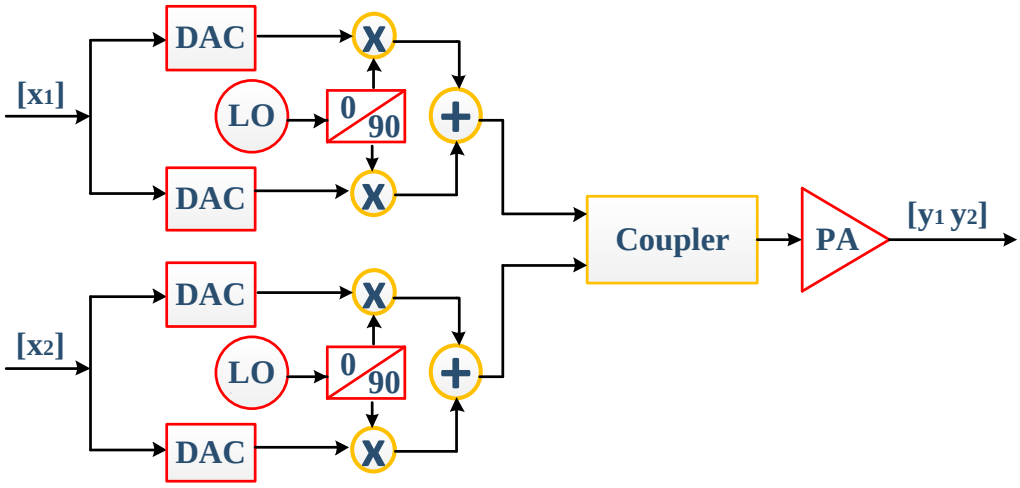

Figure 4.1: Simplified block diagram of dual-branch MIMO wireless transmitter.

As mentioned before, a PA is one of the most challenging blocks in designing a wireless transmitter. Also, the efficiency of the PA significantly affects the overall efficiency of the wireless transmitter. On the one hand, the PA that amplifies the wideband signals with a high PAPR produces distortion, which results in adjacent channel interference and in-band distortion. These significantly degrade the quality of the signal. On the other hand, if the PA operates in the linear region with a large back-off, the power efficiency will be decreased. Hence, it is desired that the PA works in the nonlinear region where it produces nonlinear distortion. The use of dual-branch MIMO wireless transmitters means that two transmission paths will be implemented on the same chipset, which will cause interaction and correlation between the signals. This interaction between the multiple paths is known as a crosstalk effect. Thus, the relation

between inputs (x_1, x_2) and outputs (y_1, y_2) of the dual-branch MIMO wireless transmitter can be presented as:

$$[y_1\ y_2] = A[x_1\ x_2]^T \tag{4.1}$$

where A is a nonlinear matrix presenting nonlinear behaviour (PA nonlinearity and crosstalk) of the dual-branch MIMO wireless transmitter [4-5].

Another component that is critical in designing a wireless transmitter is an I/Q modulator. It is responsible for up-converting the baseband signal to RF frequencies. During the up-conversion process, the I/Q modulator induces distortion to the signal, which can be manifested as an I/Q imbalance, DC offset and LO leakage. These distortions must not be disregarded since they affect the transmitted signal and will further degrade the quality of the transmitted signal. Thus, distortion introduced from the I/Q modulator must be taken into account.

In addition, the modelling process of I/Q impairments is based on the modelling of the cross coupling channels of the I and Q components of the input signal. It can be presented using the conjugate of the input signals (x_1, x_2, ${x_1}^*$, ${x_2}^*$) and the outputs (y_1, y_2):

$$[y_1\ y_2] = B[x_1\ x_2\ {x_1}^*{x_2}^*]^T \tag{4.2}$$

where B is a nonlinear matrix presenting nonlinear behaviour (I/Q impairments, PA nonlinearity and crosstalk) of the dual-branch MIMO wireless transmitter [4-6].

Due to the aforementioned distortion which exists in wireless transmitters, various models such as PH, RatF and RV, are developed for the compensation of nonlinear distortion and the improvement of the quality of signal. As it will be shown in this chapter, using these models a good performance is obtainable. However, a high complexity of the wireless transmitter is an inevitable drawback. Therefore, the two-box model is developed for joint compensation of I/Q impairments, PA nonlinearity and crosstalk effects for multi-branch MIMO wireless transmitters. The use of it brings the identification of each phase separately while the contribution of the previous phase is taken into account. Furthermore, the model is iterative, which means that it will converge after a few system-level iterations.

Figure 4.2 illustrates the steps of the proposed two-box model, which includes implementation of the two phases. System level identification is done separately for each phase. Once phase 1 is identified (Figure 4.2 a), it will be considered as being a part of a new system (Figure 4.2 b), which apart from phase 1 will include an I/Q modulator and a PA as well. Now, in phase 2, which is added to improve the performance, new parameters of the system are identified. This way, it is possible to optimise the identification of any system, which will lead to more accurate results. Accordingly, it is feasible to compensate for residual distortion.

During each iteration, only one phase is processed. Also, both phases are modelled by a lower value of the polynomial order and the memory depth. Compared with the conventional models identification complexity of the proposed two-box model is lower. In addition, the identification complexity is calculated by computing the number of multipliers needed for the identification of the model coefficients. Often, more than one system level iteration must be performed for the identification of phases. Hence, when convergence of phase 1 is finished, it can be persisted with the identification of phase 2. The two-box model is realised by implementing algorithms RatF in phase 1 and RV in phase 2.

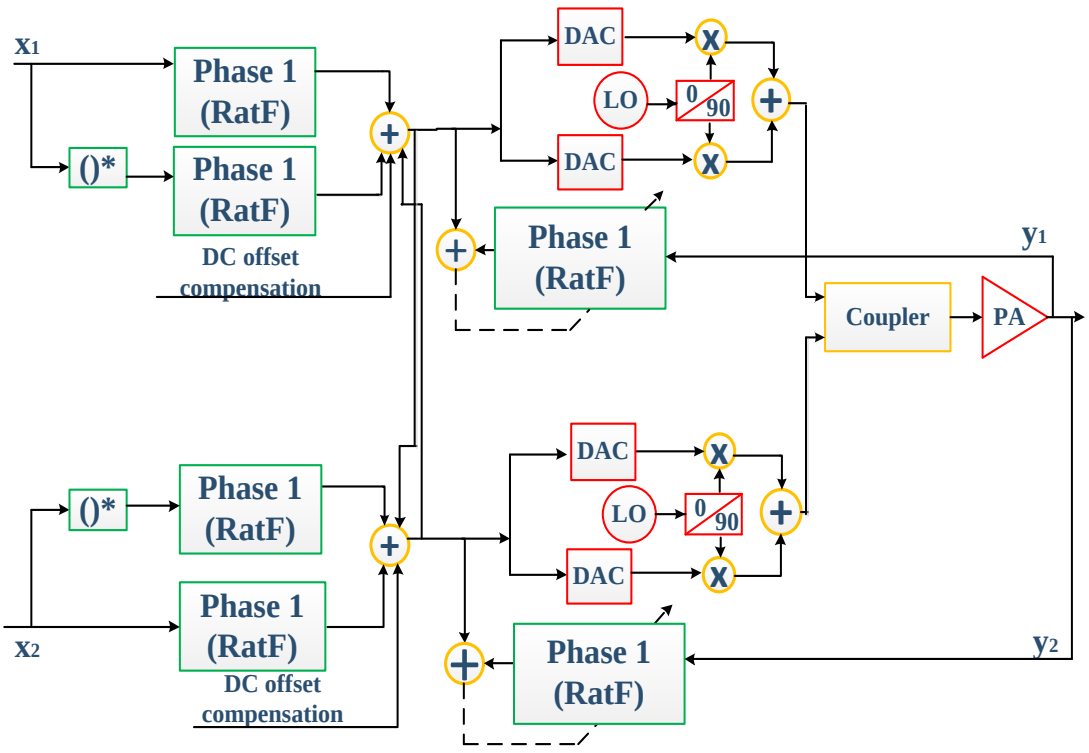

(a)

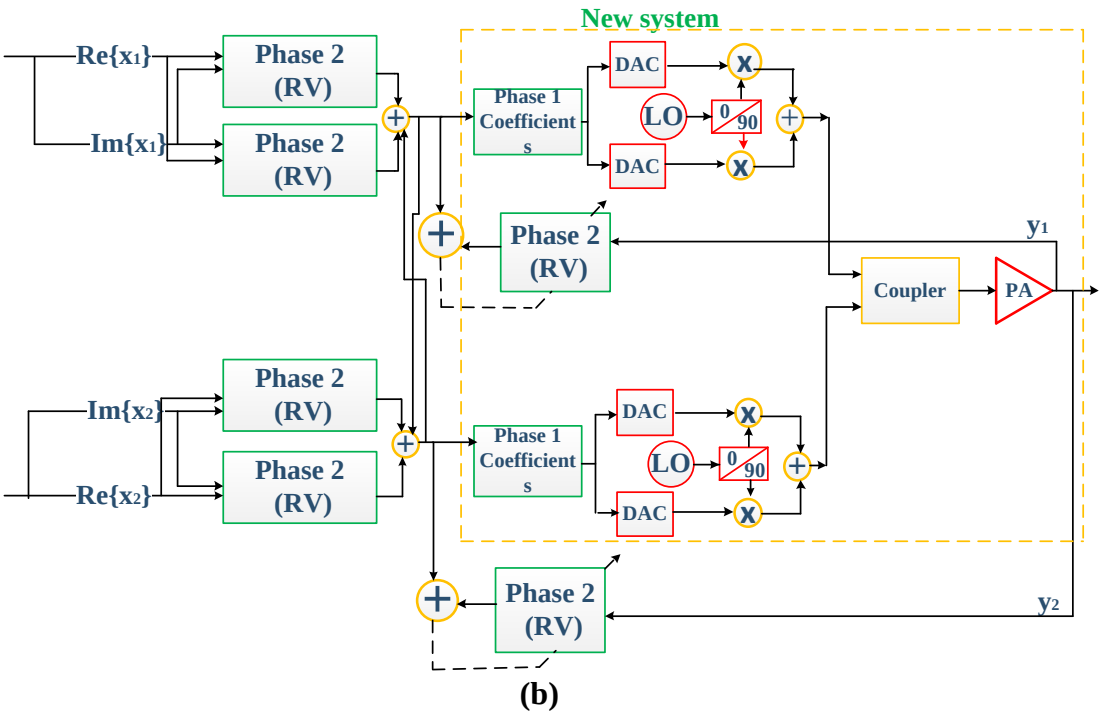

Figure 4.2: Illustration of the two-box model (a) Phase 1; (b) Phase 2.

The concept of RatF uses the ratio of two polynomials for the modelling process, where more information about the signal distortion is attained. The best results in modelling so far were obtained by implementing the Volterra model. The approximation power of RatF is the same as the Volterra model but it can be done with a lower complexity. It also has a better extrapolation ability. Despite all the benefits that are achieved by implementing RatF, the main problem is still complexity. In other words, there is a high number of parameters when a high order of RatF is used.

It is defined as:

$$RatF\{x_1(n)\} = \gamma_1 + \frac{\sum_{q=0}^{Q}\sum_{k=0}^{K} a_{k,q}x_1(n-q)|x_1(n-q)|^k}{1+\sum_{p=1}^{P} b_p x_1(n)|x_1(n)|^p} + \frac{\sum_{q=0}^{Q}\sum_{k=0}^{K} c_{k,q}x_1{}^*(n-q)|x_1(n-q)|^k}{1+\sum_{p=1}^{P} d_p x_1{}^*(n)|x_1(n)|^p} \quad (4.3)$$

where k and p denote the order of the numerator and denominator respectively, γ_1 denotes the DC offset, $a_{k,q}$, b_p, $c_{k,q}$and d_p denote the coefficients of the model, Q denotes the memory depth and $x_1(n)$ denotes the input signal of the phase 1 [4-3]. The above equation in the matrix notation can be written as:

$$\boldsymbol{y} = RatF\{x(n)\} = \boldsymbol{Rh_{phase1}} \quad (4.4)$$

The equation 4.4 is defined as follows:

$$\boldsymbol{y} = [y(1) \dots y(N)], \tag{4.5}$$

where N is the number of samples.

Matrix $\boldsymbol{R}$ represents the matrix which takes both the input and the output samples in case of the RatF structure (as described in [4-3]) and $\boldsymbol{y}$ represents the output samples.

For the mitigation of PA nonlinearity and I/Q imbalance, $\boldsymbol{R}$ matrix can be written as:

$$\boldsymbol{R} = [\boldsymbol{r_1} \vdots \boldsymbol{r_1^*}] \tag{4.6}$$

To account for I/Q compensation, $\boldsymbol{r_1^*}$ has been appended to $\boldsymbol{r_1}$ matrix, which is defined as:

$$\boldsymbol{r_1} = \begin{pmatrix} X_{i,0}(1) \dots X_{i,M}(1) - y(1)x(1)|x(1)| \dots - y(1)x(1)|x(1)|^J \\ X_{i,0}(2) \dots X_{i,M}(2) - y(2)x(1)|x(2)| \dots - y(2)x(2)|x(2)|^J \\ \vdots \\ X_{i,0}(N) \dots X_{i,M}(N) \ - y(N)x(N)|x(N)| \dots - y(N)x(N)|x(N)\ |^J \end{pmatrix} \tag{4.7}$$

Also, complex input vector is expressed as:

$$X_{i,m}(N) = [x(N-m) \dots x(N-m)|x(N-m)|^i]. \tag{4.8}$$

Using LS solution [4-7], coefficients of the model in phase 1 can be calculated as follows:

$$\boldsymbol{h_{phase1}} = (\boldsymbol{R}^H\boldsymbol{R})^{-1}\boldsymbol{R}^H\boldsymbol{y} \tag{4.9}$$

these values represent the model coefficients in phase 1 ($\boldsymbol{h_{phase1}}$).

The increase of the nonlinear order and the memory depth of the RatF model can lead to non-realistic estimated coefficients. Moreover, the nonlinearities that exist in the I and Q branches of the I/Q modulator cannot be compensated for by using RatF models. These limitations of the model can be avoided using phase 2. The advantage of using a model based on RV series in phase 2 of the proposed two-box model is a possibility to manipulate the real numbers instead of complex numbers, which reduces the complexity of the algorithm. With such implementation, not only the terms from each branch are

included, but also the cross terms between the I and Q branches. In other words, it can model both the linear and the nonlinear I/Q impairments.

The RV is described as:

$$RV_1\{x(n)^I, x(n)^Q\} = \sum_{m_1=0}^{M} \boldsymbol{h}_{1m_1}^T \boldsymbol{x}_{m_1} + \sum_{m_1=0}^{M} \sum_{m_2=m_1}^{M} \boldsymbol{h}_{1m_1m_2}^T \left(\boldsymbol{x}_{1m_1} \otimes \boldsymbol{x}_{1m_2}\right) + \\ \dots \sum_{m_1=0}^{M} \dots \sum_{m_K=m_{K-1}}^{M} \boldsymbol{h}_{1m_1\dots m_K}^T \left(\boldsymbol{x}_{1m_1} \otimes \dots \otimes \boldsymbol{x}_{1m_K}\right) \quad (4.10)$$

where $\boldsymbol{h}_{1m_1\dots m_K}$ and $k \in K$ (and$m_k \in M$) are the coefficients of the model determined in phase 2, K and M are the polynomial order and the memory depth respectively and $\boldsymbol{x}_{1m_1}$ is the input of the phase 2 [4-4]. The symbol $\otimes$ is used to denote Kronecker product and it is defined as:

$$\begin{bmatrix} a_1 \\ a_2 \end{bmatrix} \otimes \begin{bmatrix} b_1 \\ b_2 \end{bmatrix} = \begin{bmatrix} a_1 b_1 \\ a_1 b_2 \\ a_2 b_1 \\ a_2 b_2 \end{bmatrix} \quad (4.11)$$

In equation 4.6, information from I and Q signals is separately used to create dual-input real-valued coefficients for the I and Q branches. In addition, for the modelling of an I/Q modulator and its impairments, all nonlinear terms must be included, not only odd terms as in the case of PA modelling.

Also, vectors $\boldsymbol{h}$ and $\boldsymbol{x}$ are defined as:

$$\boldsymbol{h}_{m_1\dots m_p} = [h_{m_1\dots m_p,1}\ h_{m_1\dots m_p,2}\ , \dots h_{m_1\dots m_p,2^p}\ ]^T \quad (4.12)$$

and

$$\boldsymbol{x}_{m_p} = \begin{bmatrix} x^I(n-m_p) \\ x^Q(n-m_p \end{bmatrix} \quad (4.13)$$

Coefficients in phase 2 can be determined using LS solution [4-7] as follows:

$$\boldsymbol{h}_{\boldsymbol{phase2}} = (\boldsymbol{X}^H \boldsymbol{X})^{-1} \boldsymbol{X}^H \boldsymbol{y} \quad (4.14)$$

where these values represent coefficients of the model.

The block diagram of the proposed DPD, which is based on the two-box model described previously, is shown in Figure 4.3, where LS solution is used for the calculation of the DPD coefficients in both stages. For DPD implementation, ILA is utilised, where a post-inverse is identified and used as a pre-inverse. The main goal of using this structure is to progressively mitigate the linear and nonlinear distortion. The principle is based on the compensation in two phases. In phase 1, one part of distortion from I/Q modulator and PA is compensated. As the complexity of the RatF model rises fast with the increase of the nonlinear order and the memory depth, it is used as a technique which partly compensates for nonlinear distortion and prepares the signal for using the RV model. After phase 1, the predistorted signal is now used as the new input in the transmitter front-end. In other words, RatF will derive a new output signal for phase 2. This signal will be used to determine the coefficients of phase 2.

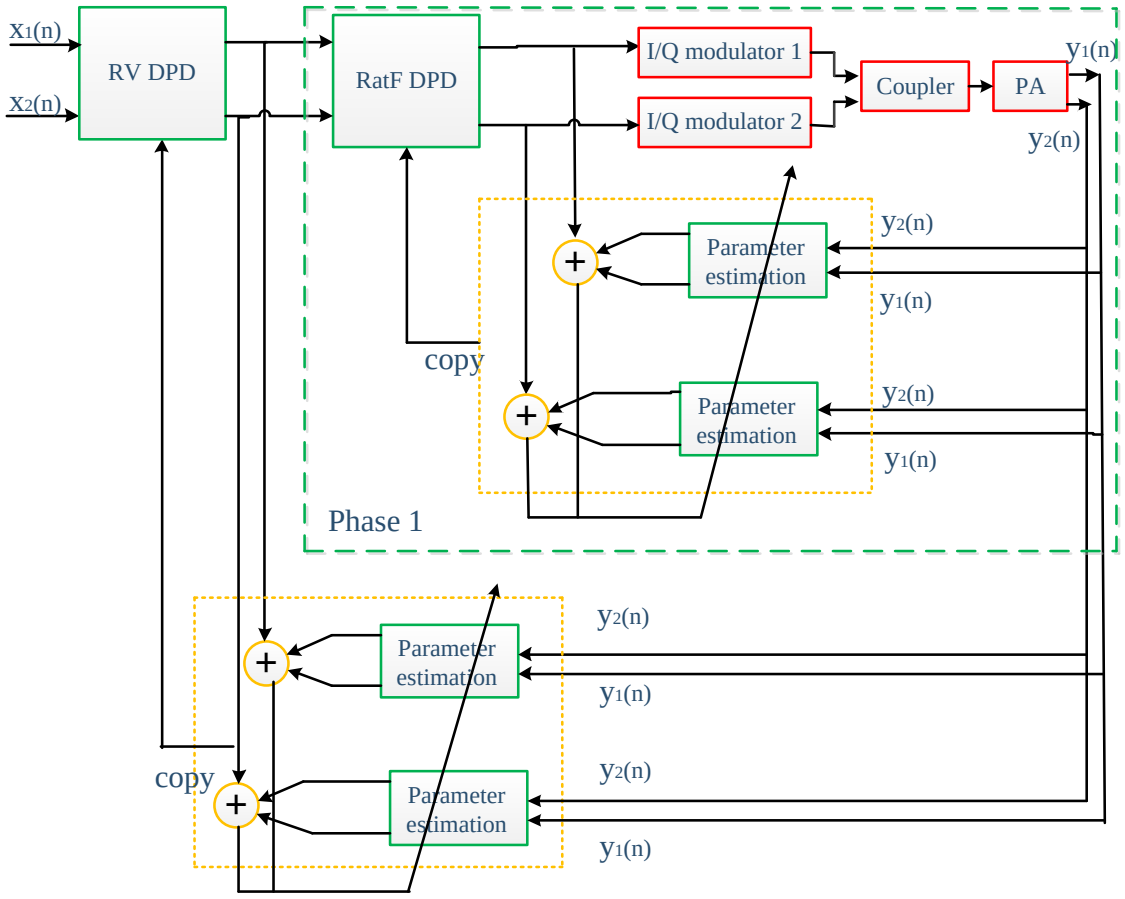

Figure 4.3: ILA of a two-box DPD.

4.3 Least Square Solution

The easiest way for estimating model coefficients using LS algorithm [4-7] is to first collect the coefficients in equations (4.3) or (4.6), into one vector $\boldsymbol{h}$ ($J \times 1$, where J is the total number of coefficients). These coefficients appear as a linear weighting of

nonlinear signals, such as in equations (4.3) and (4.6). Each component of the coefficient vector $\boldsymbol{h}$ is associated with a signal whose time samples over some period ($n = 1, 2 \ \ldots N$), are collected into a vector $\boldsymbol{h}$.

For example, in equation 4.3, coefficient a_{21} is associated with the signal $x(n-1)|x(n-1)|^2$, whose time samples define an $N \times 1$ vector. Assembling all such vectors into a $N \times J$ matrix $\boldsymbol{X}$, the model output can then be compactly expressed as:

$$\tilde{\boldsymbol{y}} = \boldsymbol{X}\boldsymbol{h} \tag{4.15}$$

Where $\tilde{\boldsymbol{y}}$ is an $N \times 1$ vector that designates an estimate of the actual output vector $\boldsymbol{y}$. Hence, the inverse modelling method used in the predistortion technique, where the input $\boldsymbol{x}$ is being estimated from the output samples $y(n)$ ($n = 1, 2 \ \ldots N$), is written as:

$$\tilde{\boldsymbol{x}} = \boldsymbol{Y}\boldsymbol{d} \tag{4.16}$$

where $\tilde{\boldsymbol{x}}$ is an $N \times 1$ vector that designates an estimate of the actual input vector $\boldsymbol{x}$, and $\boldsymbol{d}$ vector presents DPD coefficients. Matrix $\boldsymbol{Y}$ is constructed in a similar way as matrix $\boldsymbol{X}$, where $y(n-q)$ is replaced with $x(n-q)$. This is the actual form of the estimation employed in the context of predistortion applications. Also, the estimation error $e(n)$ is written:

$$e(n) = x(n) - \tilde{x}(n) \tag{4.17}$$

Similarly in vector form, estimation error is expressed:

$$\boldsymbol{e} = \boldsymbol{x} - \tilde{\boldsymbol{x}} \tag{4.18}$$

Therefore, the LS solution that minimises $\|\boldsymbol{e}\|^2$ as follows:

$$\boldsymbol{d} = (\boldsymbol{Y}^H\boldsymbol{Y})^{-1}\boldsymbol{Y}^H\boldsymbol{x}. \tag{4.19}$$

4.4 Simulation Results

The system level simulation was performed in Matlab. 3 MHz LTE (64 QAM OFDM) signals were created and passed through a four-branch MIMO wireless transmitter. In these simulations, different bit streams were sent in each of the four signal paths. Therefore, spatially multiplexed four-branch MIMO wireless transmitters were analysed. Taylor series PA model for real Mini-Circuits ZFL-500 PA was extracted experimentally and this model was used in simulations. The model from [4-8] was used

in order to simulate the non-linear distortion and linear static errors (DC offset, gain and phase imbalance) for an I/Q modulator. Also, an amount of -15 dB nonlinear crosstalk is introduced in four-branch MIMO wireless transmitters.

In order to evaluate the compensation of the nonlinear distortion, accuracy of the models and its complexity, the following parameters were calculated and are presented in Table 4.1: ACPR, EVM, NMSE, floating point operations (FLOPs) [4-9] and number of coefficients. The numbers of coefficients ($\boldsymbol{No.Coef}$) and FLOPs of tested models have been derived and the following forms are:

$$No.Coeff_{PH} = No.branches(2M\sum_{k=0}^{K}(k+1)+1) \tag{4.20}$$

$$FLOPs_{PH}(K,M) = \underbrace{No.branches[2(3+\sum_{k=1}^{K}(k+1))]}_{C_{basis}} + \underbrace{No.branches[8(2M\sum_{k=0}^{K}(k+1))-2+1]}_{C_{filter}} \tag{4.21}$$

$$No.Coeff_{RatF} = No.branches(2(K+1)(Q+1)+2P+1) \tag{4.22}$$

$$FLOPs_{RatF}(K,Q,P) = \underbrace{No.branches[3+2\max(K,P)]}_{C_{basis}} + \underbrace{No.branches\{[8(2(K+1)(Q+1))-2]+[8(2P)-2]+1+9]\}}_{C_{filter}} \tag{4.23}$$

$$No.Coeff_{RV} = \sum_{p=1}^{P}\{2^p\left[\sum_h\left(\sum_{m_1}^{M}\sum_{m_2=m_1}^{M}\cdots\sum_{m_{p=m_{p-1}}}^{M}h_{m_1m_2\ldots m_p}\right)\right]\} \tag{4.24}$$

$$FLOPs_{RV}(K,M) = \underbrace{\sum_{k=2}^{K}2^k}_{C_{basis}} + \underbrace{2No.Coeff_{RV}-1}_{C_{filter}} \tag{4.25}$$

The number of FLOPs is calculated as sum of C_{basis} and C_{filter} which is defined as in [4-9].

Moreover, the output spectra of system for different models are shown in Figure 4.4. Furthermore, the results of AM/AM and AM/PM of PA output signal are presented in Figures 4.5 and 4.6, respectively.

Model (orders K, Q, P and K, M)	ACPR (dBc) ±2.5MHz	EVM (%)	NMSE (dB)	FLOPs	No. Coeff
Without DPD	-29.0	18.4535	-17.2597	/	/
PH (5, 5)	-39.1	3.9854	-26.4829	6900	844 (complex)
(5, 3)	-38.3	4.5656	-24.8978	4212	508 (complex)
(4, 3)	-36.9	5.7841	-23.1201	3012	364 (complex)
RatF (5, 5, 4)	-40.2	2.8358	-29.8938	2636	324 (complex)
(4, 3, 2)	-39.4	3.8772	-27.5478	1476	180 (complex)
(3, 2, 1)	-37.6	4.3356	-26.2134	892	108 (complex)
RV (5, 3)	-37.7	5.8360	-24.8899	10476	8x2560(real)
(4, 3)	-36.1	6.4545	-23.6281	6364	8x768 (real)
(3, 2)	-34.8	7.2918	-22.0015	924	8x110 (real)
Two-box RatF (5, 3, 2) – RV (3, 1)	-44.0	0.9966	-34.7057	Ph.1: 1740 Ph.2: 118	Ph.1:212 (complex) Ph.2: 8x48 (real)
RatF (4, 3, 2) – RV (3, 2)	-43.4	1.1531	-33.8749	Ph.1: 1476 Ph.2: 924	Ph.1: 180(complex) Ph.2: 8x110(real)
RatF (3, 2, 1) – RV (3, 1)	-41.1	1.4471	-31.7497	Ph.1: 892 Ph.2: 118	Ph.1: 108(complex) Ph.2: 8x48(real)

Table 4.1: Performance of the models.

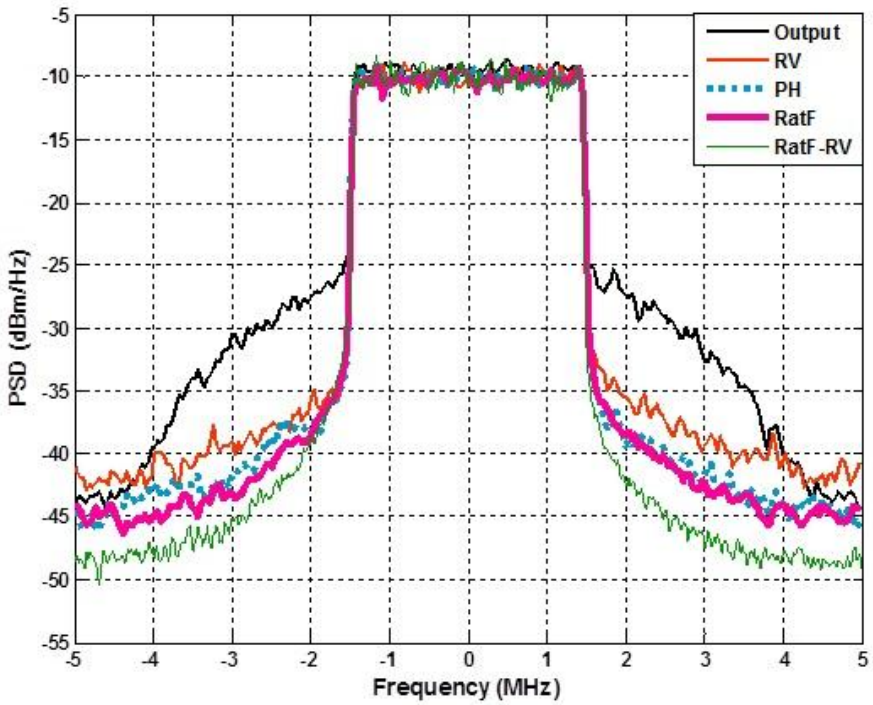

Figure 4.4: Power spectra of the proposed two-box DPD and its comparison with the existing models.

As it can be seen, the two-box model (RatF-RV) decreases the ACPR to -44 dBc. Also, EVM and NMSE go as low as 0.99 %, and -34 dB respectively, which indicate that the two-box model is able to successfully compensate for I/Q impairments and PA nonlinearity in four-branch MIMO wireless transmitters.

It is worth mentioning that RV deals with real coefficients. This leads to reduced computational load of the two-box model in comparison with studied models, since they have complex coefficients. The existence of two phases in the two-box model enables scaling down the nonlinear order and the memory depth as well. Compared with studied models, the proposed model significantly decreased the number of FLOPS.

By comparing results obtained using one model of cascade (RatF or RV), with the two-box model, it is shown that the proposed model not only achieves better performance, but also reduces the numbers of both FLOPs and coefficients. The RV model, as a modified Volterra structure can compensate for the nonlinear distortion introduced from both, I/Q modulator and PA. The main drawback is the exponential increase of the number of coefficients.

It can be seen from Table 4.1 that with decrease of the polynomial order and the memory depth the complexity of the wireless transmitter reduces accordingly. In case when the best modeling performances are achieved the proposed two-box model reduces the numbers of both FLOPs and coefficients in comparison with the studied models. The optimal results are obtained using $K = 5, Q = 3, P = 2$ for the RatF and $K = 3, M = 1$ for RV, where K, Q and P are defined as in the equation 4.3 and K and M as in the equation 4.10. It is possible to derive result which can be satisfactory for some application and reduce even more complexity, as in case $K = 3, Q = 2, P = 1$ for the RatF and $K = 3, M = 1$ for the RV.

As it can be noticed from Figures 4.5 and 4.6, strong gain and phase compression are manifested at PA output signal (DPD off case). By using the RV model this dispersion is reduced but its level is still high. Compared with the RV model, the PH and the RatF models give better results. However, the results after applying the proposed two-box model show that the AM/AM and AM/PM curves are thinner and the output amplitude has been thoroughly linearised.

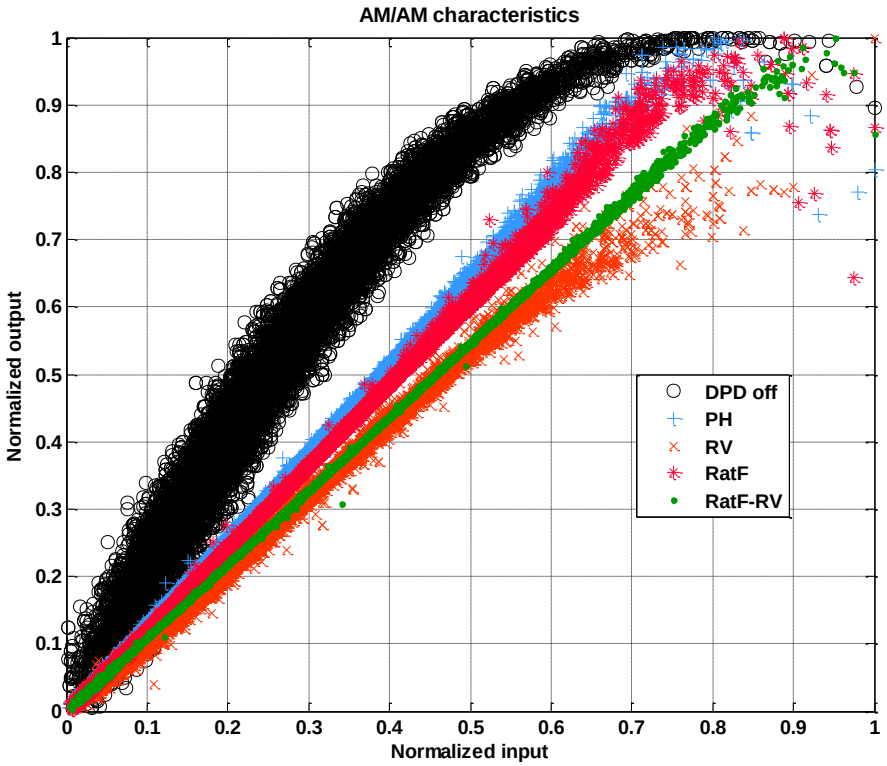

Figure 4.5: AM/AM curves of the proposed two-box DPD and its comparison with the existing models.

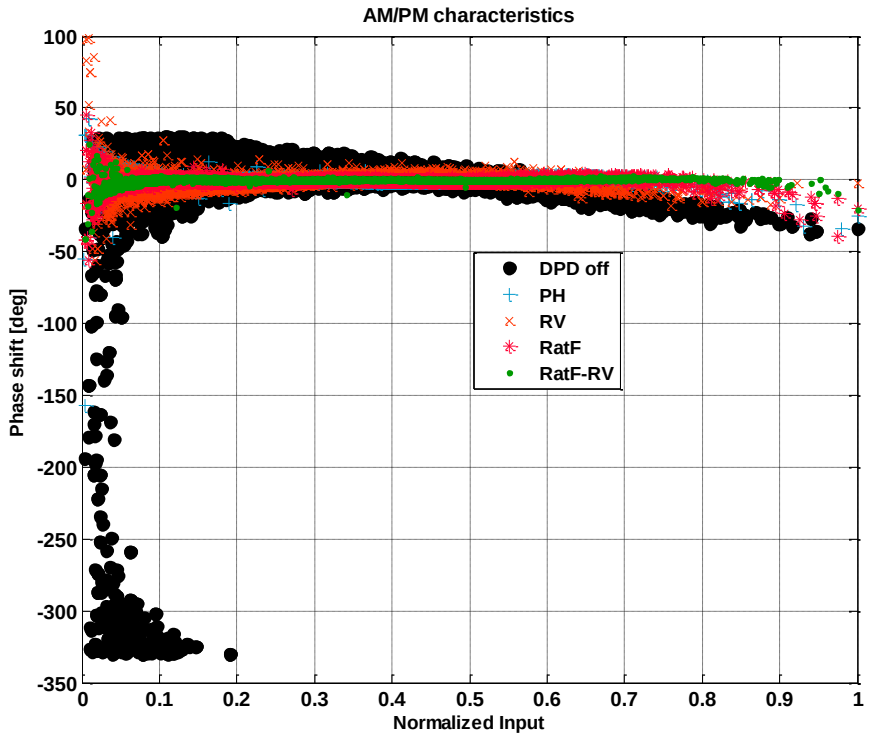

Figure 4.6: AM/PM curves of the proposed two-box DPD and its comparison with the existing models.

4.5 Experimental Results

Experiments were carried out using the measurement setup shown in Figure 4.7. It consisted of two signal generators, Keysight MXG N5182A and ESG E4433B, which were used to emulate the dual-branch MIMO wireless transmitter. The coupler was utilised in order to model the crosstalk effect that appears in the dual-branch MIMO wireless transmitter's paths. A Mini-Circuits ZFL-500 PA was used as the DUT for measurement. This DUT was fed by two WCDMA signals on the same frequency with the same input power with an imbalance artificially introduced I/Q offset of 3% and 5% respectively and 3° I/Q skew. This signal with 20 dB nonlinear crosstalk effect was passed through the model which created a predistorted signal. Finally, the predistorted signal was provided to the Keysight MXG N5182A signal generator, where it was up-converted to RF. The linearised signal was down-converted by the Keysight VSA and captured by the 89600 VSA software running on the PC. The polynomial order (K and P) and memory depth (Q and M) were varied during the measurement until the proposed and tested algorithms achieved the best performance.

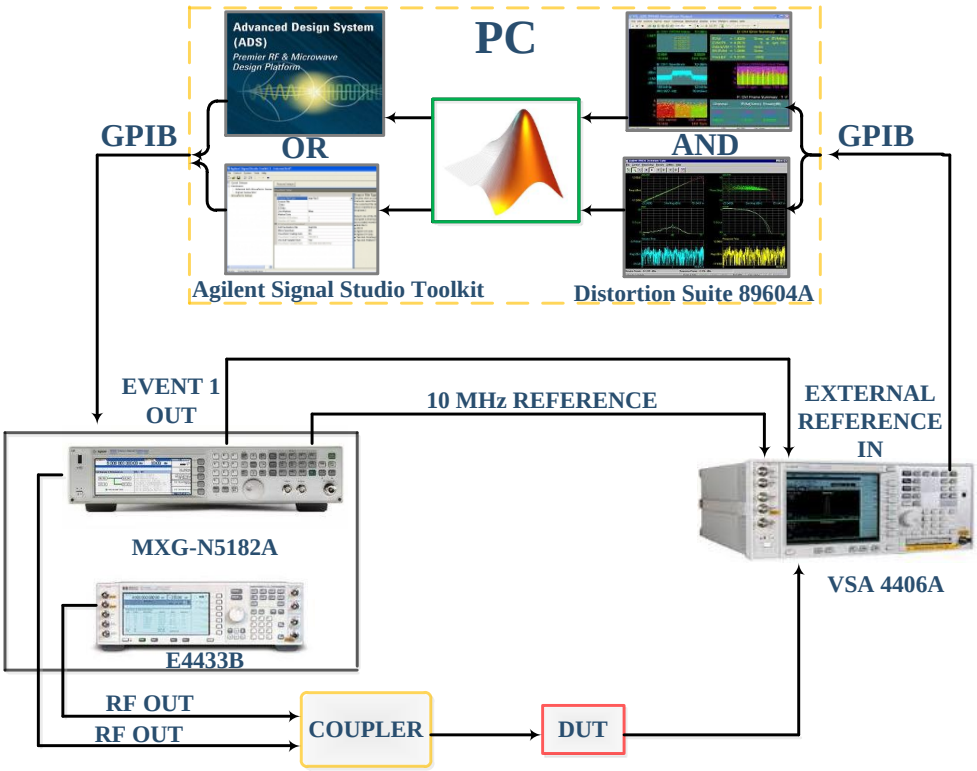

Figure 4.7: Measurement setup.

In order to evaluate the compensation of the nonlinear distortion, accuracy of the model and its complexity, the following parameters were calculated and presented in Table

4.2: ACPR, EVM, NMSE, FLOPs and the number of coefficients. The optimal values of the polynomial order (K and P) and memory depth (Q and M) for the experiment are given in the Table 4.2. These values are obtained using trial measurements. Furthermore, the output spectra of transmitter for the different models are shown in Figure 4.8.

Model (orders K, Q, P and K, M)	**ACPR (dBc) $\pm$2.5 MHz**	**EVM (%)**	**NMSE (dB)**	**FLOPs**	**No. Coeff**
Without DPD	-26.8	15.0035	-20.3568	/	/
PH (5, 4)	-32.5	3.6572	-27.7222	820	102 (complex)
RatF (5, 3, 4)	-38.2	1.5511	-31.9856	954	130 (complex)
RV (4, 2)	-29.2	6.2153	-22.1520	1578	4x382 (real)
Two-box RatF (4, 3, 2) – RV (3, 1)	-40.5	0.0973	-37.3376	Ph.1: 738 Ph.2: 118	Ph.1:90 (complex) Ph.2: 4x48 (real)

Table 4.2: Performance of the models.

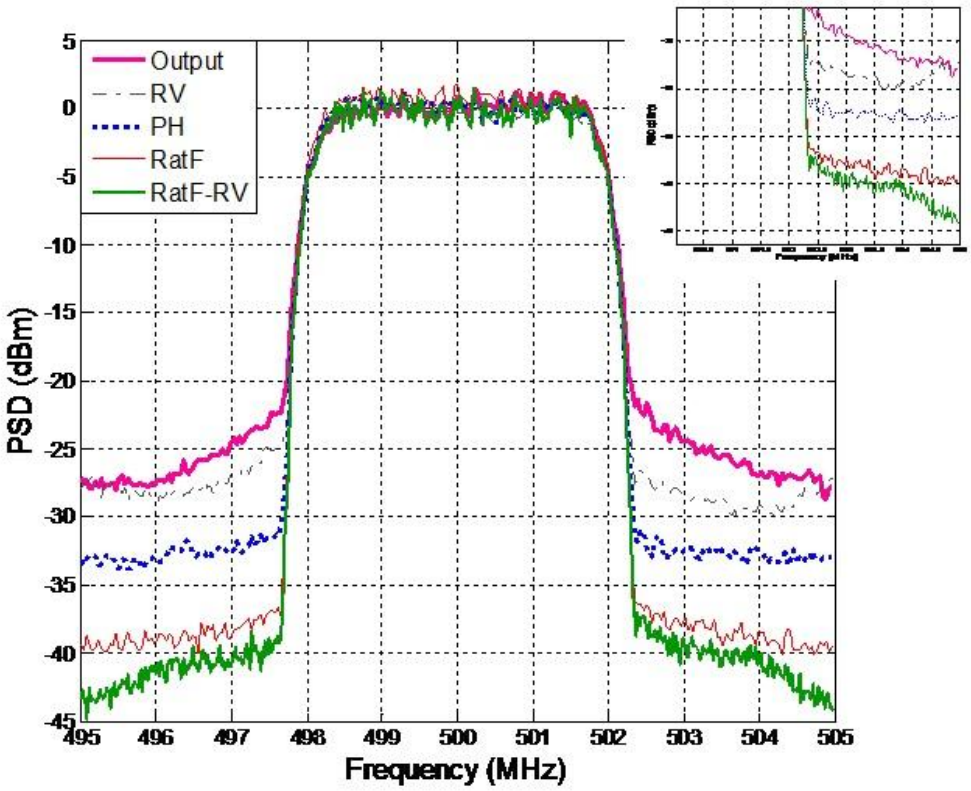

Figure 4.8: Power spectra of the proposed two-box DPD and its comparison with the existing models.

The two-box model (RatF-RV) decreases the ACPR to less than -40.5 dBc. Also, EVM and NMSE go as low as 0.09 %, and -37 dB respectively, which indicate that the two-box model is able to successfully compensate for I/Q impairments and PA nonlinearity in the dual-branch MIMO wireless transmitter.

The complexity rises very high with the increase in the polynomial order and memory depth of the RatF. It is implemented as phase 1 of the two-box model which will partly compensate for the PA nonlinearity, I/Q impairments and crosstalk effects. With such an implementation number of both, FLOPs and coefficients are lower in comparison with the studied models. Existence of phase 2 in this two-box model enables further compensation of nonlinear distortion which exists in the dual-branch MIMO wireless transmitter. Also, the computational load of the two-box model based on the RatF-RV is low. In other words, complexity is significantly reduced.

4.6 Summary

A new two-box model for the joint compensation of I/Q impairments, PA nonlinearity and crosstalk effects for multi-branch MIMO wireless transmitters has been proposed. The nonlinear distortion is compensated by implementing the PD in two phases, where each phase is identified separately and modelled by a lower order of implemented functions (RatF and RV). The model relies on the idea to gradually compensate the nonlinear distortion. This significantly minimises the complexity of the modelling process. By comparing results obtained using PH and RatF models with the proposed model, it is shown that the numbers of both, the FLOPs and the coefficients are reduced while performance is at a high level. It also achieves improvements in ACPR, EVM and NMSE.

4.7 References

[4-1] M. Bozic and D. Budimir, "Joint compensation of I/Q impairments, power amplifier nonlinearity and crosstalk in MIMO transmitters using two-box model," *European Microwave Conference (EuMC)*, vol., no., pp. 1120-1123, Sept. 2015

[4-2] L. Anttila, P. Handel and M. Valkama, “Joint mitigation of power amplifier and I/Q modulator impairments in broadband direct-conversion transmitters,” *IEEE*

Transactions on Microwave Theory and Techniques, vol 58, no.4, pp. 730-739, April 2010

[4-3] M., Aziz, M. Rawat and F.M. Ghannouchi, "Rational function based model for the joint mitigation of I/Q imbalance and PA nonlinearity," *IEEE Microwave and Wireless Components Letters*, vol. 23, no. 4, pp. 196-198, April 2013

[4-4] C. Haiying, A.S. Tehrani, C. Fager, T. Eriksson and H. Zirath, "I/Q imbalance compensation using a nonlinear modeling approach," *IEEE Transactions on Microwave Theory and Techniques*, vol. 57, no. 3, pp. 513-518, March 2009

[4-5] S. A Bassam., M. Helaoui and F. M. Ghannouchi, "Crossover Digital Predistorter for the Compensation of Crosstalk and Nonlinearity in MIMO transmitters" *IEEE Transactions on Microwave Theory and Techniques*, vol. 57, no. 5, pp. 1119-1128, May 2009

[4-6] S. A Bassam, M. Helaoui, S. Boumaiza and F. M. Ghannouchi "Experimental study of the effects of RF front-end imperfection on MIMO transmitter performance," *IEEE MTT-S International Microwave Symposium Digest*, vol., no., pp. 1187-1190, June 2008

[4-7] D. Morgan, Z. Ma, J. Kim, M. Zierdt and J. Pastalan, "A generalized memory polynomial model for digital predistortion of RF power amplifiers," *IEEE Transactions on Signal Processing*, vol. 54, no., pp. 3852–3860, Oct. 2006

[4-8] M. Li, L. Hoover, K.G. Gard and M.B. Steer, "Behavioural modelling and impact analysis of physical impairments in quadrature modulators," *IET in Microwaves, Antennas & Propagation*, vol. 4, no. 12, pp. 2144-2154, Dec. 2010

[4-9] A.S. Tehrani, C. Haiying, S. Afsardoost, T. Eriksson, M. Isaksson and C. Fager, "A comparative analysis of the complexity/accuracy tradeoff in power amplifier behavioral models," *IEEE Transactions on Microwave Theory and Techniques*, vol. 58, no. 6, pp. 1510-1520, June 2010

CHAPTER 5

COMPENSATION OF NONLINEAR DISTORTION FOR CONCURRENT DUAL-BAND WIRELESS TRANSMITTERS USING TWO-BOX MODEL

5.1 Introduction

A novel two-box model for the joint compensation of nonlinear distortion introduced from both I/Q modulator and PA for concurrent dual-band wireless transmitters is proposed [5-1]. To achieve strong service demands, wireless transmitters need to incorporate different standards at the same time, which result in processing different signals within different frequency bands [5-2]–[5-3]. This implies the use of PAs that accommodate concurrent signals at different frequency bands. The nonlinear behavior of the dual-band PA is not the same as one in the single band, but it is more emphasised. The existence of I/Q modulators ensue generating and processing the I and Q channel inputs separately. Due to hardware imperfections of an I/Q modulator, the differences may appear between I and Q signals. These differences introduce further distortion to the signals. Therefore, during the DPD development the presence of I/Q impairments must be taken into account.

Many models have already been proposed in literature [5-4]–[5-11]. Joint predistorter based on 2D-DPD model is developed for the compensation of both I/Q impairments and PA nonlinearity (2D-DPD for I/Q) [5-4]. The main problem using this model is the high complexity which is directly involved with the existence of three summations. Also, the low complexity 2D-DPD (LC 2D-DPD) model proposed in [5-5] does not take into account I/Q impairments. Therefore, this model will be extended to compensate for I/Q impairments (LC 2D-DPD I/Q). As it will be shown, LC 2D-DPD for I/Q reduces the complexity of the detriment of accuracy.

The Wiener and Hammerstein models are known as two-box models. These models adapt/employ a cascade of nonlinear function and linear filter to model the nonlinear component [5-6]. In other words, they assume that the memory effects are linear. In practice, due to thermal, non-ideal impedance matching and bias circuit modulation effects, it was found that nonlinear component exhibit nonlinear dynamics, which cannot be ignored [5-7]. Since, these models do not take into account the nonlinear memory effects and cross-terms, they limit the modeling performance. Therefore, the forward twin-nonlinear two-box (FTNTB) model as more general implementation of the Hammerstein model was proposed in [5-8]. The FTNTB model uses a memory polynomial function as the second one, which is able to take into account the nonlinear memory effects. In this way, the overall performance of the Hammerstein model was improved. The FTNTB model is developed for single band transmitters. For the compensation of nonlinear distortion introduced by the PA in concurrent dual-band wireless transmitter 2D forward twin nonlinear two-box (2D-FTNTB) model was developed in [5-9]. The proposed 2D-FTNTB model presents 2D-Hammerstein structure, which is consisted of two memoryless 2D-DPD models followed by two memory 2D-DPD. However, as the nonlinearity order and the memory depth increase, the condition number of the Vandermonde matrix that needs to be inverted while identifying memory polynomial coefficients increase drastically. It can be concluded that complexity using 2D-FTNTB rises fast with increase of the nonlinear order and the memory depth. Also, the models mentioned before are not developed to take into account the I/Q impairments.

Moreover, the RatF [5-10] characterises PA nonlinearity and linear I/Q impairments for single band wireless transmitters. As a universal approximator and a good extrapolator, RatF provides more accurate results in comparison with the MP model. The only problem is that memory needs to be incorporated in the real system, which will result in an increased model complexity. Furthermore, the dual-input nonlinear model based on the RV series for frequency-dependent linear and nonlinear I/Q impairments is also developed for single band transmitters [5-11]. In this letter, RatF and RV models will be extended for the concurrent dual-band transmitters (2D-RatF and 2D-RV). This RV model as a simplified Volterra structure is still quite impractical in real systems because the number of parameters increases exponentially with a higher nonlinear order and memory depth.

Therefore, a new two-box model for I/Q impairments and PA nonlinearity for concurrent dual-band wireless transmitter is proposed. Using the proposed two-box model, the nonlinear distortion is compensated by implementing PD in two phases, where each phase is identified separately and modelled by the lower order of implemented functions (2D-RatF and 2D-RV). The proposed two-box model relies on the idea to gradually compensate the nonlinear distortion. It will be shown that by employing the two-box model not only its complexity can be reduced, but also better performance can be achieved. The performance of the proposed model is evaluated in terms of ACPR, EVM and NMSE improvements using 1.4 MHz LTE and WCDMA signals.

5.2 Proposed Approach for Concurrent Dual-band Wireless Transmitters

Concurrent dual-band wireless transmitters support two different standards in different frequency bands. In other words, two modulated signals are transmitted simultaneously. Therefore, the nonlinear behaviour of these transmitters is much more noticeable since the in-band and out-of-band IM and CM products contribute further to the signal distortion. Around each carrier frequency, stand in-band IM products that are similar to those in single-band wireless transmitters. Out-of-band IM products are placed between two signals located far from the desired ones and can be easily filtered out. CM products represent IM products between signals in both frequency bands which appear in the same frequency bands as in-band IM products. It can be concluded that in-band IM and CM products cause bandwidth regrowth and introduce interference to the signals which is much greater than single-band wireless transmitters. Hence, new DPD model must be developed to take into account all these effects together with I/Q impairments and PA nonlinearity.

Compensation of nonlinear distortion is accomplished by using independent processing blocks for both frequency bands. In this way, the sampling rate requirements of both converters, the digital-to-analogue and analogue-to-digital, are reduced. Figure 5.1 illustrates the steps of the proposed two-box model, which includes the implementation of the two phases.

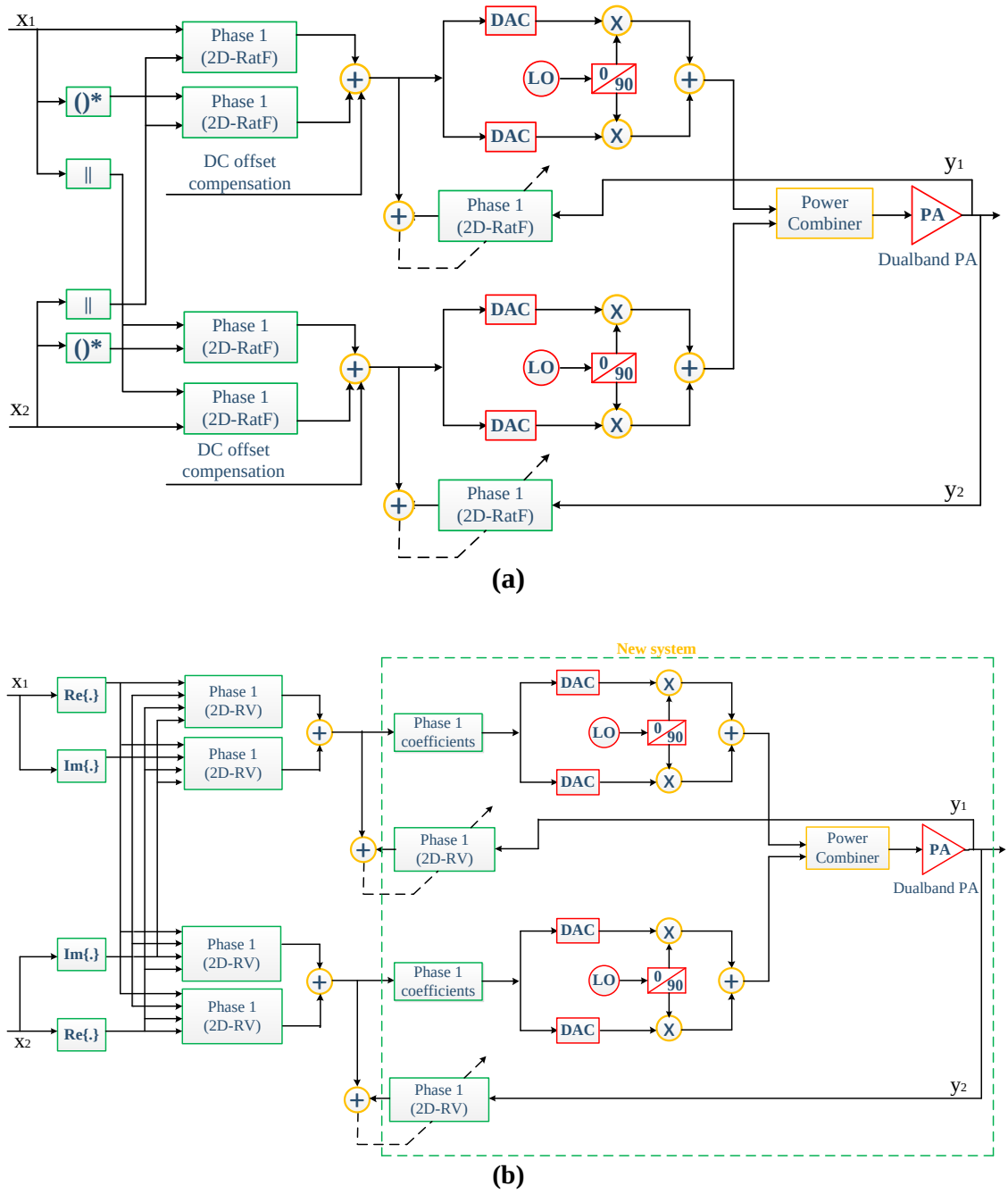

Figure 5.1: Illustration of the two-box model (a) Phase 1; (b) Phase 2.

System level identification is done separately for each phase. Once a phase 1 is identified (Figure 5.1(a)), it will be considered as being a part of a new system (Figure 5.1(b)), which, apart from phase 1, will include I/Q modulator and PA as well. Now, in phase 2, which is added to improve the performance, new parameters of the system are identified. This way, it is possible to optimise the identification of any system, which will lead to more accurate results. Accordingly, it is feasible to compensate residual distortion.

The two-box model is realised by implementing the algorithms 2D-RatF in phase 1 and 2D-RV in phase 2. The concept of 2D-RatF uses the ratio of two polynomials for the modelling process. Thus, more information about the signal distortion is attained. It is defined as:

$$2D - RatF\{x_1(n)\} = \gamma_1 + \frac{\sum_{q=0}^{Q}\sum_{k=0}^{K}\sum_{j=0}^{k} a_{k,j,q}x_1(n-q)|x_1(n-q)|^{k-j}|x_2(n-q)|^j}{1+\sum_{p=1}^{P}\sum_{m=1}^{p} b_{p,m}x_1(n)|x_1(n)|^{p-m}|x_2(n)|^m} + \frac{\sum_{q=0}^{Q}\sum_{k=0}^{K}\sum_{j=0}^{k} c_{k,j,q}x_1^*(n-q)|x_1(n-q)|^{k-j}|x_2(n-q)|^j}{1+\sum_{p=1}^{P}\sum_{m=1}^{p} d_{p,m}x_1^*(n)|x_1(n)|^{p-m}|x_2(n)|^m} \quad (5.1)$$

where k and p denote the order of the numerator and denominator respectively, $a_{k,j,q}$, $b_{p,m}$, $c_{k,j,q}$, $d_{p,m}$ and γ_1 are the model coefficients, Q is the memory depth, $x_1(n)$ and $x_2(n)$ are the input signals.

The above equation can be developed in a matrix form as follows:

$$\boldsymbol{y}_i = RatF\{x^{(i)}(n)\} = \boldsymbol{R}^{(i)}\boldsymbol{h}_{phase1}^{(i)} \quad (5.2)$$

where $i = 1, 2$ are indexes used to indicate the lower and the upper frequency bands.

The parameters in the above equation are defined as follows:

$$\boldsymbol{y}_i = [y_i(1) \dots y_i(N)], \quad (5.3)$$

where N is the number of samples.

Matrix $\boldsymbol{R}^{(i)}$ represents the matrix which takes both the input and the output samples in case of RatF structure and $\boldsymbol{y}_i$ represents the output samples.

For the mitigation of PA nonlinearity and I/Q imbalance, $\boldsymbol{R}$ matrix can be written as:

$$\boldsymbol{R}^{(i)} = \left[\boldsymbol{r}^{(i)} \vdots \boldsymbol{r}^{(i)*}\right] \quad (5.4)$$

To account for I/Q compensation, $\boldsymbol{r}_i^*$ has been appended to the $\boldsymbol{r}_i$ matrix. The $\boldsymbol{r}_i$ matrix is defined as:

$$\boldsymbol{r}^{(i)} = \begin{pmatrix} X_{0,0,0}^{(i)}(1), X_{1,0,0}^{(i)}(1), X_{1,1,0}^{(i)}(1) \ \dots X_{K,j=K,Q}^{(i)}(1) \\ -y_i(1)X_{1,1,}^{(i)}(1) \dots - y_i(1)X_{P,1}^{(i)}(1) \dots - y_i(1)X_{P,m=P}^{(i)}(1) \\ X_{0,0,0}^{(i)}(2), X_{1,0,0}^{(i)}(2), X_{1,1,0}^{(i)}(2) \ \dots X_{K,j=K,Q}^{(i)}(2) \\ -y_i(2)X_{1,1,}^{(i)}(2) \dots - y_i(2)X_{P,1}^{(i)}(2) \dots - y_i(2)X_{P,m=P}^{(i)}(2) \\ \vdots \\ X_{0,0,0}^{(i)}(N), X_{1,0,0}^{(i)}(N), X_{1,1,0}^{(i)}(N) \dots X_{K,j=K,Q}^{(i)}(N) \\ -y_i(N)X_{1,1,}^{(i)}(N) \dots - y_i(N)X_{P,1}^{(i)}(N) \dots - y_i(N)X_{P,m=P}^{(i)}(N) \end{pmatrix} \tag{5.5}$$

Also, the complex input vectors are expressed as:

$$X_{k,j,q}^{(i)}(n) = \begin{Bmatrix} x_1(n-q)|x_1(n-q)|^{k-j}|x_2(n-q)|^j \ i=1 \\ x_2(n-q)|x_2(n-q)|^{k-j}|x_1(n-q)|^j \ i=2 \end{Bmatrix}. \tag{5.6}$$

And

$$X_{p,m}^{(i)}(n) = \begin{Bmatrix} x_1(n)|x_1(n)|^{p-m}|x_2(n)|^m \ i=1 \\ x_2(n)|x_2(n)|^{p-m}|x_1(n)|^m \ i=2 \end{Bmatrix}. \tag{5.7}$$

Using LS solution, coefficients of the model in phase 1 can be calculated as follows:

$$\boldsymbol{h}_{phase1}^{(i)} = (\boldsymbol{R}^{(i)^H}\boldsymbol{R}^{(i)})^{-1}\boldsymbol{R}^{(i)^H}\boldsymbol{y}_i \tag{5.8}$$

these values represent the model coefficients in phase 1 ($\boldsymbol{h_{phase1}}$).

The increase of the nonlinear order and memory depth of the 2D-RatF model can lead to non-realistic estimated coefficients. Moreover, the nonlinearities that exist in the I and Q branches of the I/Q modulator cannot be compensated for by using 2D-RatF models. These limitations of the model can be avoided using the phase 2. The 2D-RV model is defined as following:

$$\begin{gathered} RV_1\{x_1(n)^I, x_1(n)^Q\} = \\ \sum_{m_1=0}^{M} \boldsymbol{h}_{1m_1}^T \boldsymbol{x}_{m_1} + \\ \sum_{m_1=0}^{M}\sum_{m_2=m_1}^{M} \boldsymbol{h}_{1m_1m_2}^T \left(\boldsymbol{x}_{1m_1} \otimes \boldsymbol{x}_{2m_1} \otimes \boldsymbol{x}_{1m_2} \otimes \boldsymbol{x}_{2m_2}\right) + \\ \dots \sum_{m_1=0}^{M} \dots \sum_{m_K=m_{K-1}}^{M} \boldsymbol{h}_{1m_1\dots m_K}^T \left(\boldsymbol{x}_{1m_1} \otimes \boldsymbol{x}_{2m_1} \dots \otimes \boldsymbol{x}_{1m_K} \otimes \boldsymbol{x}_{2m_K}\right) \end{gathered} \tag{5.9}$$

where $\boldsymbol{h}_{1m_1\ldots m_K}$ and $k \in K$ (and$m_k \in M$) are the coefficients of the model determined in phase 2, K and M are the polynomial order and the memory depth respectively and $\boldsymbol{x}_{1m_K}$ and $\boldsymbol{x}_{2m_K}$ are the inputs of the phase 2. Symbol $\otimes$ is used to denote Kronecker product.

Also, vectors $\boldsymbol{h}$ and $\boldsymbol{x}$ are defined as:

$$\boldsymbol{h}_{m_1\ldots m_p} = [h_{m_1\ldots m_p,1}\ h_{m_1\ldots m_p,2}\ , \ldots h_{m_1\ldots m_p,2^p}\ ]^T \tag{5.10}$$

and

$$\boldsymbol{x}_{m_p} = \begin{bmatrix} x^I(n-m_p) \\ x^Q(n-m_p) \end{bmatrix} \tag{5.11}$$

Coefficients in phase 2 can be determined using an LS solution as follows:

$$\boldsymbol{h_{phase2}} = (\boldsymbol{X}^H\boldsymbol{X})^{-1}\boldsymbol{X}^H\boldsymbol{y} \tag{5.12}$$

where these values represent coefficients of the model.

The advantage of using a model based on the 2D-RV series in phase 2, is the possibility to manipulate the real numbers instead of complex numbers, which reduces the complexity of the algorithm.

5.3 Experimental Results

Experiments were carried out using the measurement setup shown in Figure 5.2. It consists of two signal generators, Keysight MXG N5182A and Keysight ESG E4433B. The power combiner was utilised in order to model concurrent dual-band wireless transmitter. Aggregated signals are passed through Mini-Circuits ZFL-500 PA, which represents the DUT. Two signal generators were set to have baseband timing alignment and transmit signals at carrier frequencies of 400 MHz (WCDMA signal) and 500 MHz (1.4 MHz LTE signal) with an imbalance artificially introduced I/Q offset of 3% and 5%, respectively and 3 I/Q skew. The nonlinearity order and memory depth were varied during the measurement until the proposed and tested algorithms achieved the best performance.

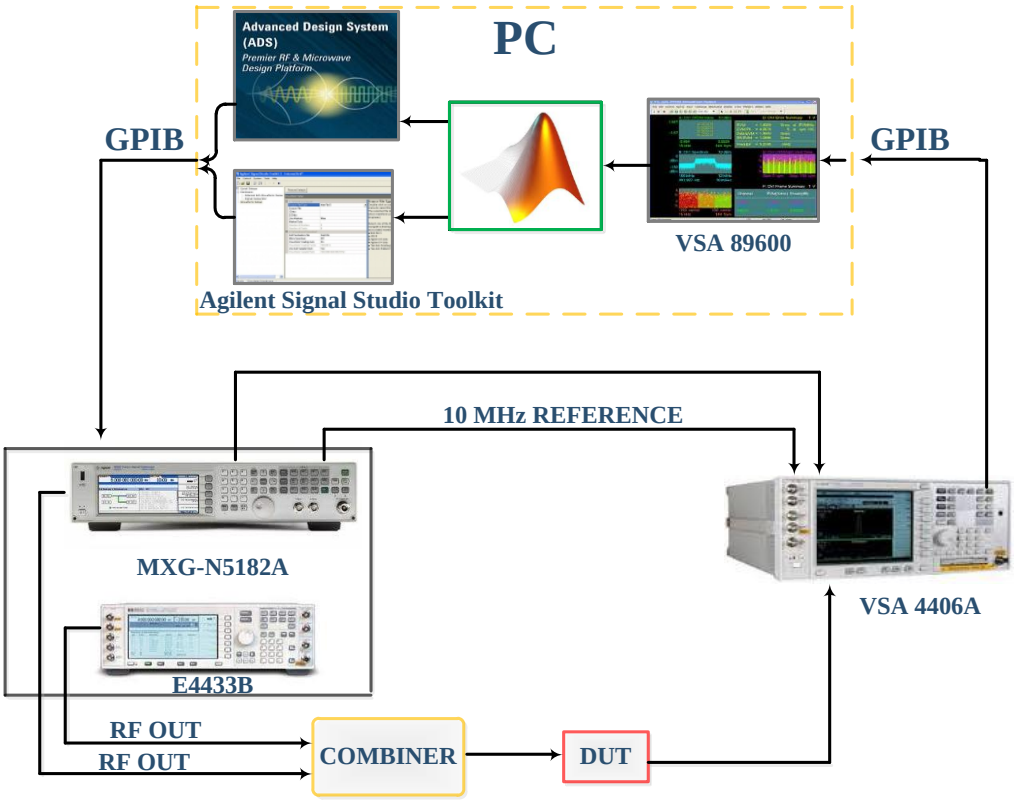

Figure 5.2: Measurement setup.

In order to evaluate the compensation of the nonlinear distortion, accuracy of the models and its complexity, the following parameters were calculated and are presented in Table 5.1, 5.2 and 5.3: ACPR, EVM, NMSE, FLOPs [5-12] and the number of coefficients. Further, the output spectra of transmitter for different models are shown in Figures 5.3 and 5.4 for the UB and LB respectively. The results of AM/AM and AM/PM of PA output signal for UB and LB are presented in Figures 5.5, 5.6, 5.7 and 5.8 respectively.

Model (orders K, Q, P and K, M)	**ACPR (dBc) ±2.5 MHz UB**	**EVM (%) UB**	**NMSE (dB) UB**
Without DPD	-26.45	16.0035	-23.9833
2D-DPD I/Q (5, 5)	-46.50	1.3996	-38.0830
LC 2D-DPD I/Q (5, 5)	-44.51	1.5327	-36.8759
(5, 7)	-45.33	1.4879	-37.0014
2D-RV (4, 3)	-45.20	3.9391	-28.7741
(5, 3)	-45.45	3.2425	-29.8787
2D-RatF (5, 5, 4)	-46.52	1.3774	-39.0062
2D-RatF (4, 3, 2) – RV (3, 2)	-48.28	0.7286	-42.7489
2D-RatF (3, 2, 1) – RV (3, 1)	-46.83	1.2954	-39.3013

Table 5.1: Performance of the models for UB.

Model (orders K, Q, P and K, M)	**ACPR (dBc) ±2.5 MHz LB**	**EVM (%) LB**	**NMSE (dB) LB**
Without DPD	-32.20	16.0035	-26.7804
2D-DPD I/Q (5, 5)	-42.00	1.0512	-40.4337
LC 2D-DPD I/Q (5, 5) (5, 7)	-41.20 -41.88	1.2172 1.1874	-38.2920 -38.7845
2D-RV (4, 3) (5, 3)	-37.95 -39.78	2.8255 2.1289	-31.6127 -32.0033
2D-RatF (5, 5, 4)	-42.08	0.9986	-40.4938
2D-RatF (4, 3, 2) – RV (3, 2)	-45.65	0.5832	-44.6830
2D-RatF (3, 2, 1) – RV (3, 1)	-42.35	0.9304	-40.7589

Table 5.2: Performance of the models for LB.

Model (orders K, Q, P and K, M)	**FLOPs**	**No. Coeff**
Without DPD	/	/
2D-DPD I/Q (5, 5)	3450	422 (complex)
LC 2D-DPD I/Q (5, 5) (5, 7)	1008 1356	122 (complex) 162 (complex)
2D-RV (4, 3) (5, 3)	3182 5238	4x768 (real) 4x2560 (real)
2D-RatF (5, 5, 4)	1318	162 (complex)
2D-RatF (4, 3, 2) – RV (3, 2)	Ph.1: 738 Ph.2: 462	Ph.1:90 (complex) Ph.2: 4x110 (real)
2D-RatF (3, 2, 1) – RV (3, 1)	Ph.1: 446 Ph.2: 118	Ph.1:58 (complex) Ph.2: 4x48 (real)

Table 5.3: Performance of the models.

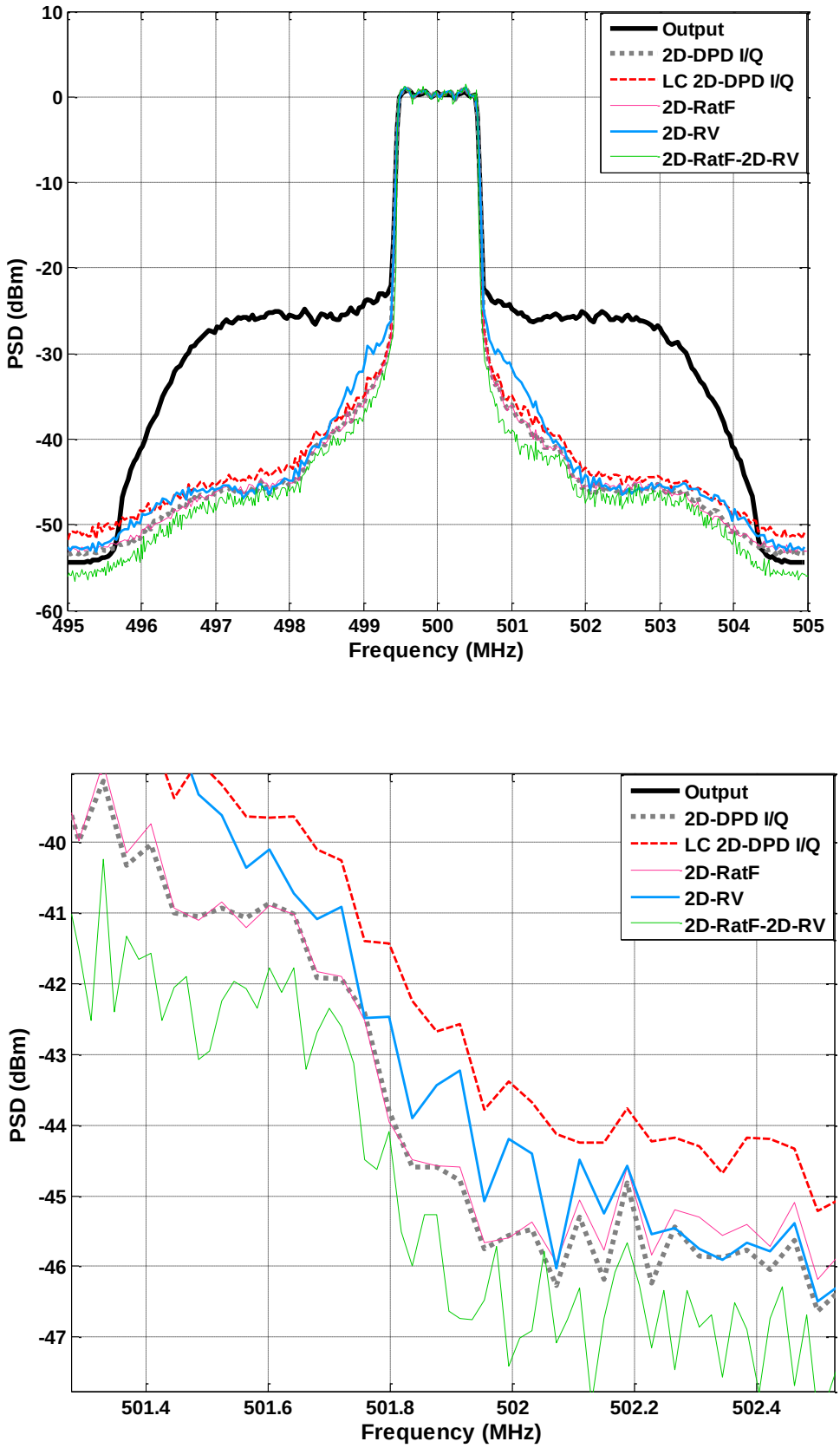

Figure 5.3: Power spectra of the proposed two-box DPD and its comparison with the existing models UB.

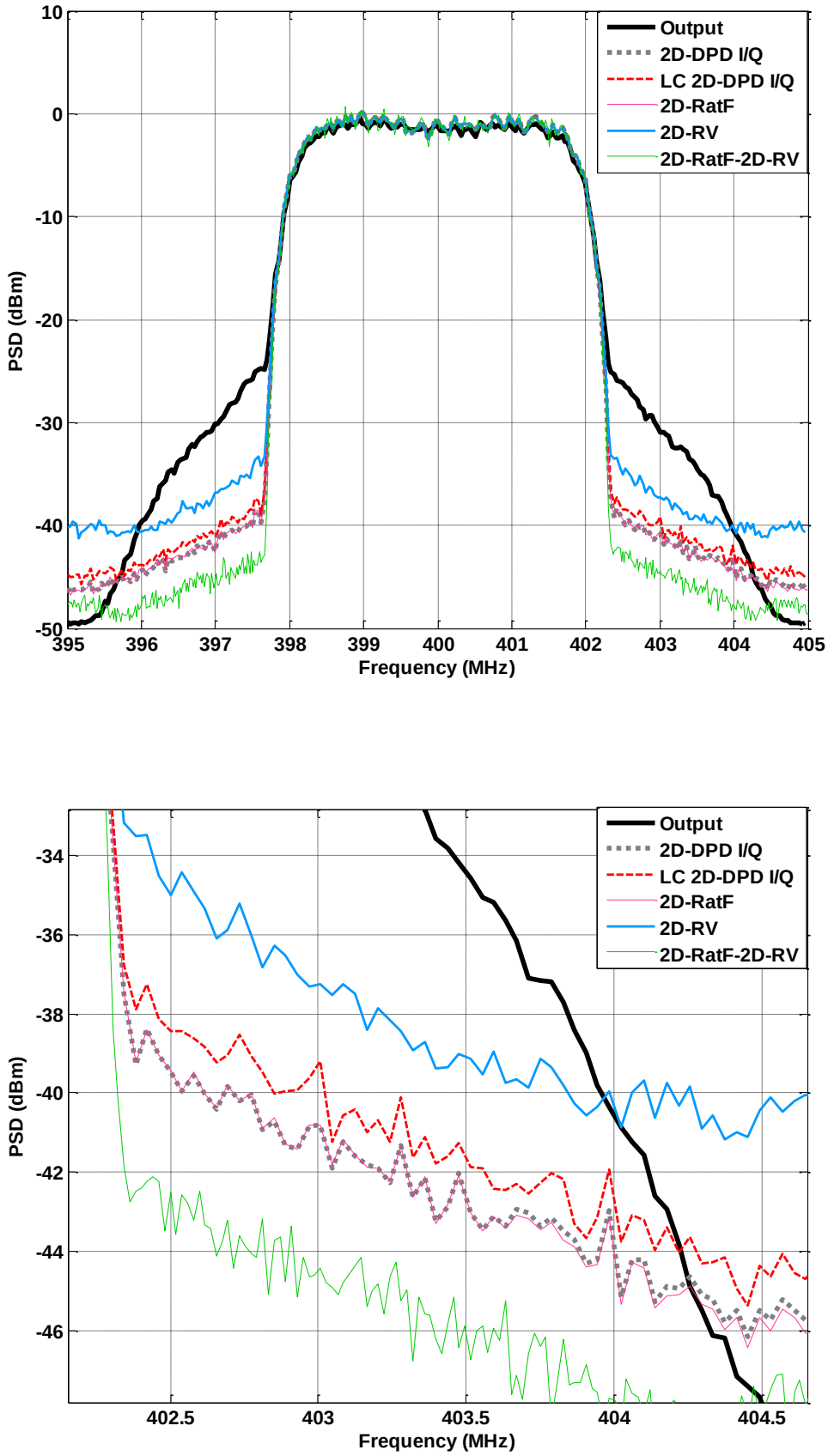

Figure 5.4: Power spectra of the proposed two-box DPD and its comparison with the existing models LB.

As can be seen, the two-box model (2D-RatF-2D-RV) decreases the ACPR to less than -48 dBc for the UP and less than -45 dBc for the LB. Also, EVM and NMSE go as low as 0.72% for the UB and 0.58% for LB, and -42 dB for the UB and -44 dB for the LB respectively. By comparing the results obtained using one model of cascade (2D-RatF or 2D-RV) with the two-box model, it is shown that the proposed model not only achieves a better performance, but also reduces the numbers of both the FLOPs and the coefficients.

As RV deals with real coefficients, the computational load of phase 2 in the two-box model is almost the same as for the LC 2D-DPD for I/Q, since it has complex coefficients. The existence of two phases in the two-box model enables scaling down the nonlinear order and memory depth. Also, the number of FLOPs is significantly reduced in comparison with all the studied models.

As can be noticed from Figures 5.5, 5.6, 5.7 and 5.8, significant dispersion is manifested at the PA output signal (DPD off case). By using the 2D-RV model dispersion is reduced but its level is still high. 2D-DPD I/Q and LC 2D-DPD I/Q models give better results in comparison with 2D-RV model, while with 2D-RatF, AM/AM and AM/PM curves for both bands are thinner. However, the proposed two-box model gives best AM/AM and AM/PM performance. The AM/AM and AM/PM curves are thinner in comparison with the 2D-RatF model. Also, the output amplitude has been thoroughly linearised using the proposed two-box model. All the results prove that the proposed two-box model is able to successfully compensate for I/Q impairments, PA nonlinearity and CM products in concurrent dual-band transmitters.

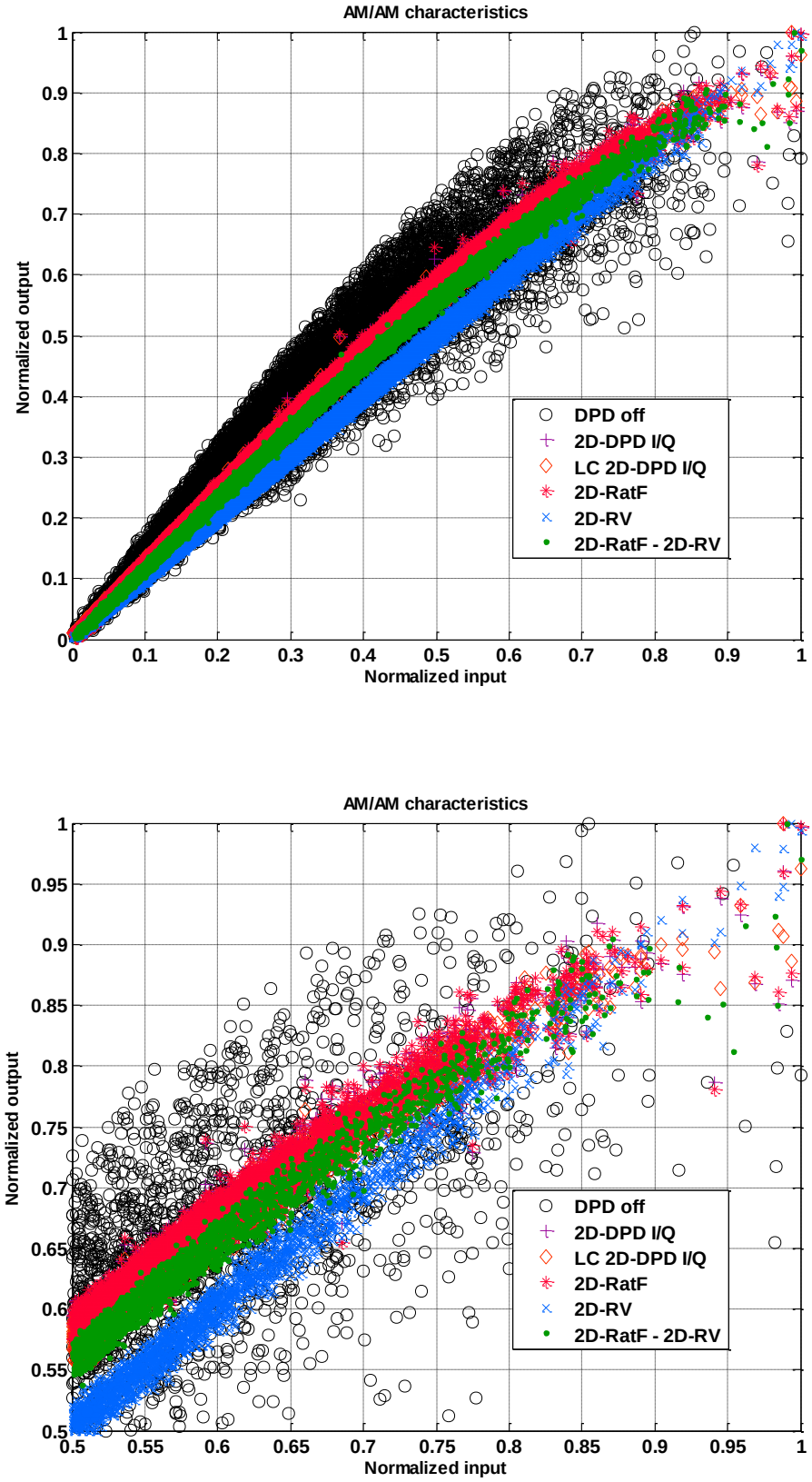

Figure 5.5: AM/AM curves of the proposed two-box DPD and its comparison with the existing models UB.

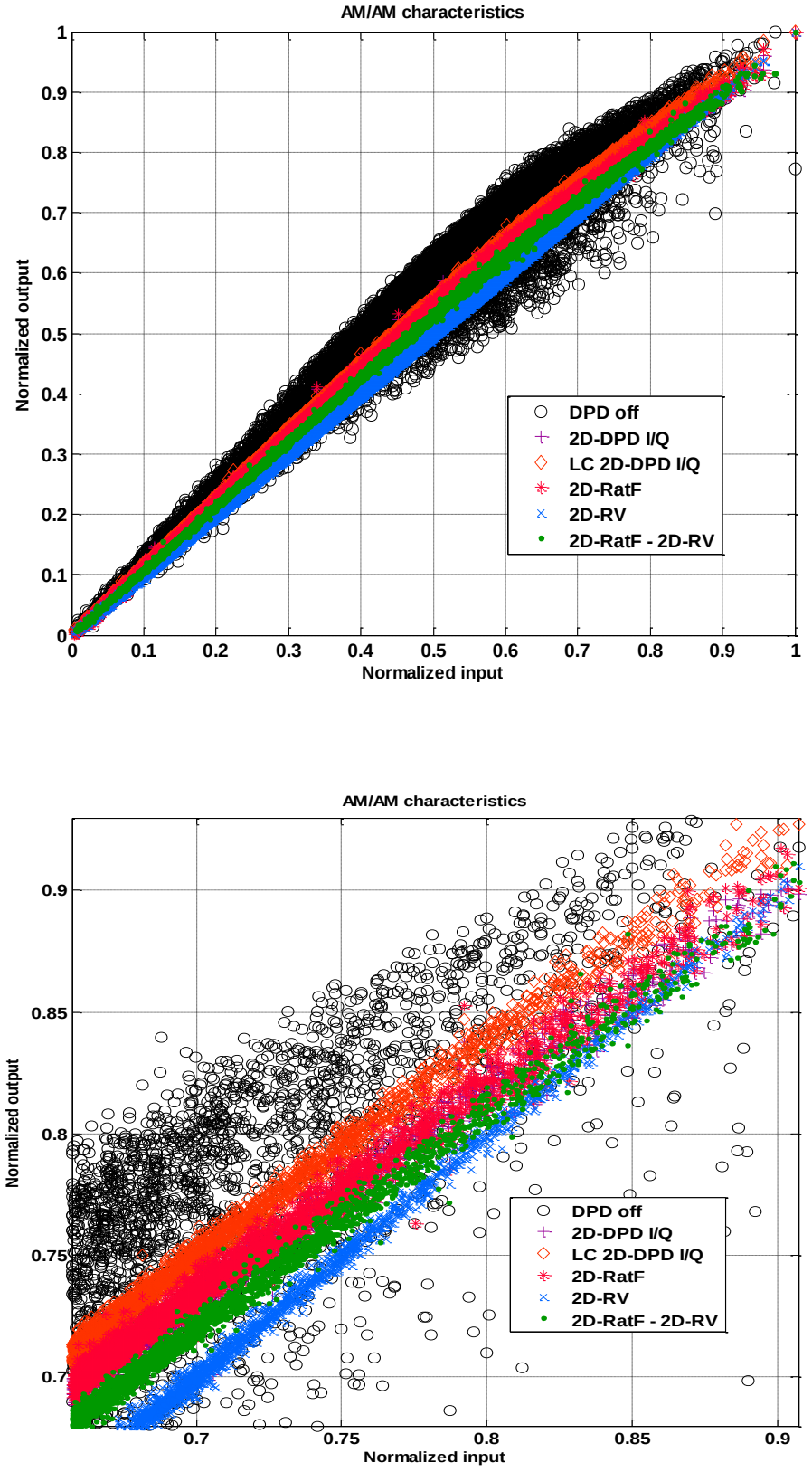

Figure 5.6: AM/AM curves of the proposed two-box DPD and its comparison with the existing models LB.

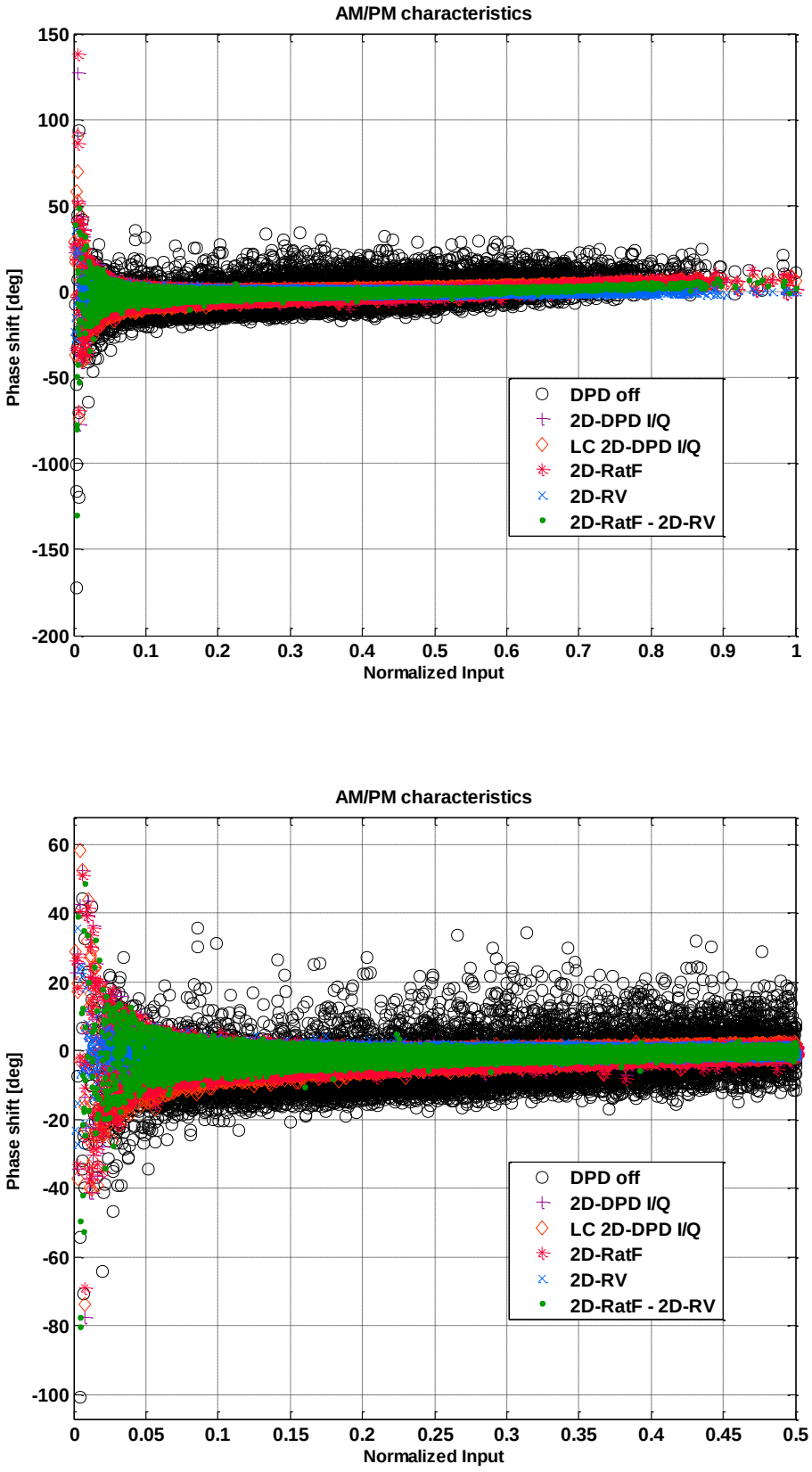

Figure 5.7: AM/AM curves of the proposed two-box DPD and its comparison with the existing models UB.

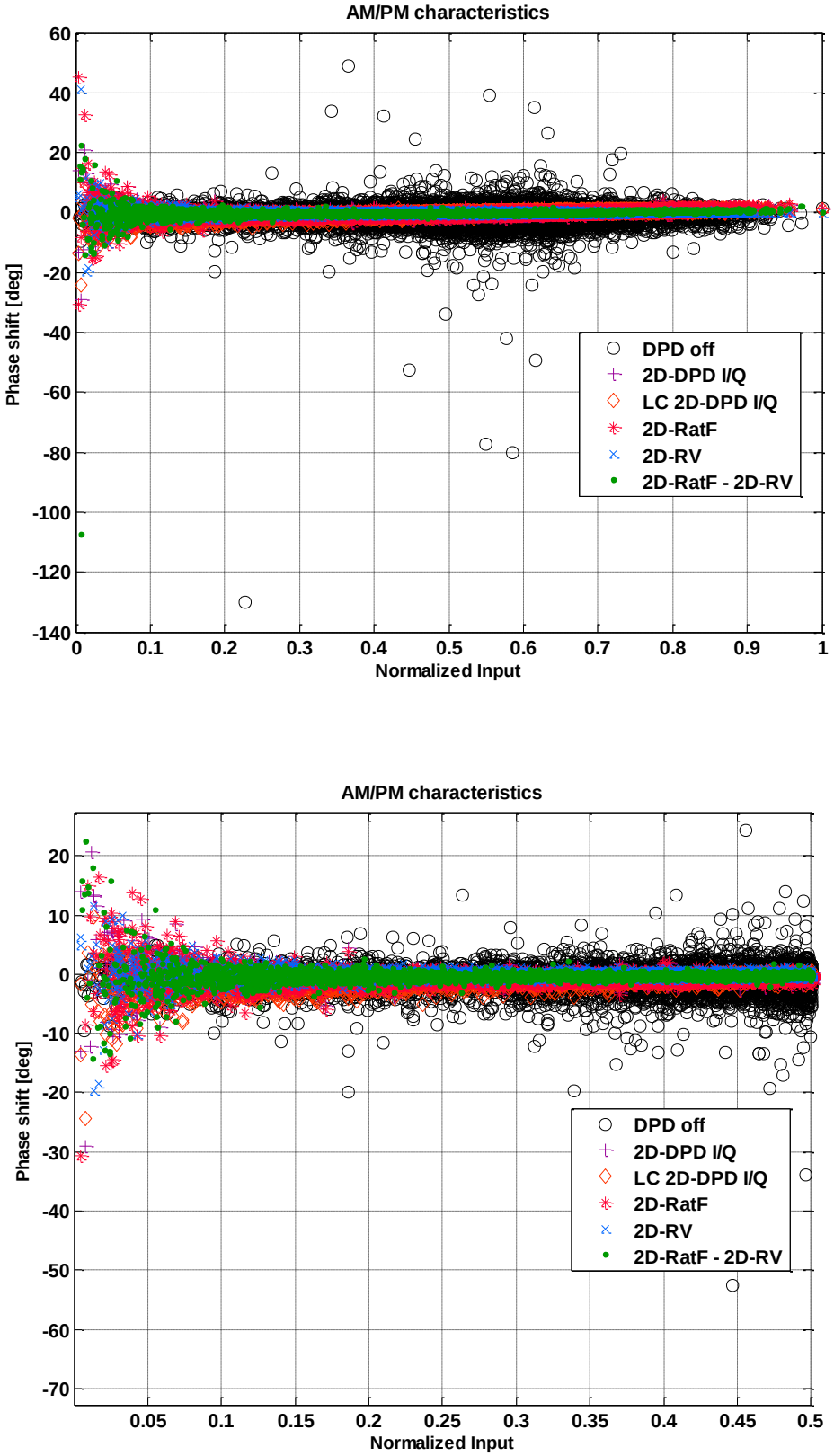

Figure 5.8: AM/AM curves of the proposed two-box DPD and its comparison with the existing models LB.

5.4 Summary

A new two-box model for the joint compensation of I/Q impairments and PA nonlinearity, as well as CM products for concurrent dual-band wireless transmitter has been proposed. The nonlinear distortion is compensated by implementing PD in two phases, where each phase is identified separately and modelled by the lower order of implemented functions (2D-RatF and 2D-RV). The proposed model relies on the idea to gradually compensate the nonlinear distortion. This significantly minimises the complexity of the modelling process. It also achieves improvements in ACPR, EVM and NMSE.

5.5 References

[5-1] M. Bozic and D. Budimir, "Joint Compensation of I/Q Impairments and Power Amplifier Nonlinearity for Concurrent Dual-Band Transmitters Using Two-Box Model," *IEEE Microwave and Wireless Components Letters*, vol. 25, no. 5, pp. 340-342, May 2015

[5-2] Y.J. Liu, W. Chen, J. Zhou, B.H. Zhou, and F. Ghannouchi, "Digital predistortion for concurrent dual-band transmitters using 2-D modified memory polynomials," *IEEE Transactions on Microwave Theory and Techniques*, vol. 61, no. 1, pp. 281–290, Jan. 2013

[5-3] S. A. Bassam, C. Wenhua, M. Helaoui, F. M. Ghannouchi and F. Zhenghe, "Linearization of concurrent dual-band power amplifier based on 2D-DPD technique," *IEEE Microwave and Wireless Components Letters*, vol. 21, no. 12, pp. 685–687, Dec. 2011

[5-4] Y.J. Liu, W. Chen, J. Zhou, B.-H. Zhou and Y.N. Liu, "Joint predistortion of IQ impairments and PA nonlinearity in concurrent dual-band transmitters," *42nd European Microwave Conference (EuMC)*, vol., no., pp. 132–135, Nov. 2012

[5-5] Y.J. Liu, J. Zhou, W. Chen, B. Zhou and F. M. Ghannouchi, "Low complexity 2D behavioural model for concurrent dual-band power amplifiers," *Electronics Letters*, vol. 48, no. 11, pp. 620–621, May 2012

[5-6] J. Moon and B. Kim, "Enhanced Hammerstein Behavioral Model for Broadband Wireless Transmitters," in IEEE Transactions on Microwave Theory and Techniques, vol. 59, no. 4, pp. 924-933, April 2011.

[5-7] Y. Xu, J. Wang, X. Zhu and J. Zhai, "Dynamic extended Hammerstein model of RF power amplifiers for digital predistortion," *Microwave Integrated Circuits Conference (EuMIC)*, pp. 276-279, 2011.

[5-8] O. Hammi, "Orthogonal polynomial based Hammerstein behavioral model for power amplifiers with strong memory effects," *2010 Asia-Pacific Microwave Conference*, Yokohama, pp. 441-444, 2010.

[5-9] C. Quindroit, N. Naraharisetti, P. Roblin, S. Gheitanchi, V. Mauer and M. Fitton, "2D forward twin nonlinear two-box model for concurrent dual-band digital predistortion," *IEEE Topical Conference on Power Amplifiers for Wireless and Radio Applications (PAWR)*, pp. 1-3, 2014.

[5-10] M. Aziz, M. Rawat and F. M. Ghannouchi, "Rational function based model for the joint mitigation of I/Q imbalance and PA nonlinearity," *IEEE Microwave and Wireless Components Letters*, vol. 23, no. 4, pp. 196–198, April 2013

[5-11] C. Haiying, A. S. Tehrani, C. Fager, T. Eriksson and H. Zirath, "I/Q imbalance compensation using a nonlinear modeling approach," *IEEE Transactions on Microwave Theory and Techniques*, vol. 57, no. 3, pp. 513–518, March 2009

[5-12] A. S. Tehrani, C. Haiying, S. Afsardoost, T. Eriksson, M. Isaksson and C. Fager, "A comparative analysis of the complexity/accuracy tradeoff in power amplifier behavioral models," *IEEE Transactions on Microwave Theory and Techniques*, vol. 58, no. 6, pp. 1510–1520, June 2010

CHAPTER 6
CONCLUSION AND FUTURE WORK

This chapter summarises the contributions made in this thesis and reiterates the potential for future work, both of which have already been covered in some detail at the end of previous chapters. The main focus of this thesis was to develop and investigate an accurate and low complexity DPD technique for compensation of I/Q impairments, PA nonlinearity, crosstalk effects and CM products that appears in multi-branch MIMO and concurrent dual-band wireless transmitters. The thesis therefore, has addressed some of the challenges that appear during this process, such as modelling accuracy, complexity and linearity of wireless transmitters. This was achieved by evaluating nonlinear distortion that appears in the wireless transmitters and demonstrating the effects of distortion on the transmitted signal. After that, a new two-box model was developed that successfully modelled and compensated for undesired effects in multi-branch MIMO and concurrent dual-band wireless transmitters.

Chapter 1 has provided an outline of the thesis and introduced the aims and objectives as well as a brief discussion of the past research work that has been carried out with regards to modelling and compensation process of nonlinear distortion that appears in wireless transmitters.

The basic background theory, which was relevant to the subject of this thesis has been given in Chapter 2. A brief overview of requirements of the parameters for linearity in wireless transmitters has been provided with a description of nonlinear distortion introduced from I/Q modulator and PA. Also, main system parameters have been demonstrated together with metrics that are needed for evaluating performances of wireless transmitters. Then explanation of OFDM technology as basis of LTE wireless system has been addressed. The chapter has also highlighted the distortion that is additionally introduced in wireless transmitters using multi-branch or multi-frequency MIMO systems, such as crosstalk effect and CM products, respectively.

Overview of behavioural models of I/Q modulator and PA has been addressed in Chapter 3. Then, adaptive DPD architectures, such as DLA and ILA have been

explained. Also, the problem relating to the joint compensation of I/Q impairments and PA nonlinearity together with crosstalk effects or CM products have been demonstrated.

Chapter 4 has introduced a new two-box model for joint compensation of I/Q impairments, PA nonlinearity and crosstalk effects for multi-branch MIMO wireless transmitters. The key idea was to gradually compensate for the nonlinear distortion by implementing predistorter in two phases. When identification of phase 1 is finished, it will belong to a new system, a cascade of I/Q modulator and PA. This enables reduction of model complexity, since only one phase is processed by iteration. In addition, model complexity depends on the number of parameters that are needed for identification process, which are minimised with the existence of two phases. Then, phase 2 can be identified and new coefficients are calculated. Phase 2 is added to compensate for residual distortion or improve linearity of the new system. Phase 1 of two-box model is realised using RatF and phase 2 using RV model, where both models are modified so they can take into account crosstalk effect. The two-box model was verified through Matlab simulation and experimental measurement.

In Chapter 5, the proposed technique that was described in Chapter 4 was developed for concurrent dual-band wireless transmitters. In other words, a two-box model was introduced to compensate for I/Q impairments, PA nonlinearity and CM products. As explained in Chapter 4, the model was implemented in two phases, where each was identified separately. Therefore, the identification of any system was optimised. The identification complexity was much lower in comparison with conventional systems, since only one phase was processed during iteration. In addition, the identification algorithm has used an ILA and LS method for parameter identification. The two-box model was realised by implementing algorithms 2D-RatF in phase 1 and 2D-RV in phase 2, which were modified to take into account CM products that appear in concurrent dual-band wireless transmitters. 2D-RatF was chosen as its approximation power is the same as Volterra model, which so far gives the best modelling results. Also, in comparison to the Volterra model, complexity of 2D-RatF is lower. Implementation of phase 2 enables scaling down the nonlinear order and memory depth of 2D-RatF (phase 1), since increase of those parameters can lead to non-realistic estimated coefficients. 2D-RV model was able to compensate nonlinear distortion that appears in I/Q modulator. In addition, experimental verification of the proposed two-box model for compensation of I/Q impairments, PA nonlinearity and CM products for concurrent dual-band wireless transmitters has been demonstrated in this Chapter.

6.1 Contributions of the Thesis

The research work presented in this thesis has made the following list of contributions.

1. The problems of I/Q impairments, PA nonlinearity and crosstalk effects which appear in multi-branch MIMO wireless transmitters have been addressed. Also, the development of a novel two-box model, which jointly compensates for these impairments, has been conducted. In order to show the influence of the distortion which appears in multi-branch MIMO wireless transmitters, evaluation has been done using Matlab simulations and experimental measurements. The proposed two-box model has been validated through Matlab simulation as well as experimental measurements. In comparison with the RatF model, it was shown that two-box model improves ACPR by about 2.3 dB and reduces the number of both the FLOPs and the coefficients.

2. For the first time, the development of a two-box model for the joint compensation of I/Q impairments, PA nonlinearity and CM products for concurrent dual-band wireless transmitters has been presented. This model enables the compensation of nonlinear distortion gradually, which leads to a reduced complexity. This is possible since the identification is done separately for each phase. Phase 1 is implemented using the 2D-RatF which has the same approximation power as the Volterra model. To overcome the problem of non-realistic estimated coefficients which can be manifested using the RatF, phase 2 of the two-box model is implemented. Ability to use the 2D-RV model as phase 2 has demonstrated the improvements in ACPR, EVM and NMSE. Moreover, the number of both the FLOPs and the coefficients has been decreased. Experimental verification of the proposed two-box model has been provided.

6.2 Suggestions for Future Work

The research work detailed in this thesis has addressed some of the challenges that pertain to model and compensate nonlinear distortion, which appears in multi-branch and multi-frequency MIMO wireless transmitters. However, there is still some scope for expansion. Future work in this field could therefore address several possible areas.

1. The two-box model which was proposed in Chapter 4 was experimentally verified using the PA ZFL 500 for multi-branch MIMO wireless transmitters.

Nevertheless, with the increase in the efficiency of wireless transmitters, new experimental verification will be needed. Therefore, the proposed model will be further investigated engaging the new high-power high-efficiency types of power amplifiers (Doherty, class F, inverse class F or class J PAs that exhibit strong memory effects) as DUT. Also, these new tests will conduct multi-branch and multi-frequency MIMO wireless transmitters architecture.

2. The thesis has introduced a two-box model for the joint compensation of nonlinear distortion introduced in multi-branch and multi-frequency MIMO wireless transmitters using 4G signals. Therefore, a second suggestion for future work is the implementation of different digitally modulated signals in different types of wireless transmitters. Also, new experiments can be conducted with a new modulated signal with different and wider frequency bands using the two-box model proposed in Chapter 4 and 5 respectively.

3. The possibility of the extension of the concurrent dual-band wireless transmitters to more multi-frequency wireless transmitter will open up new opportunities for further development of the proposed two-box model. This property might be beneficial, since the model has significantly lower complexity in comparison with the studied models. It also improves the performances of the wireless transmitters. Generally speaking, the further reduction in the complexity of DPD technique and improvement of efficiency wireless transmitters could be carried out.

List of Publications

[1] **M. Bozic**, M. Cabarkapa, D. Budimir, N. Neskovic and A. Neskovic “Evaluation of Nonlinear Distortion in MIMO Transmitters”, *42nd European Microwave Conference (EuMC)*, vol., no., pp. 908-911, Nov. 2012

[2] **M. Bozic** and D. Budimir, "Joint compensation of I/Q impairments, power amplifier nonlinearity and crosstalk in MIMO transmitters using two-box model," *European Microwave Conference (EuMC)*, vol., no., pp. 1120-1123, Sept. 2015

[3] **M. Bozic** and D. Budimir, "Joint Compensation of I/Q Impairments and Power Amplifier Nonlinearity for Concurrent Dual-Band Transmitters Using Two-Box Model," *IEEE Microwave and Wireless Components Letters*, vol. 25, no. 5, pp. 340-342, May 2015

[4] M. Cabarkapa, **M. Bozic**, N. Neskovic, A. Neskovic and D. Budimir, “Compensation of Undesired Effects in MIMO Wireless Transceivers”, *IEEE International Symposium on Antennas and Propagation and CNC/USNC/URSI National Radio Science Meeting (APS2012)*, vol., no., pp. 1-2, July 2012

[5] **M. Bozic**, M. Cabarkapa, N. Neskovic, A. Neskovic and D. Budimir, "Compensation of nonlinear distortion in MIMO OFDM wireless communication systems," *Telecommunications Forum (TELFOR), 2011 19th* , vol., no., pp.425-428, Nov. 2011

[6] **M. Bozic**, M. Cabarkapa and D. Budimir, " Combined Baseband Injection - Real Volterra Digital Predistortion for 4G Wireless Transmitters," *IEEE Microwave and Wireless Components Letters*, Oct 2015 (submitted)

APPENDIX

Data Sheets for the Power Amplifiers

Coaxial
Amplifier

ZFL-500+
ZFL-500

50Ω Low Power 0.05 to 500 MHz

SMA version shown
CASE STYLE: Y460

Features
- wideband, 0.05 to 500 MHz
- rugged, shielded case
- low noise, 5.3 dB typ.
- protected by US Patent, 6,943,629

Applications
- instrumentation
- lab use
- VHF/UHF

Connectors	Model	Price	Qty.
SMA	ZFL-500(+)	$69.95	(1-9)
BNC	ZFL-500-BNC	$74.95	(1-9)
BRACKET (OPTION "B")		$5.00	(1+)

+RoHS Compliant
The +Suffix identifies RoHS Compliance. See our web site for RoHS Compliance methodologies and qualifications

Amplifier Electrical Specifications

MODEL NO.	FREQUENCY (MHz)		GAIN (dB)		MAXIMUM POWER (dBm)		DYNAMIC RANGE		VSWR (:1) Typ.		DC POWER	
					Output (1 dB Compr.)	Input (no damage)	NF (dB)	IP3 (dBm)			Volt (V)	Current (mA)
	f_L	f_U	Min.	Flatness Max.			Typ.	Typ.	In	Out	Nom.	Max.
ZFL-500(+)	0.05	500	20	±1.0	+9	+5	5.3	+18	1.9	1.9	15	80

Open load is not recommended, potentially can cause damage.
With no load derate max input power by 20 dB

Maximum Ratings

Operating Temperature	-20°C to 71°C
Storage Temperature	-55°C to 100°C
DC Voltage	+17V Max.

Permanent damage may occur if any of these limits are exceeded.

Outline Drawing

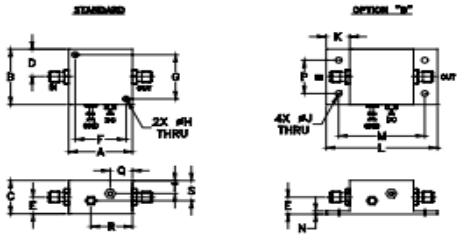

Outline Dimensions (inch / mm)

A	B	C	D	E	F	G	H	J	K	L	M	N	P	Q	R	S	T	wt.
1.25	1.25	.75	.63	.36	1.000	1.000	.125	.125	.46	2.18	1.688	.06	.750	.50	.80	.45	.29	grams
31.75	31.75	19.05	16.00	9.14	25.40	25.40	3.18	3.18	11.68	55.37	42.88	1.52	19.05	12.70	20.32	11.43	7.37	38

Notes
A. Performance and quality attributes and conditions not expressly stated in this specification document are intended to be excluded and do not form a part of this specification document.
B. Electrical specifications and performance data contained in this specification document are based on Mini-Circuit's applicable established test performance criteria and measurement instructions.
C. The parts covered by this specification document are subject to Mini-Circuits standard limited warranty and terms and conditions (collectively, "Standard Terms"); Purchasers of this part are entitled to the rights and benefits contained therein. For a full statement of the Standard Terms and the exclusive rights and remedies thereunder, please visit Mini-Circuits' website at www.minicircuits.com/MCLStore/terms.jsp

Mini-Circuits®
www.minicircuits.com P.O. Box 35166, Brooklyn, NY 11235-0003 (718) 934-4500 sales@minicircuits.com
REV. B
M125292
ZFL-500
131015
Page 1 of 2

Typical Performance Data/Curves

FREQUENCY (MHz)	GAIN (dB)			DIRECTIVITY (dB)			VSWR (:1) 15V		NOISE FIGURE (dB)	POUT at 1 dB COMPR. (dBm)
	12V	15V	16V	12V	15V	16V	IN	OUT	15V	15V
0.05	20.18	21.24	21.41	18.10	17.50	17.40	1.59	1.69	—	10.52
0.33	21.00	22.06	22.23	16.40	15.70	15.60	1.17	1.11	—	10.82
3.90	21.03	22.08	22.27	16.30	15.60	15.50	1.09	1.11	—	10.84
47.90	21.08	22.13	22.30	16.10	15.40	15.30	1.07	1.11	5.72	10.87
192.30	20.96	21.93	22.07	15.40	15.90	17.10	1.01	1.01	5.74	10.31
243.60	20.79	21.74	21.90	16.80	17.20	16.80	1.01	1.01	5.76	10.28
307.70	20.74	21.70	21.84	16.20	16.60	16.60	1.01	1.02	5.77	10.26
371.80	20.58	21.55	21.70	16.40	17.20	17.60	1.01	1.02	5.77	10.23
435.90	20.69	21.65	21.80	15.70	16.80	16.10	1.01	1.03	5.78	10.14
500.00	20.40	21.36	21.52	17.10	17.70	16.70	1.01	1.02	5.79	10.05

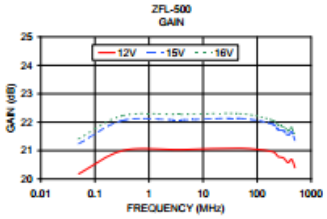

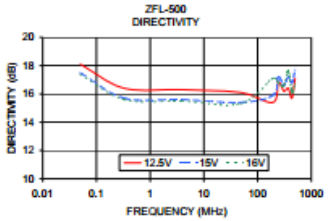

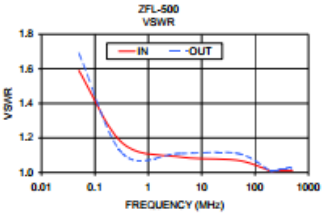

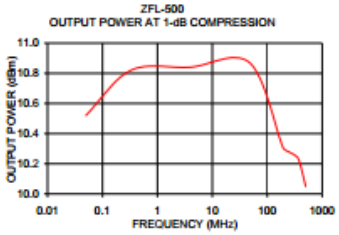

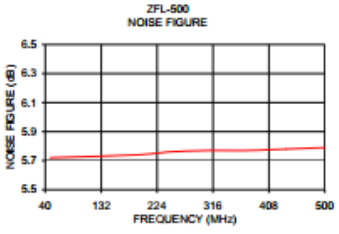

Notes
A. Performance and quality attributes and conditions not expressly stated in this specification document are intended to be excluded and do not form a part of this specification document.
B. Electrical specifications and performance data contained in this specification document are based on Mini-Circuit's applicable established test performance criteria and measurement instructions.
C. The parts covered by this specification document are subject to Mini-Circuits standard limited warranty and terms and conditions (collectively, "Standard Terms"); Purchasers of this part are entitled to the rights and benefits contained therein. For a full statement of the Standard Terms and the exclusive rights and remedies thereunder, please visit Mini-Circuits' website at www.minicircuits.com/MCLStore/terms.jsp

Coaxial

Amplifier

ZHL-1042J+
ZHL-1042J

50Ω Medium Power 10 to 4200 MHz

Features
- wideband, 10 to 4200 MHz
- high IP3, +30 dBm typ.
- low noise, 6 dB typ.

Applications
- laboratory
- communication systems

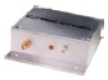

ZHL-1042JX-S

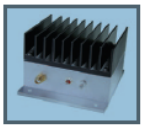

ZHL-1042J-S

CASE STYLE: NN92

Connectors	Model	Price	Qty.
SMA	ZHL-1042J(+)	$495.00 ea.	(1-9)
SMA	ZHL-1042JX	$485.00 ea.	(1-9)

+RoHS Compliant
The +Suffix identifies RoHS Compliance. See our web site for RoHS Compliance methodologies and qualifications

Electrical Specifications

MODEL NO.	FREQ. (MHz)		GAIN (dB)			MAXIMUM POWER OUTPUT (dBm)		DYNAMIC RANGE		VSWR (:1) Typ.		DC POWER	
	f_L	f_U	Typ.	Min.	Flatness Max.	(1 dB Compr.) Min.	Input (no damage)	NF (dB) Typ.	IP3 (dBm) Typ.	In	Out	Volt (V) Nom.	Current (A) Max.
ZHL-1042J(+)	10	4200	—	25	±1.5	+20	+10	6	+30	2.5	2.5	15	0.330
ZHL-1042JX*	10	4200	—	25	±1.5	+20	+10	6	+30	2.5	2.5	15	0.330

* Heat sink not included
Open load is not recommended, potentially can cause damage.
With no load derate max input power by 20 dB

To order without heat sink, add suffix X to model number. Alternative heat sinking and heat removal must be provided by the user to limit maximum temperature to 65°C, in order to ensure proper performance. For reference, this requires thermal resistance of user's external heat sink to be 2.2°C/W Max.

Maximum Ratings

Operating Temperature	-20°C to 65°C
Storage Temperature	-55°C to 100°C
DC Voltage	+20V Max.

Permanent damage may occur if any of these limits are exceeded.

Outline Drawing

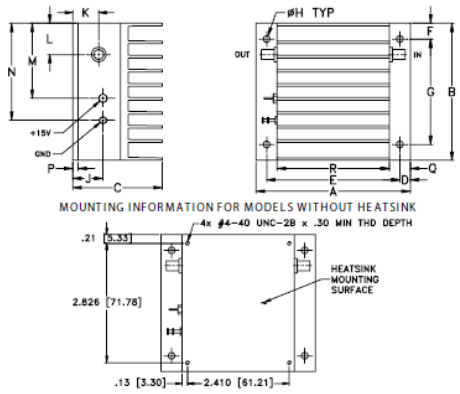

Outline Dimensions (inch / mm)

A	B	C	D	E	F	G	H	J	K	L	M	N	P	Q	R	wt
3.66	3.25	2.13	.25	3.16	.38	2.50	.156	.72	.64	.74	1.78	2.30	.125	.50	2.66	grams*
92.96	82.55	54.10	6.35	80.26	9.65	63.50	3.96	18.29	16.26	18.80	45.21	58.42	3.18	12.70	67.56	500.0

*362 grams without heatsink

REV.C
M129211
ZHL-1042J
130528
Page 1 of 2

Typical Performance Data/Curves

FREQUENCY (MHz)	GAIN (dB)			DIRECTIVITY (dB)			VSWR (:1)		NOISE FIGURE (dB)	POUT at 1 dB COMPR. (dBm)
	12V	15V	16V	12V	15V	16V	IN	OUT	15V	15V
10.00	27.55	28.68	28.68	33.40	32.60	33.80	1.60	1.57	19.14	22.32
21.40	28.01	29.08	29.09	30.70	19.80	26.40	1.56	1.83	17.99	23.20
67.00	27.31	28.36	28.37	28.30	27.70	27.50	1.57	1.84	13.37	22.82
209.90	27.41	28.43	28.44	32.30	29.80	34.40	1.52	1.78	7.36	22.75
258.50	26.30	27.16	27.18	29.70	23.10	24.80	1.65	1.10	5.34	21.04
657.20	27.06	28.06	28.06	29.80	23.00	30.50	1.24	1.43	5.90	21.80
1514.10	27.81	28.70	28.71	29.50	29.10	27.40	1.53	1.62	5.28	20.96
1836.40	27.53	28.29	28.28	30.00	26.70	27.70	1.88	1.47	5.40	21.14
2158.70	26.69	27.44	27.44	25.50	26.20	27.90	1.94	1.29	5.39	20.59
2373.60	26.44	27.26	27.27	25.00	26.00	28.50	1.83	1.20	5.30	20.84
2910.80	26.45	27.38	27.41	23.90	28.10	23.20	1.48	1.12	5.41	20.61
3233.10	26.74	27.60	27.60	23.50	31.50	25.70	1.45	1.34	5.43	20.72
3555.40	26.87	27.63	27.64	28.60	25.90	25.80	1.17	1.64	5.43	20.61
3877.70	27.26	28.14	28.15	22.20	20.80	22.20	1.31	1.75	5.55	21.22
4200.00	27.17	28.06	28.08	21.90	18.30	21.20	1.46	1.66	5.58	20.82